The Photochemistry of (η^6-arene)$M(CO)_3$ (M = Cr, Mo, or W) and $[(\eta^6\text{-arene})_2Cr]^+$

A thesis presented for the degree of Doctor of Philosophy

at

Dublin City University

by

Siobhan O'Keeffe B.Sc.

under the supervision of Dr. Conor Long

School of Chemical Sciences

1997

The Photochemistry of (η^6-arene)$M(CO)_3$ (M = Cr, Mo, or W) and $[(\eta^6\text{-arene})_2Cr]^+$

A thesis presented for the degree of Doctor of Philosophy

at

Dublin City University

by

Siobhan O'Keeffe B.Sc.

under the supervision of Dr. Conor Long

School of Chemical Sciences

1997

Declaration

I hereby certify that this thesis, which I now submit for assessment on the programme of study leading to the award of Ph.D. is entirely my own work and has not been taken from the work of others save and to the extent that such work has been cited and acknowledged within the text of my work.

Signed: Siobhán O'Keeffe **Date:** 6-11-'97

Siobhan O'Keeffe

Acknowledgements

Firstly I would like to thank Dr. Conor Long for all his help, encouragement and great patience over the last few years. Many thanks to Mary for her help in my early postgrad. days and especially during the writing of this thesis; the use of the office, the proof reading and most importantly the sweets!

Thanks to all the technical staff here who were always so helpful when I was usually in a fluster; Veronica, Mick, Damien, Maurice, Ann, Vinny and all the others who have passed through.

To all the past and present members of the research group; Mary, Ciara, Charlie, Deirdre, and Bronagh who have all been a great help and fun over the years.....it *almost* makes me want to hang around for another Xmas dinner! Thanks also to the other occupants of AGO7 who kept me laughing, and added that little something extra to the lab (smelly organics for one!), and of course I can't forget the neighbours in AG12, and the many other postgrads.

Many thanks to all my friends, the girlies of 165; Ger, Marie, Ciara, and Teresa, to Orla (the mountain goat!),who has been with me all the way, Ciara H. Monica, Susan, Anna, Shivaun and Mick. A huge and very special thanks to Tom .....now where is Figure 1.8?!

Finally I want to thank my family for their love and support in my seemingly endless student life; to Mum who's the best and Dad who would have enjoyed the celebrations, and to Aine and Donie who may eventually have a big sister to bum from.

To Mum, Aine, Donie
and the memory of Dad.

Table of Contents

Chapter 2

Electronic structure and the photochemistry of (η^6-arene)$M(CO)_3$ complexes (M = Cr, Mo, or W).

Chapter 3

The photochemistry of $[(\eta^6\text{-benzene})_2Cr]^+$

Chapter 4

The photochemistry of $[(\eta^6$-*cis and trans*-1,2-diphenylethene$)(Cr(CO)_3)_2]$

Abstract

Recent research has shown ring-slip processes to be important in the photochemistry of organometallic complexes of the type (η^6-arene)$M(CO)_3$, (M = Cr, Mo, or W). Previously CO-loss was thought to be the dominant photoprocess. This thesis attempts to investigate alternative photoprocesses to CO-loss showing a direct link between the ground state electronic configurations of these systems and their photochemistry.

Chapter 1 provides a general introduction to the history of organometallic chemistry. A brief description of bonding in the complexes of interest is given along with descriptions of any techniques either employed in the research or of significance to the literature survey. The bulk of this chapter deals with a literature survey of the theoretical descriptions of the electronic structure of (η^6-arene)$M(CO)_3$ (M = Cr, Mo, or W) and [(η^6-arene)$_2$M] (M = Cr) complexes.

Chapter 2 begins with a review of the photochemistry of (η^6-arene)$M(CO)_3$ complexes (M = Cr, Mo, or W). The quantum yield for photoinduced CO-loss in (η^6-mesitylene)$Mo(CO)_3$ was measured at a variety of wavelengths and found to increase with decreasing wavelengths of irradiation. The variations in the electronic transitions for (η^6-mesitylene)$M(CO)_3$, on changing the metal centre from Cr, Mo, and W were investigated using a peak fit programme. An emission spectrum of (η^6-mesitylene)$W(CO)_3$ at 77 K is presented. This further confirms the assignments derived from the UV/vis analysis. The photochemistry of (η^6-allylbenzene)$Cr(CO)_3$ was examined at low temperature by I.R. spectroscopy in an attempt to "trap" any ring-slip intermediate.

In chapter 3 studies into the photochemistry of [(η^6-arene)$_2$Cr]$^+$I$^-$ are detailed. Deligation of the arene rings resulted upon irradiation. Both steady state photolysis and laser flash photolysis was employed to detect and identify the intermediates of the photochemical reactions. Results suggest that the intermediates involved in aqueous solution differed from those in acetonitrile solutions.

The results of investigations into the photochemistry of the bimetallic complexes [(η^6-*cis* and *trans*-1,2-diphenylethene)($Cr(CO)_3)_2$] are presented in Chapter 4. These complexes contain low energy MLCT transitions. In the *cis* complex

low energy irradiation resulted in *cis* to *trans* isomerization while higher energy irradiation resulted in CO-loss. The molecular structural details of [(η^6-*trans*-1,2-diphenylethene)($Cr(CO)_3)_2$] are also included.

Finally experimental details on the syntheses and techniques used during the research are given.

CHAPTER 1

Introduction

1.1 A Brief History of Organometallic Chemistry

The earliest organometallic compound was synthesised and characterised by Zeise in 1827[1] which has a formulation $K[PtCl_3(C_2H_4)]$ and is known as Zeise's salt. The report was viewed with some scepticism initially. In 1918 the first π-arene complexes of chromium(1) were synthesised by Hein. In fact these were the first π-arene complexes of any transition metal. Cotton[2] said of these complexes "The reactions and properties of these complexes seem at face value, so completely unorthodox, and the isolation of the compounds so tedious that there has been scepticism, covert and overt, as to the validity of Hein's claims." It was only in the 1950's with the development of physical methods of structural determination such as infrared, NMR, and single crystal X-ray diffraction that the correct structures of Zeise's and Hein's products together with complexes such as ferrocene[3,4] were elucidated. The elucidation of such structures lead to the synthesis of a plethora of organometallic compounds.

The growth of organometallic chemistry in the middle of this century can also be linked to the emergence of the polymer industry in the 40's and 50's. Metal based catalysts provided efficient methods for the production of monomers. A catalyst acts by producing an alternative low energy pathway, which speeds up the reaction without losing it's chemical identity. The use of heterogeneous catalysts in industrial processes is more dominant than that of homogeneous catalysts. The Ziegler-Natta catalyst ($TiCl_3$), employed in the production of polyethylene from alkenes, is an example of a heterogeneous catalyst of immense significance. More recently the use of homogeneous catalysts in some processes has become almost exclusive.[5] Homogeneous catalysis in solution has advantages in that high activities are possible, the selectivity can be "fine-tuned" by altering electronic and steric factors through ligand substitution, and the reaction mechanisms can be studied by spectroscopic methods. A number of important homogeneous catalysts are in use in industrial processes. Of particular importance are $RhH(CO)(PPh)_3$ which catalyses the hydroformylation of alkenes and $[PdCl_3]^{2-}$ which catalyses the synthesis of acetaldehyde from ethylene(Wacker process).

1.2 Applications of Organometallic Photochemistry

While most catalytic processes are thermally based, photoinduced reactions of functionalised monomers and polymers have increasing commercial applications. Examples include UV curing of coatings and in production of photoimaging of semiconducting chips. If the functionalised monomers are photoinert then a photoinitiator is required; irradiation of this can yield highly reactive intermediates which can interact with the starting materials to yield the desired product. Typically organic compounds which generated radicals upon irradiation are used. However transition metal complexes are now being viewed as useful photoinitiators. For example the thermally stable flourinated titanocene derivatives undergo efficient radical production when irradiated at wavelengths of the argon ion laser. Further examples include cobalt(III)ammine complexes which photochemically liberate multi-equivalents of Lewis base,[6] a chromium(III) complex that photoreleases an initiator for the anionic polymerisation of an acrylate monomer [7] and a series of iron(II)-sandwich compounds that photodecompose to cationic Lewis acids.[8] Also photoinduced deligation of both arene rings in $[(\eta^6\text{-toluene})_2Cr]^+$ generates cationic Lewis acids which exhibit possibilities for initiating cross-linking of epoxides.[9]

Schützenberger initiated research into metal carbonyl compounds as early as 1868. By the 1920s metal carbonyl chemistry and catalytic reactions of carbonyl compounds began to assume importance. Metal carbonyls are particularly suited to act as homogeneous catalysts. The efficient production of a vacant site in the metal is of utmost importance and $Cr(CO)_6$ has a quantum yield of 0.67 for the photochemical expulsion of a CO ligand,[10] resulting in a co-ordinately unsaturated species with the required vacant site for co-ordination. This can be employed in catalysis of the hydrogenation of 1,3 dienes providing good yields and selectivity.[11] It was also found that the $Cr(CO)_6$-catalysed water-gas shift reaction was accelerated by UV irradiation.[12]

1.3 Bonding in Organometallic Compounds

An organometallic compound can be defined as an organic compound that contains at least one direct metal-carbon bond. In this study the metals are group 6 transition metals and bonding involves the partially filled metal d-orbitals. In order to bond with the metal an unsaturated organic molecule must possess vacant orbitals of suitable symmetry to interact with the filled d-orbitals of the metal.

1.31 Carbon monoxide as a ligand

Carbon monoxide is an unsaturated ligand by virtue of its multiple bond. Metal carbonyl species are amongst the most intensively investigated of the organometallic compounds. Figure 1.1 depicts the interaction between the CO molecule and the metal for bond formation. Carbon monoxide possesses a filled σ-orbital and two filled π-orbitals localised mainly between the carbon and the oxygen. Directed away from the molecule are two lone pairs, one on oxygen and one on carbon. Carbon is less electronegative than the oxygen, so the spacial arrangement of the lone pair is greater on the carbon. Donation of this lone pair to the partially filled d-orbital of the metal forms a σ-bond of the donor-acceptor type. The CO also has two unoccupied π-antibonding orbitals which are of the correct symmetry to accept electron density from the occupied metal d-orbitals forming a π-bond. So the metal-carbonyl bond represents a synergic interaction where the CO σ-donation is supplemented by a back donation from the metal to the π^* orbitals of the CO.

The σ-bond is the main contributor to the bond energy, however the π-bond does have important consequences; the electron density at the metal is decreased stabilising metals in low oxidation states and strengthening the metal-CO bond. As the CO has accepted electrons into its anti-bonding orbitals the bond order in the CO molecule decreases and so the bond strength decreases. This is reflected in a shift of the carbonyl absorption frequency in the infrared spectrum to lower frequency on complexation; free CO exhibits a $\nu_{co} = 2149 cm^{-1}$, while $Cr(CO)_6$ has a $\nu_{co} = \sim 1985\ cm^{-1}$.

The number of carbonyls that are complexed by the metal is dictated by the 18 electron rule. The metal must achieve an effective atomic number of the next noble gas.

For example chromium being a d^6 metal has 6 valence electrons, so to fulfil the 18 electron rule it must complex 6 CO molecules, resulting in $Cr(CO)_6$. Photoinduced loss of a CO ligand results in a highly reactive $16e^-$ intermediate.

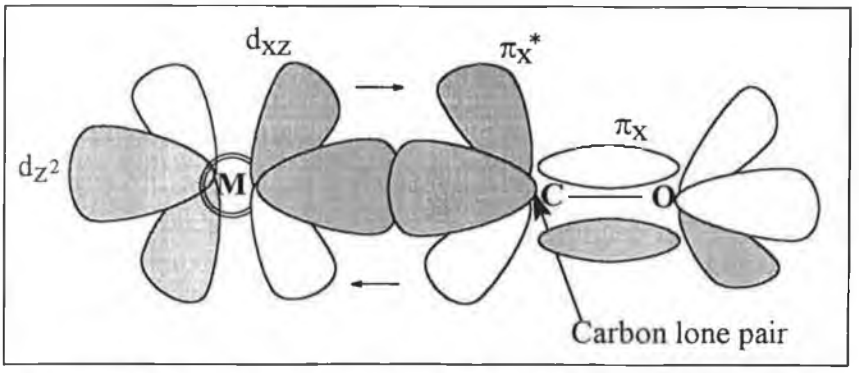

Figure 1.1 Bonding interactions of CO with transition metals

1.32 Arenes as ligands

Arene ligands are important in organometallic chemistry. The planar ligand lies perpendicular to the metal arene centroid vector. Figure 1.2 depicts the π-molecular orbitals of benzene. If the z-axis is taken as the direction from the metal to the arene centre then filled the a_{2u} orbital of the arene has the correct symmetry to interact with the d_z^2 orbital of the metal. However, these orbitals are not aligned to give large overlap, the d_z^2 being directed at the hole in the centre of the a_{2u} orbital. The degenerate e_{1ga} and e_{1gb} orbitals can donate an electron via π interaction with the d_{xz} and d_{yz} orbitals giving large overlap, this forms the principle metal arene bond. The unoccupied e_{2u} is only capable by symmetry of very weak interaction with the metal d_{xy} and $d_{x^2-y^2}$, so benzene is a good electron donor but a poor electron acceptor. The electron accepting ability of arenes can be altered by varying the nature of the arene substituents. Again the 18 electron rule must be satisfied so commonly known metal arene complexes include (η^6- arene)$Cr(CO)_3$ and (η^6-arene)$_2$Cr.

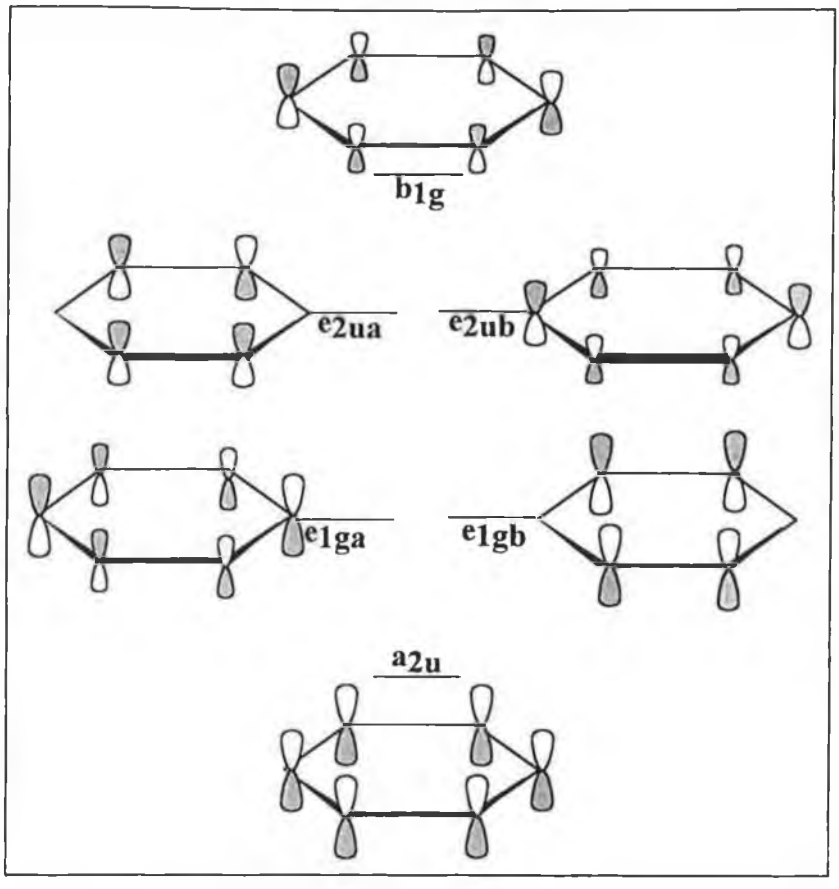

Figure 1.2 Benzene π-molecular orbitals

1.4 Excited States in Organometallic Complexes

Organometallic compounds possess a variety of low-lying excited states which are readily populated by irradiation in the near-Infrared, visible, or ultra-violet region of the spectrum, i.e. 200nm -1100nm. A number of these are encountered and discussed in this study.

1.41 Ligand field excited states

Ligand field (LF) transitions involve electron transitions between the d-orbitals of the metal and are thus also referred to as d-d transitions. This would imply that such a transition would have little consequence for the binding of the ligand to the metal-ligand bond. The metal d-orbitals are not totally metal in character however, as they are involved in the metal to ligand bonding. This ligand character of the orbitals allows a relaxation of the selection rules so that the absorptivities of the LF transitions in organometallic complexes far exceed those of metals ions. Consequently LF transition

states have been identified as the photoactive states in many substitution reactions. For the d^6 low-spin complexes such as $M(CO)_6$ (M = Cr, Mo, or W) LF transitions involve an electron transition from filled t_{2g} orbitals, which are π-bonding with respect to the metal-CO interaction to unoccupied e_g orbitals, which are σ-antibonding with respect to the metal-CO linkage. This transition labilises the metal-CO bond due both to the population of the σ-antibonding orbital and depopulation of the π-bonding orbital.

1.42 Metal to ligand charge transfer excited states

Metal to Ligand Charge Transfer(MLCT) transitions as their title implies originate in a metal centred orbital and terminate in a ligand localised orbital. In its crudest form it may be viewed as an oxidation of the metal and reduction of the ligand. For such a transition to occur the complex must possess low-lying ligand acceptor orbitals and an easily oxidised metal centre. The depopulation of the metal d-orbital and the population of the ligand localised π-orbital is thought to have little influence on the metal ligand bond explaining why dissociative photochemistry does not result following MLCT transitions. Furthermore the ligand becomes anionic and the metal cationic in nature which generates an electrostatic attraction. This inertness to ligand lability can be exploited as they allow other photochemical processes to be investigated. MLCT absorption bands can generally be identified by their solvent sensitivity as solvent molecules can readily interact with the π-orbitals of complexed ligands and affect the stability of polarised excited states.

1.43 Ligand to metal charge transfer excited states

For a complex to exhibit ligand to metal charge transfer (LMCT) transitions it must possess low-lying unoccupied metal acceptor orbitals and an easily oxidised ligand. This is a rare scenario as unfilled metal orbitals are generally at high energy due to the high ligand field strengths associated with organometallic complexes. One example is the sandwich complex $[(\eta^6\text{-benzene})_2Cr]^+$ which has a LMCT transition in the UV/vis region of the spectrum. There are few claims that the LMCT state is photoreactive and they are generally associated with homolytic cleavage of metal and ligand bond.

1.5 Techniques Employed to Study Transient Species

The intermediates formed in photoinduced reactions are an important piece in the jigsaw of the reaction mechanism, and need to be accurately identified. Today there are various methods available to detect and aid in identifying these transient species.

1.51 UV/visible monitored laser flash photolysis

This technique was developed by Norrish and Porter [13] in the 1950's, for which they later won the Nobel prize. It allows the initiation and monitoring of primary photochemical processes. The photoprocess is initiated by a high intensity light striking the sample. Absorption of this light results in the generation of a high concentration of excited molecules or photoproducts. These can be monitored by changes in the original UV/vis spectrum of the sample. Changes in the complete absorption spectrum can be studied, or, as was employed in this study a single wavelength can be monitored and the kinetics studied. Nasielki *et al.*[14] pioneered the use of UV/vis monitored laser flash photolysis for the study of $Cr(CO)_6$ intermediates. Metal carbonyl intermediates are easily detected because of their high quantum yields and the striking differences in their absorption characteristics compared to the parent species. The technique is also applicable to metal sandwich systems as is outlined in Chapter 3 of this thesis. This is a highly sensitive technique allowing the study of low concentrations of reactive intermediates. Investigations can be carried out on very rapid reaction systems; i.e. in the femtosecond time domain. However the technique does have a number of disadvantages; for example, an intermediate with low extinction coefficients may not be detected, or very complex spectra may be obtained if the absorption bands overlap. Also it is not possible to obtain any structural information from this technique. This technique does however effectively establish a broad outline of the photochemistry of particular systems, and used in conjunction with other characterisation methods provide fundamental data on the photophysical and photochemical processes involved.

1.52 Low temperature techniques

Low temperature techniques allow structural determination of intermediates that would not be observed at room temperature. The parent species is trapped in a matrix and irradiated. Any unstable intermediates generated are trapped in the matrix and can be studied at leisure. Matrices are generally solid inert gases or frozen hydrocarbons, held at temperatures between 10 and 30 K. An alternative matrix is cast polymers into which the parent species is incorporated. This technique allows even greater temperature ranges to be employed.

The trapped intermediate can be investigated using most commonly IR or UV/vis spectroscopy. IR detection is well suited to the study of metal crabonyl fragments due to their characteristic carbonyl stretches in the IR region of the spectrum. As the intermediates are studied in a low temperature rigid environment, there are limitations to this technique; little kenetic data can be obtained from this technique and the observations cannot be translated directly to behaviour in solution. They are however invaluable in assisting in interpretation of results obtained in solution.

1.6 Techniques to Determine Electronic Structures

This literature survey will focus on the investigations to determine the electronic structures of (η^6-arene)M(CO)$_3$ (M = Cr, Mo, or W) and (η^6-arene)$_2$Cr. Methods employed included experimental techniques such as photoelectron spectroscopy and various theoretical methods.

1.61 Photoelectron Spectroscopy

Photoelectron spectroscopy provides a very direct experimental probe for the electronic structure of organometallic compounds. The basis for the experiment is ejection of an electron from an electronic bound state using incident photons of known energy ($h\nu$). The kinetic energy, $E_k(e^-)$, of the ejected electron is measured and the ionisation energy or binding energy, E_I, can be calculated;

$$\mathbf{E_I = h\nu - E_k(e^-)}$$

For low energy photons (hν less than ~50ev) electrons are ejected from the valence shell, and the technique is Ultraviolet Photoelectron Spectroscopy (UPS). For higher energy photons (hν greater than ~1000ev), the electrons ejected are from the atomic core and the technique is known as X-ray Photoelectron Spectroscopy (XPS). The PES studies discussed in this survey probe the valence orbitals of the molecules and so UPS was employed.

The source of energy for ejecting valence electrons is provided by a helium discharge lamp. Low pressure helium gas is excited by an electric discharge. Radiation arises when the excited atoms return to their ground state. This results in a stream of photons each of energy hν = 21.2 eV, from a He(I) source. Discharges in helium can also generate a series of resonance lines from ionised He, He(II), resulting in a stream of photons each of energy hν = 40.8 eV.

The first UPS studies of organometallic complexes were reported in 1969 for a series of manganese pentacarbonyl complexes.[15] The valence spectra reflect the electronic configuration in metal d-orbitals. The ionisation band characteristics which provide information on the electronic structure are its energy, width, shape, resolved fine structures, and relative intensity. The metal based d ionisation's generally occur at the lowest energy in the photoelectron spectrum and are separated from the mainly ligand based ionisation's. The t_{2g} metal orbital ionisation's in $M(CO)_6$ (M = W, Mo, or Cr) are observed in the region of 8.5 eV. The ionisation band intensities vary depending on whether the excitation source is He(I) or He(II). Main group(C, N, O, P, and S) s and p orbitals generally show relatively high He(I) intensities and relatively low He(II) intensities in comparison to those of the transition metal d-orbitals.[16,17] This is an invaluable method for the deduction of the metal or ligand character of the orbital involved in the ionisation.

1.62 Theoretical electronic structure calculations

A number of molecular orbital calculations of varying degrees of difficulty exist. The more difficult the calculations the less applicable they are to complex molecules. Four types of molecular orbital calculations are listed below in order of decreasing difficulty:

(a) Hartree-Fock (HF) and *ab initio* self consistent field(SCF) calculations;

(b) Xα calculations;

(c) Semiempirical calculations;

(d) Empirical calculations;

(a) These methods calculate the orbital energies using Koopmans' approximation; Koopmans theorem defines molecular orbital energies as the difference in energy between an electron at an infinite distance from the molecular ion and the same electron in the molecule. This theorem essentially equates ionisation energy with orbital energy, and requires a molecular orbital model based on one-electron orbitals. Such a model is the SCF model.[18] In transition metal complexes electron repulsion must be fully allowed for and this is achieved in the SCF model. Each electron is taken singly and treated as moving in a repulsion field generated by the other included electrons. The repulsive field is averaged and taken as that experienced by the selected electron, which will modify its orbital accordingly. The selected electron is then placed in this modified orbital. This procedure is repeated for all of the electrons until the input and output arrangements are essentially the same.

These one-electron orbitals are solutions of a Schrödinger equation and the HF and *ab initio* calculations attempt to obtain very close approximations to an exact solution of the Schrödinger equation. In the HF method no terms are excluded and no further improvement of the total energy can be obtained by expanding the basis set; the set of orbitals, atomic or otherwise, out of which the molecular orbitals are built. In the *ab initio* calculations the basis set is contracted, this simplifies the mathematics and allows calculations on larger molecules. However, as the molecules become larger the

ionisation energies predicted by Koopmans' theorem become less accurate. Both these methods require a considerable computational investment.

(b) The Xα method makes less computer demands. The molecule is divided up into its' individual atoms with a spherical shell being placed around each atom. Pictorially the shell is referred to as a 'muffin tin'.[19] Each sphere is treated individually and as in the previous methods an electron is selected, however the calculations are now on isolated atoms rather than an atom incorporated into a large molecular structure. This simplifies calculations considerably.

(c) Semiempirical methods involve further simplifications to the HF calculations. Computer time is decreased by replacing certain integrals in the calculations with parameters determined by experimental methods. These methods are generally used to interpret photoelectron spectra, calculations determining the character of the molecular orbitals. There are a number of methods used in conjunction with PES results; CNDO, INDO, and MINDO (NDO = neglect of differential overlap, C = complete, I = intermediate, M = modified) and a method due to Fenske and Hall.[20]

(d) The extended Hückel method is the main empirical method. Originally the Hückel calculations were used to elucidate delocalised π molecular orbitals. This original model was extended for calculations involving more complex inorganic molecules. The Hückel method assumes that only interactions between directly bonded atoms are significant. Basically the method involves assigning an energy obtained from spectral data to each orbital to be included. The interaction energy between two orbitals is then calculated by multiplying the overlap integral by the average of the energy of the interacting orbitals. Due to its relative simplicity it is a widely used method.

1.7 Literature Survey of the Electronic Structure of Sandwich and Half Sandwich Compounds

In order to explain the photochemistry of organometallic complexes a detailed knowledge of the electronic structure is necessary. The molecular orbitals of [(η^6-benzene)$_2$Cr] (DBC) and its cation DBC^+ and of (η^6- arene)$M(CO)_3$ (M = W, Mo, or Cr) have been elucidated by a combination of experimental methods such as UV/vis spectroscopy, electron resonance spectroscopy (ESR), and in particular photoelectron spectroscopy (PES) and a number of theoretical molecular orbital calculations.

1.71 Ground state electronic structure of $(C_6H_6)_2Cr$ and $[(C_6H_6)_2Cr]^+$

The D_{6h} symmetry of DBC with eclipsed rings has been firmly established by low-temperature crystal data,[21] electron diffraction measurements,[22] and vapour phase infrared studies.[23] The first report of the UV/vis spectrum of DBC and its cation was by Feltham.[24] For the neutral species and the cation the weak low energy absorption (at 650 and 1160 nm respectively) were tentatively assigned to a LF transition. The intense bands at 308nm for DBC and at 334nm and 272 nm for DBC^+ were assigned to CT transitions due to their intensity, though their types were not specified.[25,26] In an attempt to elucidate the electronic structure a number of photoelectron[17, 27,28 29] and electron resonance[30] experiments were carried out on the sandwich complexes. On the basis of He(1) PES Green *et al.*[27] proposed the molecular orbital structure presented in Figure 1.3.

Figure 1.3 describes the bonding in DBC within a delocalised MO framework. The a_{1g}, a_{2u}, and e_{1u} benzene π-orbitals are stabilised by the chromium s and p orbitals The benzene e_{1g} orbital is stabilised by metal dxz and dyz orbitals. This results in six strong bonding interactions between the benzene rings and the chromium. The metal dx^2-y^2 and dxy orbitals form a weak π-antibonding interaction with the empty benzene e_{2g} orbital resulting in slightly stabilised $1e_{2g}$ MO. The HOMO is of a_{1g} symmetry, which results from the interaction of the benzene a_{1g} π set with the metal d_z^2 orbital albeit with poor overlap. Thus the $2a_{1g}$ MO is essentially metal in character and nonbonding.

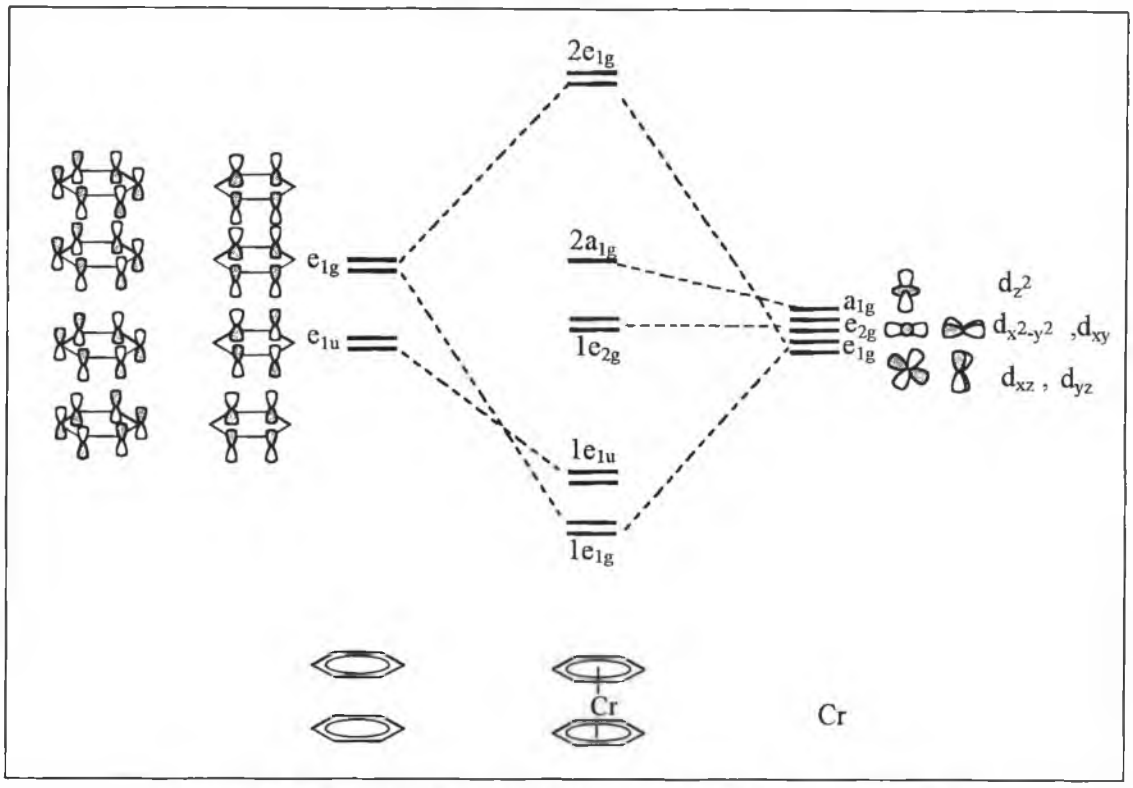

Figure 1.3 Molecular orbital diagram for [(η^6-benzene)$_2$Cr]

This interpretation of experimental results needed to be confirmed by theoretical methods. Guest *et al.*[17] presented a detailed study of the electronic structure of DBC employing PES and *ab initio* SCF MO calculations. As concluded by Evans and co-workers from analysis of He(1) spectra,[27] the lowest energy bands are assigned to ionisation from mainly metal a_{1g} and e_{2g} molecular orbitals respectively with a separation of 1.0 eV. This is substantiated by an increase in intensity of these bands on changing from a He(I) to a He(II) ionisation source. This increase is in fact due to a decrease in the intensity of the benzene ionisation intensities on changing from He1 to He2.[17] The bands beyond 8 eV were assigned to ligand based ionisations as they correlated well with the photoelectron spectrum of free benzene.

Previous semiempirical calculations[31,27] also assigned the metal based a_{1g} type orbital as the HOMO, however there were discrepancies in the energy separation between the a_{1g} and e_{2g} molecular orbitals. Guest *et al.*[17] employed *ab initio* self consistent field molecular orbital calculations to describe the ground state electronic

structure of DBC. These predicted an inversion of the highest filled molecular orbitals as compared with the ordering interpreted from the PES results, an e_{2g} type orbital being the HOMO. The difference in energy between the e_{2g} and the a_{1g} type orbitals was calculated as 0.2 eV. Koopmans' theorem (which does not allow for orbital relaxation upon ionisation) was also employed to predict the orbital energies. The energies predicted were higher than those calculated by other methods. A comparison of the theoretical and the experimental methods is given in Table 1.1.

Orbital	**Experimental I.P.**	**Koopmans I.P.**	**ΔSCF I.P.**
a_{1g}	5.5	11.3	5.1
e_{2g}	6.5	7.5	4.9

Table 1.1 Calculated and experimental ionisation potentials(I.P.) (eV) of DBC.

The charge distribution was calculated using the Koopmans ionisation potentials. From these results presented in Table 1.2 it is clear that the e_{2g} orbital having 43% ligand π character provides the largest contribution to the metal arene bond. The a_{1g} type is confirmed as being almost totally metal d in character. The rest of the predicted molecular orbitals correlated with those of the free ligand. From orbital and overlap populations the chromium configuration was predicted as $3d^{3.34}$, (i.e., a positive charge of 2.66 on the Cr atom).

		Charge Distribution (%)				
		Chromium			Carbon	
Symmetry	**Energy (eV)**	3d	4s	4p	$2p_\sigma$	$2p_\pi$
e_{2g}	-7.5	53	-	-	04	43
a_{1g}	-11.3	92	2	-	03	01

Table 1.2 Valence Molecular Orbitals of DBC using Koopmans' I.P.s.[17]

The lack of correlation between the experimental and the theoretical results lead Weber *et al.*[19] to carry out further theoretical studies on DBC and also on the cation DBC^+. Using the Xα molecular orbital method the a_{1g} type orbital was predicted as the HOMO, while the e_{2g} type orbital was predicted as the second HOMO. This agreed with previous interpretations of photelectron spectra.[17,27]. These calculations also confirmed an e_{2g} to be the LUMO (see Figure 1.3) which previous extended Hückel calculations failed to do.[28,30] The percentage charge distribution for the LUMO and two HOMOs is presented in Table 1.3. These results indicate that the SHOMO (e_{2g} type orbital) is the largest contributor to the metal arene bond.

		Charge Distribution(%)				
		Chromium			Carbon	
Symmetry	**Energy(eV)**	3d	4s	4p	$2p_\sigma$	$2p_\pi$
e_{1g}	-	75	-	-	02	10
a_{1g}	6.6	77	-	-	01	-
e_{2g}	7.33	43	-	-	01	22

Table 1.3 Valence Molecular Orbitals calculated using the Xα method [19]

Weber *et al.*[19] also applied these calculations to elucidating the ground state electronic structure for DBC^+. Figure 1.4 depicts a comparison of the ground-state valance energy levels for $Cr(C_6H_6)_2$ and $[Cr(C_6H_6)_2]^+$. While the ordering of the energy levels is unchanged on ionisation, the orbital levels of the cation are found at significantly lower energies than those of the neutral compound. The stabilisation was calculated to be of the order of 5-6 eV for each level. The ordering of the predominantly 3d metal orbitals is again $e_{2g} < a_{1g} < e_{1g}$, where the e_{2g} is fully occupied, the a_{1g} contains the unpaired electron, and e_{1g} is unoccupied. The a_{1g} orbital was predicted to be 79% metal character with no ligand π character, while the e_{2g} orbital was 56% metal character and 15% ligand π character. So again the e_{2g} MO is the main contributor to the metal arene bond. The calculated electronic configuration of the chromium in the cation was higher than that for the neutral compound, $3d^{4.96}$ compared with $3d^{5.14}$. The increase in positive charge on the chromium to +1.04 was interpreted as a charge transfer relaxation toward the d shell of the chromium.

Weber also used the calculated $X\alpha$ ionisation values for both the neutral and the cation species to elucidate their electronic excitation energies. This allowed detailed assignment of the absorption bands in the optical and UV absorption spectrum of compounds.

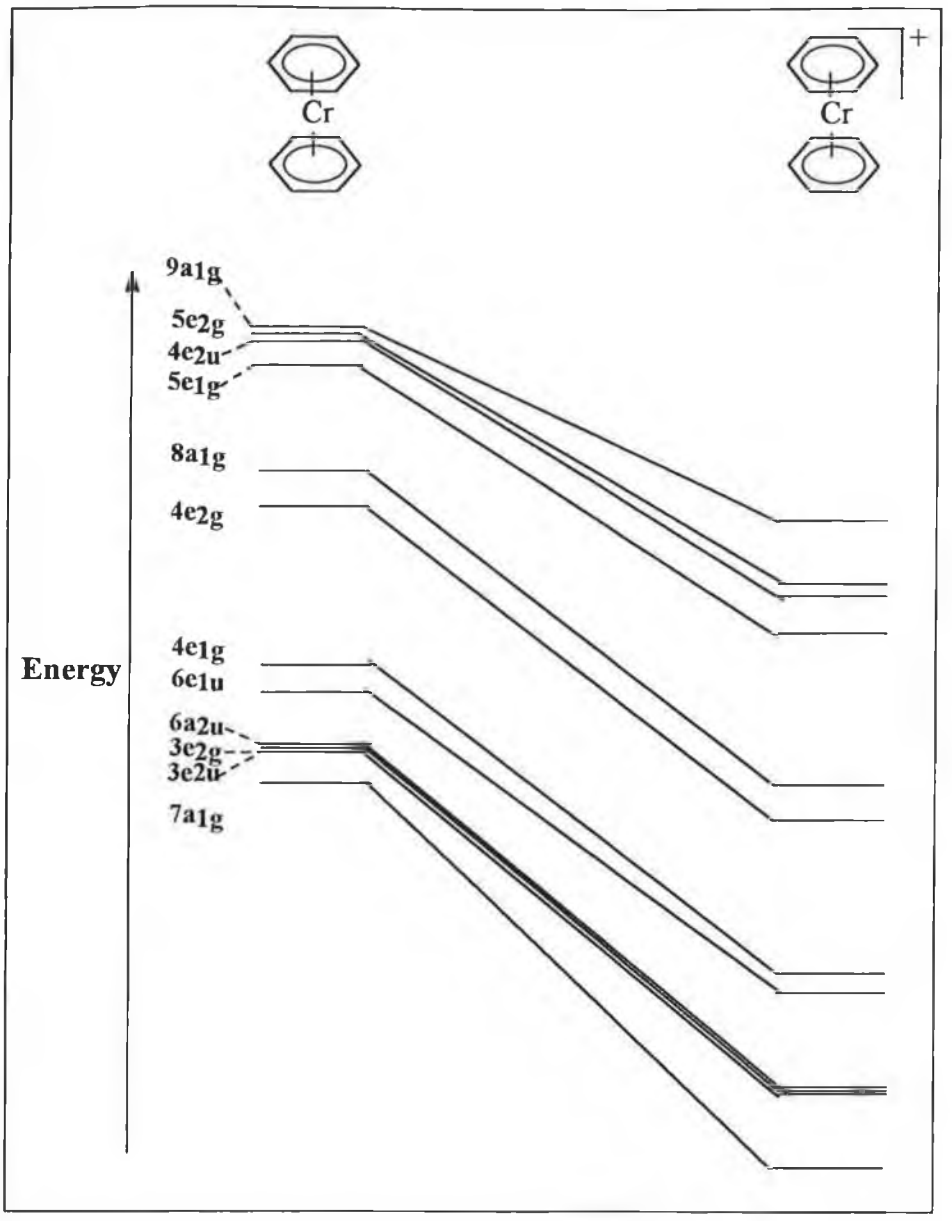

Figure 1.4 Ground-state valence energy levels for DBC and DBC^+. The HOMO is $8a_{1g}$ with 2 electrons in DBC and 1 electron in DBC^+.

1.72 Electronic excitation energies of $Cr(C_6H_6)_2$

A comparison of the experimental and calculated electronic excitation energies are presented in Table 1.4. The calculated electron transitions correlate well with those found experimentally.[24] Due to the mixing of the MO character some of the transitions cannot be unambiguously assigned as solely LF or CT(ie. the $8a_{1g} \rightarrow 5e_{2g}$ transition). The low intensity of the band at 641nm correlates well with its assignment as a d-d transition.

Transition	Assignment	Calculated(nm)	Experiment(nm)
$8a_{1g} \rightarrow 5e_{1g}$	LF	623	641
$8a_{1g} \rightarrow 5e_{2g}$	LF/ MLCT	500	417
$8a_{1g} \rightarrow 4e_{2u}$	MLCT	459	
$4e_{2g} \rightarrow 5e_{1g}$	LF	398	
$4e_{2g} \rightarrow 5e_{2g}$	LF/MLCT	365	
$4e_{2g} \rightarrow 4e_{2u}$	MLCT	359	320
$4e_{1g} \rightarrow 4e_{2u}$	IL	209	
$4e_{1g} \rightarrow 5e_{1g}$	LMCT	207	
$4e_{1g} \rightarrow 5e_{2g}$	IL/LMCT	203	
$6e_{1u} \rightarrow 4e_{2u}$	IL	194	200
$6e_{1u} \rightarrow 5e_{1g}$	MLCT	190	
$6e_{1u} \rightarrow 5e_{2g}$	IL/MLCT	188	

Table 1.4 Comparison of calculated and experimental electronic transitions of DBC. [19] (See Figure 1.5 for assignments)

1.73 Electronic excitation energies of $[Cr(C_6H_6)_2]^+$

As would be expected the absorption energies of the cation are of lower energy than those of the neutral species. Thus the lowest energy absorption band is in the near-infrared region of the spectrum. Feltham [24] assigned this low intensity band to a symmetry forbidden transition from a d-orbital to ligand π orbital. However the assignment of Scott *et al.* [32] is supported by the calculated transition assignment; a LF transition due to excitation of the electron from the filled $4e_{2g}$ orbital to the half-filled $8a_{1g}$ orbital. Further LF transitions observed experimentally[33] have been assigned to absorption bands in the visible region of the spectrum. Those centred at 395nm appear as a shoulder of moderate intensity on the first intense UV absorption peak. The UV part of the spectrum shows well defined and intense bands. These are all orbitally and

Laporte-allowed transitions of a CT nature. Table 1.5 gives a comparison of the experimental and the calculated results. As for the neutral species all the transitions cannot be unambiguously assigned as solely LF or CT due to the mixing of the orbital character.

Transition	Assignment	Calculated(nm)	Experiment(nm)
$4e_{2g} \rightarrow 8a_{1g}$	LF	1724	1176
$8a_{1g} \rightarrow 5e_{1g}$	LF	608	578
$4e_{2g} \rightarrow 5e_{1g}$	LF	455	
$8a_{1g} \rightarrow 5e_{2g}$	LF/MLCT	404	395
$4e_{1g} \rightarrow 8a_{1g}$	MLCT	385	
$6e_{1u} \rightarrow 8a_{1g}$	MLCT	341	340
$4e_{2g} \rightarrow 4e_{2u}$	MLCT	306	270
$6a_{2u} \rightarrow 8a_{1g}$	MLCT	249	238
$6e_{1u} \rightarrow 5e_{1g}$	MLCT	220	
$4e_{1g} \rightarrow 4e_{2u}$	LL	206	
$6e_{1u} \rightarrow 5e_{2g}$	LL/LMCT	202	200
$4e_{2g} \rightarrow 3b_{1u}$	MLCT	194	

Table 1.5 Comparison of Experimental and Calculated Electronic Transitions of DBC[19] (see Figure 1.5 for assignments).

1.74 The electronic structure of (η^6-arene)$Cr(CO)_3$

The Molecular structure of (η^6- benzene)$Cr(CO)_3$ has been studied in the solid state using both X-ray crystallography and neutron diffraction.[34,35] This showed the three equivalent carbonyl groups to lie in a staggered configuration with respect to the carbons in the benzene ring. X-ray diffraction revealed the benzene ring to be distorted from the D_{6h} symmetry of the isolated ring to give an overall symmetry of C_{3v}.

In order to elucidate the ground state electronic structure of half sandwich compounds of C_{3v} symmetry various methods of calculation have been employed since the late 60's. Carroll and McGlynn[36] carried out semiempirical molecular orbital calculations on (η^6-benzene)$Cr(CO)_3$. Analysis of the charge distribution on the compound showed a net charge transfer from the arene to the metal; 0.261e. However the chromium was still positively charged, +0.566, due to the electron withdrawing nature of the carbonyls. Glynn *et al.* concluded that the back donation of electron density from the metal to the CO exceeded the σ donation of electrons from the CO to the metal. Calculations of the valence molecular orbitals predicted the HOMO to be an e-type orbital and the SHOMO to be the 2 almost degenerate a-type orbitals.

In the 70's detailed extended Hückel type calculations were carried out.[37,38,39] These reports examined the fragments of the compound, treating the $Cr(CO)_3$ and the ring separately and then combining the predicted molecular orbitals. Firstly considering the $Cr(CO)_3$ fragment, the C_{3v} arrangement is achieved by removing three facile CO ligands from a $Cr(CO)_6$ molecule which is of O_h symmetry. This results in a slight perturbation of the filled t_{2g} orbitals, stabilising them and splitting them into three low-lying orbitals, a_1+ e (Figure 1.5). The a_1 level is primarily metal $3d_z^2$ and lies at lower energy to the e set which is primarily $3d_x^2$- $_y^2$, $3d_{xy}$. The unfilled e_g orbitals of the O_h arrangement are destabilised in the C_{3v} symmetry and become a set of e-type orbital. These are mainly of xz and yz character, and are antibonding to the σ levels of the ligands. There is some character mixing in e sets, between the xy and the xz and between the x^2-y^2 and the yz[38,39]. At higher energy again is an sp hybrid orbital which is of e-type symmetry.

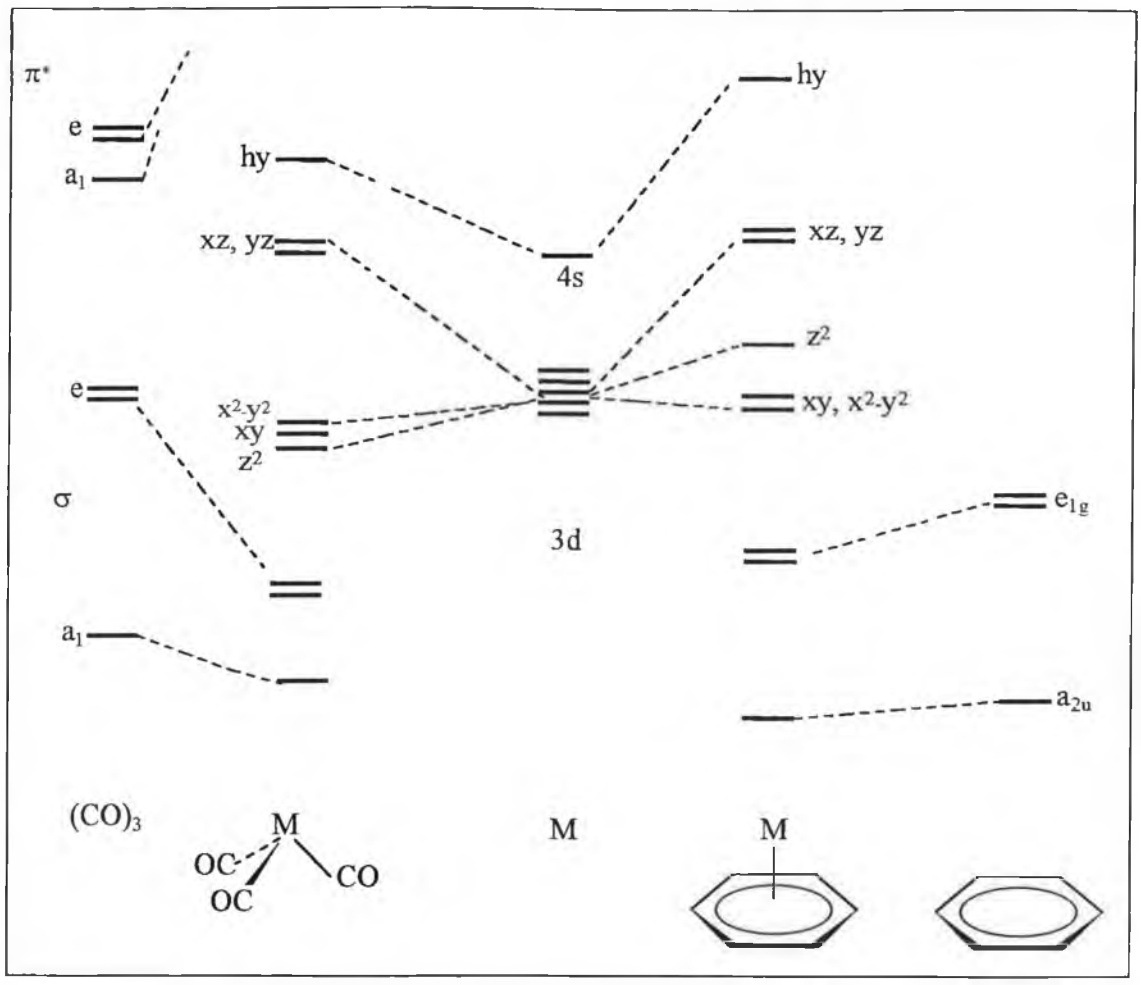

Figure 1.5 Interaction diagram for the formation of fragment molecular orbitals of $M(CO)_3$ and $M(C_6H_6)$ from the metal orbitals. Labelling of the molecular orbitals is according to their metal character.

In the case of the arene-metal fragment the metal d orbitals are again split into the a+e levels(Figure 1.5). The a_1 level which is primarily $3dz^2$ is destabilised because the a-type benzene orbital is filled. This means that in the benzene-metal molecular orbitals the a_1 level is the HOMO, this is in contrast to the $M(CO)_3$ fragment. The $e_2(xy,x^2- y^2)$ and the a_1 level are nonbonding. The e_1 set which is metal xz and yz is antibonding with respect to the benzene e_{1g} orbital.

Extended Hückel type calculations[39] elucidated the interaction for (η^6-benzene)$Cr(CO)_3$ as depicted in Figure 1.6. This shows the interaction between the

molecular orbitals of $M(CO)_3$ fragment and the benzene molecule. The HOMO is the a_1 orbital originating from the $3dz^2$ orbital. The principal interactions inferred from Figure are between the 1e, $_{e2u}$ and 2e, e_{1g} fragment orbitals. The a_1 orbital is essentially nonbonding with respect to the arene ring.

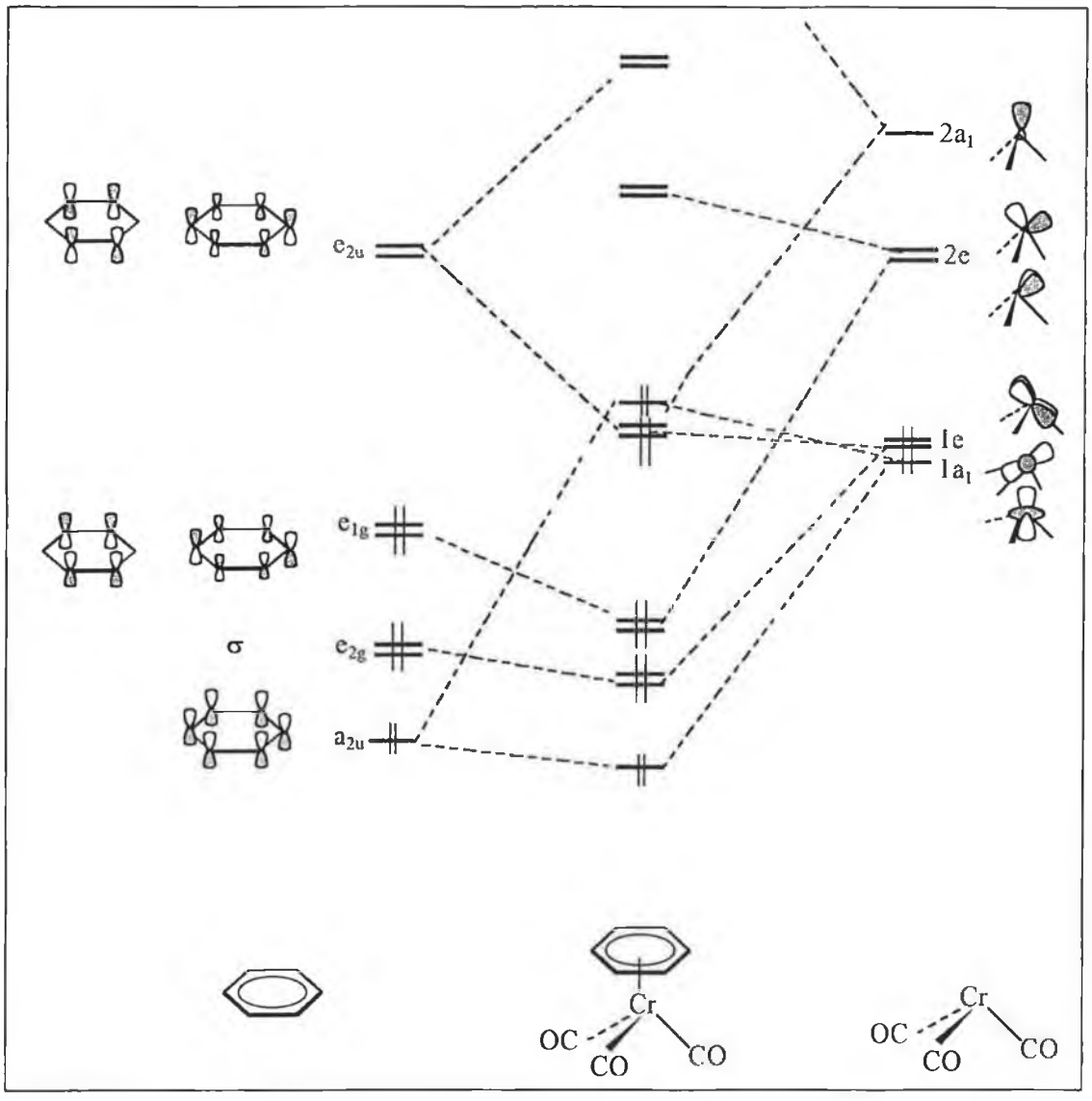

Figure 1.6 Interaction diagram for (η^6-benzene)$Cr(CO)_3$.

To further probe the electronic structure of (η^6-arene)$Cr(CO)_3$ Guest *et al.* [17]carried out the first PES studies on these complexes, these were combined with *ab initio* calculations. In the He(1) and He(2) photelectron spectra, there is only one ionisation band, ~7.4 eV, in the region where metal 3d ionisations are expected. This implies that the e_2 and the $2a_1$ are degenerate. While calculations employing Koopmans theorem predicted the HOMO to be the e_2 orbital, calculations allowing for orbital relaxation upon ionisation(SCF method) predicted the levels to be degenerate. This is consistent with the single band in the PES(see Table 1.6).

Orbital	**Experimental I.P.**	**Koopmans I.P.**	**ΔSCF I.P.**
e_2	7.5	8.4	6.1
$2a_1$	7.5	11.1	6.1

Table1.6 Calculated and Experimental I.P.(eV) of (η^6-benzene)$Cr(CO)_3$.[19]

Again, as was the case for the DBC complex, there is a change in intensity on changing from a He1 to He2 ionisation source. As the first ionisation band preserves its intensity this supports its assignment to ionisation from the valence metal orbital. The results of population analysis on the HOMOs of the molecule are given in Table 1.7. These results show the two HOMO to be predominantly metal 3d. The $2a_1$ orbital is nonbonding with respect to the arene, as was concluded from other theoretical studies, [38,40] while the e_2 orbital provides the largest contribution to the metal 3d carbonyl π and the metal 3d benzene π interactions.

		Population Analysis(%)		
Symmetry	Energy(eV)	Cr(3d)	CO(2p)	$C_6H_6(2p_\pi)$
e_2	-8.4	51	31	13
$2a_1$	-11.1	79	19	0

Table 1.7 Population analysis of (η^6-benzene)$Cr(CO)_3$

Byers and Hall [40] carried out PES studies on the (η^6-arene)$Cr(CO)_3$ complexes using Fenske-Hall calculations to assign the bands of the spectra. Their calculations predicted the a_1 orbital as the HOMO and the 2e orbital as the SHOMO. This agreed with the extended Hückel type calculations but is an inversion of the *ab initio* results. The energy difference between the two levels is only 0.27eV. The character of the valence orbitals reflects that determined by Hillier *et al*; the a_1 orbital having 99.58% metal carbonyl character and the 2e orbital having 86.16% metal carbonyl character with 9.19% arene character. Byers and Hall also included the tungsten and molybdenum in their calculations and their PES studies. The calculations showed that Figure 1.6 is a representative MO for the three metal complexes.

The photoelectron spectra of (η^6-arene)$M(CO)_3$ (M = Cr, Mo, or W) were obtained. The first ionisation band (ie. a_1+2e ionisations) is split in the tungsten complex. This has been attributed to spin-orbital coupling.[41] From calculations the first band in the split peak was assigned to the a_1 orbital and the second to the 2e orbital. A recent publication continues the variation in the ordering of the two HOMOs. [42] It is proposed that although calculations predict the a_1 to be slightly lower in energy than the 2e orbital the a_1 would experience greater relaxation on ionisation. This will result in a decrease in its ionisation energy.

1.75 Electronic excitation energies in (η^6- arene)$M(CO)_3$ (M = Cr, Mo, or W)

The absorption spectra of these complexes are dominated by MLCT absorptions Carroll and McGlynn[36] reported a comparison between experimental transitions and calculated transitions in the UV/vis spectrum of (η^6-benzene)$Cr(CO)_3$. The prominent spectral feature is a sharp, intense band at ~ 320 nm. This was assigned to a Cr $\rightarrow$ benzene CT transition with some Cr $\rightarrow$ π*CO CT character. A shoulder at ~ 220 nm is assigned to a Cr $\rightarrow$ π*CO CT. The lower energy region of the spectrum has not been studied in detail. The tungsten and the molybdenum complexes exhibit weak low energy features which have been attributed to low energy d-d transitions.[24] Beech and Gray assigned the low energy component in the spectra of W / Mo $(CO)_6$ as a spin forbidden $^1A_{1g} \rightarrow {}^1T_{1g}$ (d-d) transition. This transition is not seen in the Cr complex and is more intense in the W than the Mo complex. This enhanced intensity with increasing atomic weight of the metal centre is attributed to greater spin-orbit coupling in the heavier metals.

REFERENCES

[1] Zeise, W. C.; *Progg. Ann.* **9**, 632, 1827.

[2] Cotton, A. F.; *Chem. Rev.* **55**, 551, 1955.

[3] Kealy, T. J.; Pauson, P. L.; *Nature* **168**, 1039, 1951.

[4] Wilkinson, G.; Rosenblum, M.; Whiting M. C.; *J. Amer. Chem. Soc.*; **74**, 2125, 1952.

[5] Masters, C.; *Homogeneous transition-metal Catalysis*, Chapman and Hall, London, 1981.

[6] Kutal, C.; Weit, S.K.; MacDonald, S.A.; Willson, C.G.; *J. Coatings Tecnol.* **62**, 63, 1990.

[7] Kutal, C.; Grutsch, P.A.; Yang,, D.B.; Macromolecules, **24**, 6872,1994.

[8] Meier, K.; Zweifel, H.; *J. Imaging Sci.* **30**, 174,1986.

[9] Gamble, g.; Kutal, C.; *Polymers for Advanced Technolgies* **5**, 63, 1994.

[10] Nasielski, J.; Colas, A.; *J. Organomet. Chem.* **101**, 215, 1975.

[11] Wrighton, M.; Schroeder, M. A.; *J. Amer. Chem. Soc.* **95**, 5764, 1973.

[12] Nigorski H.; Mirbach, M. J.; Mirbach, M. F.; *J. Organomet. Chem.* **297**, 171, 1985.

[13] Norrish, R.G.; Porter, G.; *Nature* **164**, 683, 1950.

[14] Nasielski, J.; Kirsch, P.; Wilputte-Steiner, L.; *J.Organomet. Chem.* **29**, 269, 1971.

[15] Evans, S.; Green, J. C.; Orchard M. L. H; Turner, D.W.; *Discuss. Faraday Soc.* **47**, 112, 1969.

[16] Green, J. C.; *Struct. Bonding (Berlin)* **43**, 37, 1981.

[17] Guest, J. C.; Hillier, I. H.; Higginson, B. R.; Lloyd, B. R.; *Mol. Phys.* **29**, 113, 1975.

[18] Slater, J. C.; *Quantum Theory Of Molecules and Solids* , Mcgraw-Hill, New York, N.Y., 1974.

[19] Weber, J. G.; Goursot, A.; Penigault, E.; *J. Amer. Chem. Soc.* **100**, 3995, 1978.

[20] Hall, M. B.; Fenske, R. F.; *Inorg. Chem.* **11**, 768, 1972.

[21] Keulen, E.; Jellinek, F.; *J. Organomet. Chem.* **5**, 490, 1966.

[22] Haaland, A.; *Acta Chem. Scand.* **19**, 41, 1965.

[23] Ngai, L. H.; Stafford, F. E.; Schäfer, L.; *J. Amer. Chem. Soc.* **91**, 48, 1969.

[24] Feltham, R. D.; J. *Inorg. Nucl. Chem.* **16,** 197, 1961.

[25] Traverso, O.; Scandola, F.; Balzani, V.; *Mol. photochem.* **1**, 289, 1969.

[26] Geoffroy, G. L.; Wrighton, M. S.; *Organometallic Photochemistry*, Academic Press, New York, 1979.

[27] Evans, S.; Green, J. C.; Jackson, S. C.; *J. Chem. Soc. Farady Trans.* **2**, 249, 1972.

[28] Pignataro, S.; Foffani, A.; Distefano, G.; *Chem. Phys. Lett.* **20**, 350, 1973.

[29] Evans, S.; Green, J. C.; Jackson, S. E.; *J. Chem. Soc. Dalton Trans.* 304, 1974.

[30] Anderson, S.E.; Drago, R. S.; *Inorg. Chem.* **11**, 1564, 1972.

[31] Hillier, I. H.; Canadine, R. M.; *Discuss. Faraday Soc.* **47**, 27, 1969.

[32] Scott, D. R.; Becker, R. S.; *J. Phys. Chem.* **69**, 3207, 1969.

[33] Yamada, S.; Yamazaki, H.; Nishikawa, H.; Tsuchida, R.; *Bull. Chem. Soc. Jpn.* **33**, 481, 1960.

[34] Rees, B.; Coppens, P.; *J. Organomet. Chem.* **42**, c102, 1972.

[35] Rees, B.; Coppens, P.; *Acta Crystallogr.* **16**,188, 1973.

[36] Carroll, D. G.; McGlynn, S. P.; *Inorg. Chem.* 7, 1285, 1968.

[37] Elian, M.; Hoffman, R.; *Inorg. Chem.* **14**, 1058, 1975.

[38] Albright , T. A.; Hoffman, P.; Hoffman, R.; J. *Amer. Chem. Soc.* **99**, 7546, 1977.

[39] Elian, M.; Chen, M. M. L.; Mingos, M. P.; Hoffman,R.; *Inorg. Chem.* **15,** 1149, 1976.

[40] Byers, B. P.; Hall, M. P.; *Organometallics,* **6**, 2319, 1986.

[41] Lichtenberger, D. L.; Kellogg, G. E.; *Acc. Chem. Res.* **20**, 379, 1987.

[42] Field C. N.; Green, J. C.; Moody, A. G. J.; Siggel, M. R. F.; *Chem. Phys.* **206**, 211, 1996.

CHAPTER 2

Electronic Structure and the Photochemistry of (η^6-Arene)M(CO)$_3$ complexes M = (Cr, Mo, or W)

2.1 Introduction

2.11 The photochemistry of (η^6-arene)M(CO)$_3$ complexes, M = (Cr, Mo, or W)

Earliest reports on the photochemistry of (η^6-arene)M(CO)$_3$ proposed that both arene (reaction 2.1) and CO (reaction 2.2) exchange were photoinduced reactions.[1]

Reaction 1.1

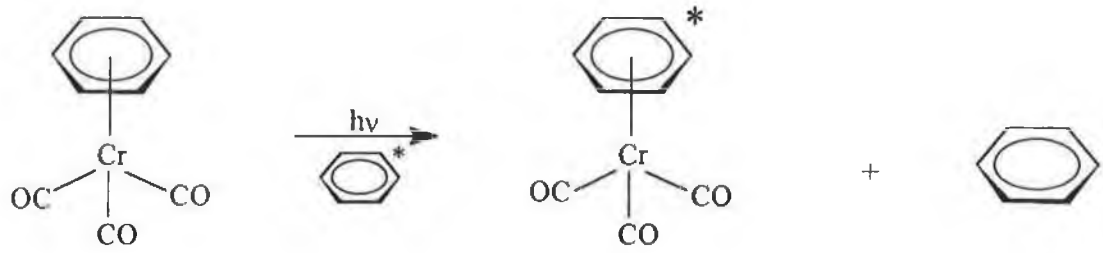

Reaction 2.2

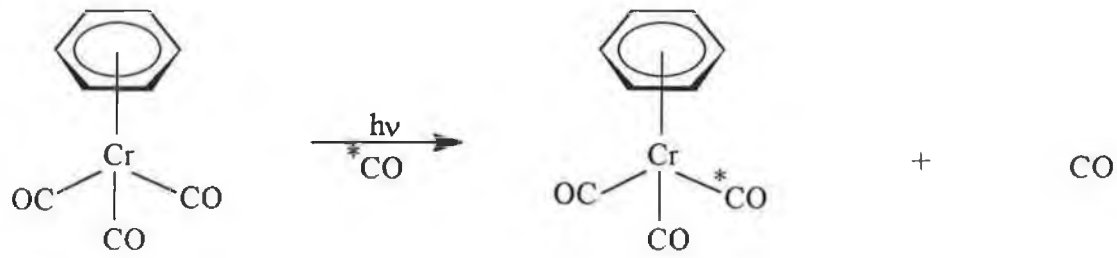

The exchange was determined by irradiating the complexes in the presence of either ^{14}CO or ^{14}C-labelled arene. Both reaction 2.1 and 2.2 were found to occur where M = Cr or Mo, however the W complexes were found to be photochemically inert. Arene exchange where M = Mo was reported to be nearly twice that of the M = Cr complexes (Table 2.1).

Complex	Exchanging Arene	% Exchange (t = 3hrs)
$(CH_3C_6H_5)Mo(CO)_3$	$CH_3{}^*C_6H_5$	28.2
$(CH_3C_6H_5)Cr(CO)_3$	$CH_3{}^*C_6H_5$	17.4

Table 2.1 Photoinduced arene exchange of *arene in (η^6-arene)$M(CO)_3$, (M = Mo or Cr) $\lambda_{irrad.}$ = 366 nm [1(a)]

When M = Cr, CO exchange was found to be very efficient. Wrighton and Haverty[2] reported a quantum yield (Φ) of 0.72 for the photochemical replacement of CO with pyridine (arene = benzene or mesitylene). No arene exchange was reported and no chemical change was observed upon irradiation in a constant stream of CO. A higher Φ of 0.9 was reported for the displacement of CO from (η^6-mesitylene)$Cr(CO)_3$ by n-dodecylmaleimide in benzene, $\lambda_{irrad.}$ = 313 nm.[3] No exchange of the benzene and mesitylene was observed. Gilbert *et al.*[4] confirmed CO displacement to be the dominant photoprocess. The extent of arene exchange was approximated as one sixth that of CO exchange. CO was found to suppress arene exchange and this lead to the conclusion that CO expulsion was important in the mechanism of arene exchange. The dicarbonyl intermediate was proposed to be involved in arene exchange. CO exchange was not affected by the presence of excess arene.

Trembovler and co-workers[5] reported on the UV/vis monitored photolysis of (η^6-arene)$Cr(CO)_3$. Continuous photolysis with visible irradiation produced both the uncomplexed arene and $Cr(CO)_6$. The substituents on the benzene ring were found to have no major effect on the rate of the decomposition. The photodecay process was deemed to be dependent on light intensity. Similar photoproducts were also reported by Bramford *et al.* Addition of CCl_4 was found to increase the rate of arene generation, while in the absence of CCl_4, CO suppressed the production of free arene.[6]

Characterisation of the intermediates was initiated by Rest *et al.*[7] using frozen gas matrices at 12K. Photolysis of (η^6-benzene)$Cr(CO)_3$ in argon or methane matrices

resulted in formation of the sixteen electron dicarbonyl species. There were no observations to suggest formation of free arene or $Cr(CO)_3$. Bitterwolf *et al* reported similar results upon photolysis of Nujol mulls at 77K.[8] CO expulsion was also observed in the gas phase.[9] Upon excitation at 355 nm the dicarbonyl species was formed, while at 266 nm excitation the dicarbonyl and the monocarbonyl were formed in a 2:5 ratio.

Oxidative addition of trisubstituted silanes to (η^6-arene)$Cr(CO)_2$ was established to originate from the photochemical generation of the dicarbonyl species from the tricarbonyl,[10] highlighting the applications of photochemical CO expulsion. The efficient loss of CO was also exploited in the co-ordination of H_2 and N_2 to (η^6-arene)$Cr(CO)_2$/ Cr(CO).[11] The monocarbonyl and dicarbonyl were generated photochemically in the gas phase and the co-ordination was monitored by FTIR. There was little difference in the CO stretching bands between the N_2 complex and the H_2 complexes. These were considered to be nontypical bonds as a shift to higher wavenumber would be expected due to oxidation of the metal centre.

More recently ring-slip processes have been have been identified as significant in the photochemistry of (η^6-arene)$Cr(CO)_3$ complexes.[12] The photochemistry of (η^6-pyridine)$Cr(CO)_3$ and its 2,6-disubstituted derivatives were investigated by matrix isolation and TRIR. Photolysis of (η^6-pyridine)$Cr(CO)_3$ in the presence of CO resulted in the formation of (η^1-pyridine)$Cr(CO)_5$ and finally $Cr(CO)_6$. This demonstrated that CO expulsion was not the only photoprocess of the complex. The $\eta^6 \rightarrow \eta^1$ photoinduced haptotropic rearrangement was proposed to occur via a solvent assisted ring-slip process. The photochemistry was shown to be wavelength dependent, high energy irradiation resulted in CO expulsion while lower energy irradiation resulted in the ring slip-process.

2.12 The thermal chemistry of (η^6-arene)M(CO)$_3$ complexes, M = (Cr, Mo, or W)

Strohmeier carried out early investigations into the thermal chemistry of (η^6-arene)Cr(CO)$_3$.[13] Arene exchange was found to be the dominant thermal process. Experiments were carried out at 140°C in heptane or heptane/THF. Kinetic data lead to the proposal of two separate mechanisms being operative, with a simultaneous exchange of two complex molecules as depicted in Scheme 2.1. A major component of the mechanism was reported to involve second order kinetics, independent of arene concentration.

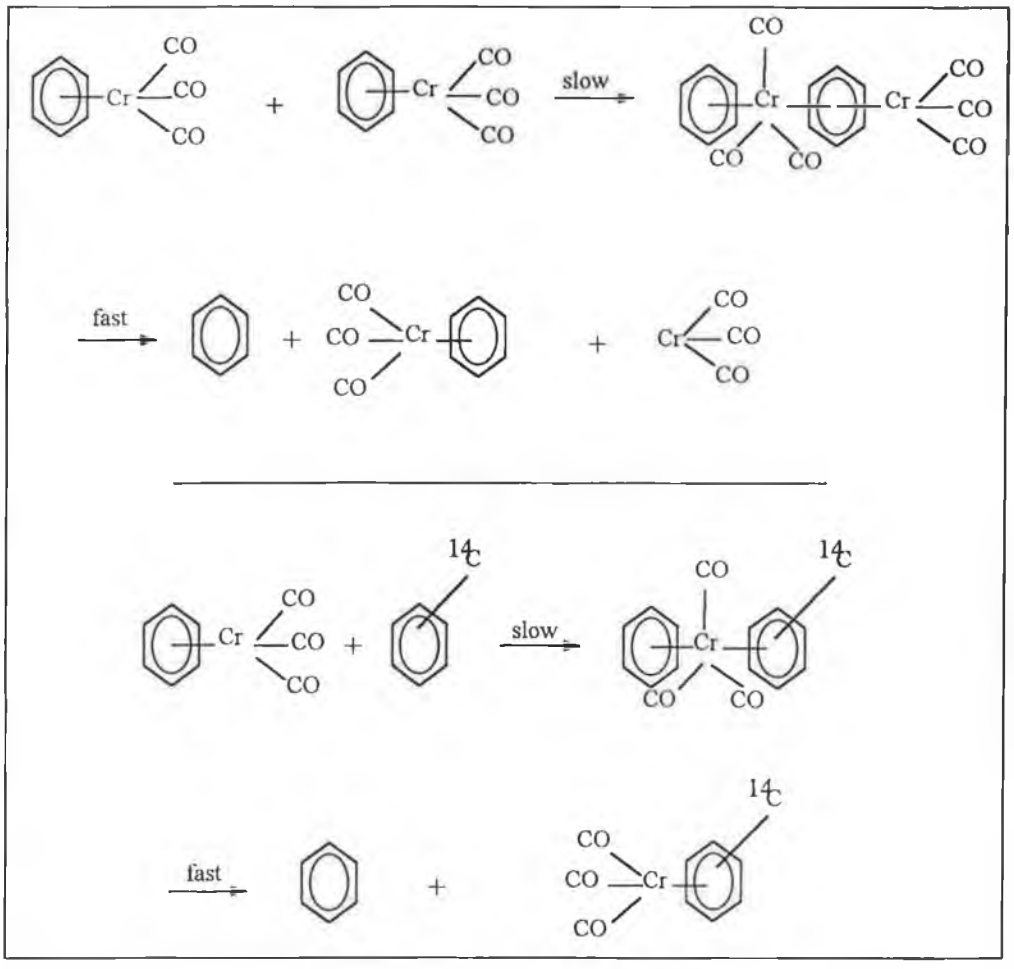

Scheme 2.1 Proposed mechanism for arene displacement.[13]

Strohmeier had not considered the participation of the donor solvent in the arene exchange mechanism.[13] Mahaffy and Pauson[14] realised the importance of donor solvents in the mechanism of arene exchange. The exchange was proposed to occur via a solvent displacement of the arene from $\eta^6 \rightarrow \eta^4$, and in the absence of a donor solvent a second

parent molecule would catalyse the reaction, by co-ordination through the oxygen of the CO molecule. Reaction 2.3 displays the mechanism for partial displacement.

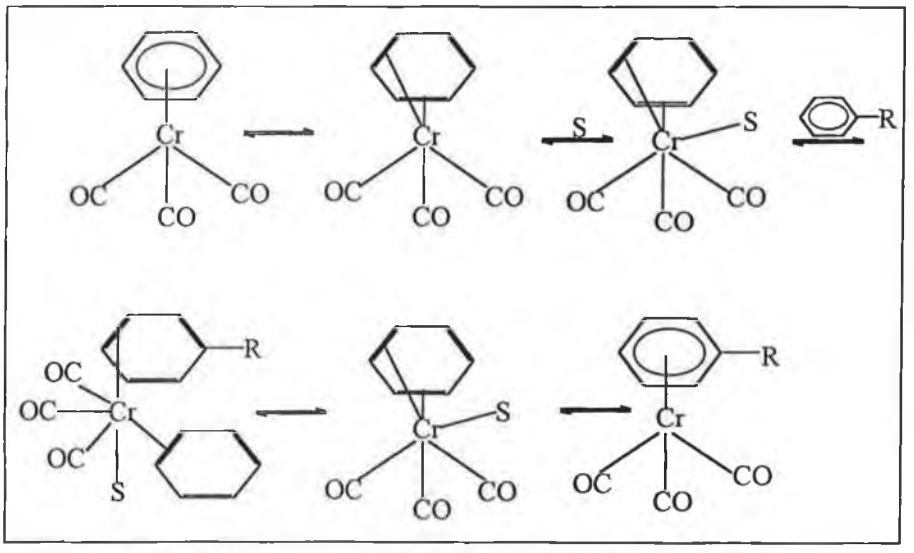

Reaction 2.3 Solvent initiated arene displacement.[14]

The possibility of a solvent stabilised $Cr(CO)_3$ moiety was also proposed.[15] Rates of exchange of arenes with hexamethylbenzene were determined in cyclohexane at temperatures in the range 80°-140°, the reaction was proposed to be first order in the complex and occur via a solvent stabilised $Cr(CO)_3$ intermediate. Traylor *et al.*[16] carried out extensive studies on the displacement of benzene or substituted benzene's from the arene metal carbonyl complexes. The observations suggested that the bound CO group acted as a nucleophilic catalyst in the arene exchange process.[16a,16b] Neighbouring group participation in the exchange was investigated by extending the π system of the arene complexes. This provided evidence for the proposed stepwise process in which the bonding in the displaced arene proceeds from $\eta^6 \rightarrow \eta^4 \rightarrow \eta^2$.

2.13 Haptotropic rearrangements in (η^6-arene)$Cr(CO)_3$

A haptotropic rearrangement refers to instances where the ML_n moiety changes its connectivity (hapto number) to a ligand with more than one co-ordinating site. The ligand is generally a polyene. Albright *et al.*[17] conducted extensive theoretical investigations into the migration of the ML_n unit from one ring to the other in a bicyclic polyene. In the (η^6-naphthalene)$Cr(CO)_3$ the least motion transit would require the $Cr(CO)_3$ fragment to transit the bisection of C_9 and C_{10} in the naphthalene, resulting in an η^2 geometry (Figure 2.1) Molecular orbital calculations showed that during the least motion transit the two dominant bonding interactions between the $Cr(CO)_3$ and the naphthalene (the two LUMO's of the $Cr(CO)_3$ and the two HOMO's of the naphthalene) are lost. A detailed investigation into the potential energy surface on shifting the Cr(CO)3 group from one ring to the other lead to the proposal that the rearrangement occurs along the pathway of lowest energy. This results in an intermediate which is essentially a 16 electron η^3- allyl-$Cr(CO)_3$ anion with a heptatrienyl cation fused to the allyl portion (Figure 2.2).

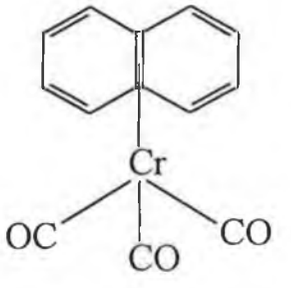

Figure 2.1 Least motion pathway for haptotropic rearrangement in (η^6-naphthalene) $Cr(CO)_3$

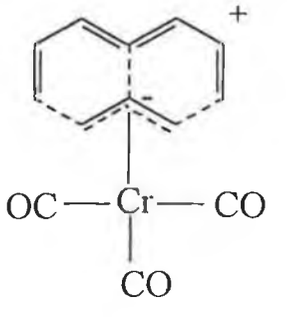

Figure 2.2 Least energy pathway for haptotropic rearrangement in (η^6-naphthalene) $Cr(CO)_3$.

Migration between non-adjacent rings has also been reported.[18] 9-Phenyl anthracene incorporates biphenyl and anthracene systems in one molecule. Heating to reflux of 9-phenylanthracene and $Cr(CO)_6$ in dioxan resulted in a $Cr(CO)_3$ moiety complexing the terminal anthracene ring. When this was allowed to stand in the dark over night the metal moiety was found to have migrated to the phenyl ring.

Kriss *et al.* [19] determined the haptotropic rearrangements in naphthalene chromium tricarbonyl systems experimentally. Dimethoxynaphthalene $Cr(CO)_3$ complexes were employed and one of the naphthalene rings was deuterium labelled. In benzene-d^6 solution migration of the $Cr(CO)_3$ moiety was observed. No significant arene exchange with the benzene-d^6 was observed.

Howell *et al.*[20] reported on kinetic studies of uncatalysed arene exchange of polyenes and heterocyclic substrates. This was an extension of Strohmeier's studies many years previously.[12(c)] Extended Hückel type calculations were employed to elucidate the dynamics of ring-slippage in $Cr(CO)_3$ complexes of benzene, naphthalene and pyrene. By creating a potential energy surface for the slippage of a MnCp group in benzene-MnCp (this is a good analogue to a (η^6-arene)$Cr(CO)_3$ system) it was calculated that an η^4 intermediate could not exist. An $\eta^6 \rightarrow \eta^2$ path was found to be the most favourable path for the (naphthalene)$Cr(CO)_3$ complex, while an $\eta^6 \rightarrow \eta^1$ path was the most energetically favoured path for the (η^6- pyrene)$Cr(CO)_3$ system. Both pathways were calculated to be comparable in energy to the (η^6-benzene)$Cr(CO)_3$.

2.2 Results and Discussion

2.21 Quantum yields for CO-loss from (η^6-mesitylene)$Mo(CO)_3$

While the photochemistry of (η^6-arene)$Cr(CO)_3$ has been extensively investigated, the photochemistry of analogous Mo systems have not been as extensively studied. As discussed in the introduction, the quantum efficiency for CO-loss ($\Phi_{CO\text{-}loss}$) in (η^6-arene)$Cr(CO)_3$ is high, 0.72[2], however no data exists for the analogous reaction in the Mo system. The changes in the UV/vis spectrum upon photolysis of (η^6-mesitylene) $Mo(CO)_3$ in cyclohexane with excess pyridine (pyr) are presented in Figure 2.3. The arrows indicate the depletion of the parent and the formation of (η^6-mesitylene)$Mo(CO)_2$(pyr). The quantum yields for CO-loss in (η^6-mesitylene)$Mo(CO)_3$ were measured for λ_{exc} = 266, 313, or 334 nm. The results are presented in Table 2.2.

$\lambda_{irrad.}$ (nm)	$\Phi_{CO\text{-}loss}$
266*	0.5887
313	0.1061
334	0.0409

Table 2.2 The quantum yields for CO displacement by pyridine in (η^6-mesitylene) $Mo(CO)_3$.* Z-cyclooctene was employed as the trapping ligand.

It is clear from these results that the quantum efficiency of CO loss in the molybdenum species is wavelength dependent. This is in contrast to its Cr analogue; Φ = 0.7 for excitation wavelengths between 436 and 313 nm[2,3] The absorption spectra of (η^6-arene)$M(CO)_3$ (M= W, Mo, or Cr) are dominated by MLCT transitions, however CO-loss is accepted to arise *via* a LF transition.[21] In the chromium system the LF state is populated either directly or *via* a radiationless decay from a higher energy MLCT state. The results obtained here indicate that this is not the case for the Mo system. Photoelectron spectra and *ab initio* studies carried out by Byers and Hall[22] found that the HOMO in the three metal complexes is similar in energy, however it is generally accepted that the 10Dq increases on going down the triad. It is then possible that the LF

excited state in the Mo system is shifted to higher energy. A lower energy MLCT excited state may then be populated, decreasing the efficiency of the LF state population and ultimately reducing $\Phi_{CO\text{-}loss}$ at long wavelength photolysis.

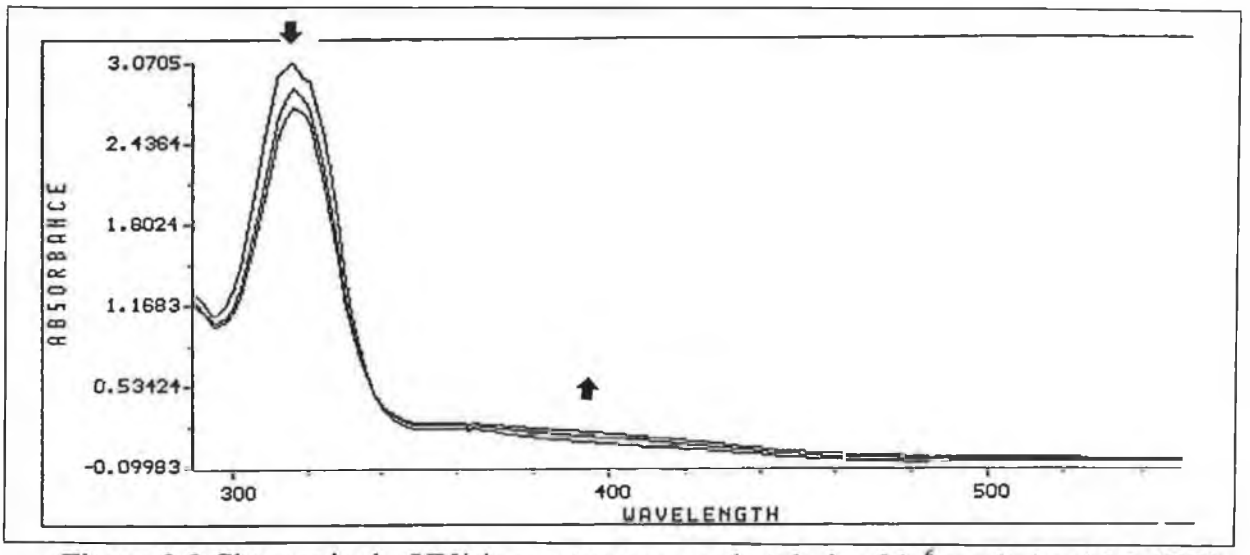

Figure 2.3 Changes in the UV/vis spectrum upon photolysis of (η^6-mesitylene) $Mo(CO)_3$ in cyclohexane with excess pyridine.

Figure 2.4 presents the UV/vis spectra of (η^6-mesitylene)$M(CO)_3$ (M= Cr, Mo, or W). The dominant spectral feature at ~320 nm has been assigned as a M → mesitylene CT with some M → π* CO CT character.[23] A pronounced band can be seen on the low energy side of the λ_{max} in the Mo and W complexes. This has previously been assigned to a LF spin forbidden singlet to triplet transition.[22] The enhanced intensity of this transition with increasing atomic weight of the central metal is typical of the larger spin orbit coupling in the heavier metal. In PES studies on (η^6-arene)$M(CO)_3$ (M= Cr, Mo, or W)[24] the spin orbital coupling in the W complex is evident, however it is not observed in the Mo complex. This discounts the assignment of the low energy feature in the UV/vis spectrum of the molybdenum complex to a transition directly populating the triplet state from the ground state. This band is tentatively assigned to a MLCT transition. The nature of the CT transition cannot be definitively assigned.

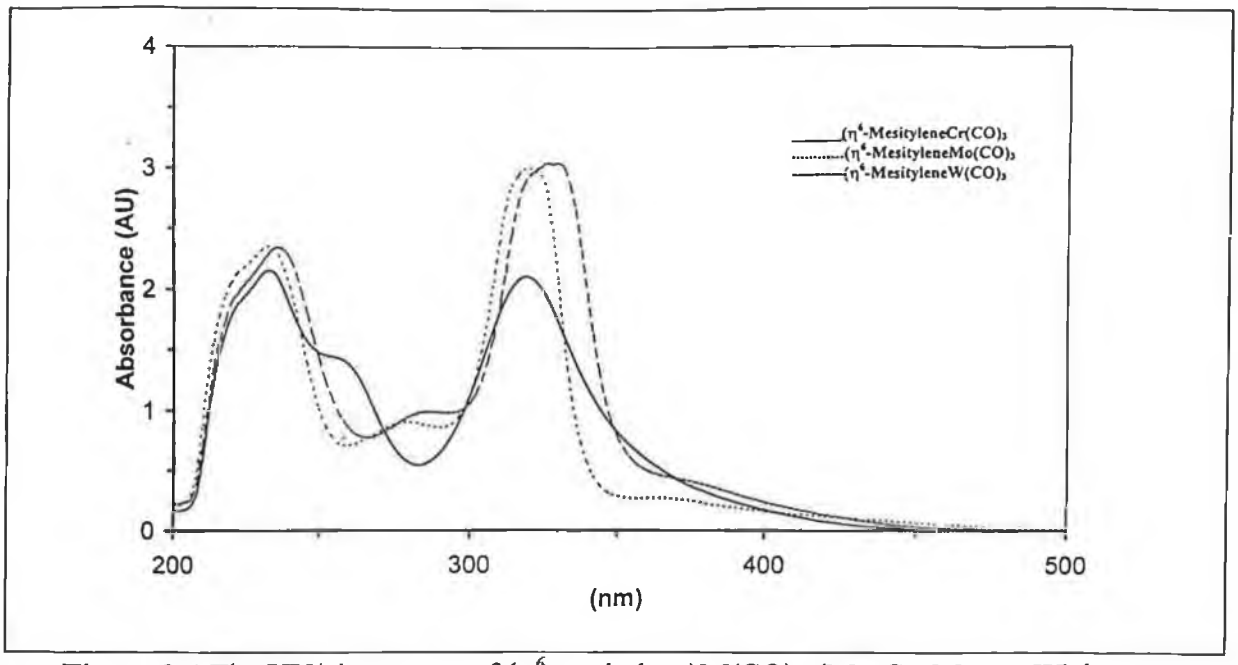

Figure 2.4 The UV/vis spectra of (η^6 mesitylene)$M(CO)_3$ (M= Cr, Mo, or W) in cyclohexane (1 x 10^{-4}M).

The UV/vis spectra of (η^6-mesitylene)$M(CO)_3$ (M = Cr or Mo) were analysed employing a PeakPick package (see experimental). This allows low intensity, overlapped peaks to be deconvoluted. The peak fit analysis for (η^6-mesitylene) $Cr(CO)_3$ in cyclohexane is presented in Figure 2.5. Deconvolution of the spectrum reveals 5 components in the UV/vis spectrum. The intensity of the two dominant absorption bands would suggest that they are CT in nature while the lowest energy transition is assigned to a LF transition. The assignments are given in Table 2.3

Wavenumber(cm^{-1})	Assignment
27935	LF
31238	M→π*CO CT
44717	M→areneπ* CT

Table 2.3 Proposed assignments for the electronic transition in (η^6-mesitylene)$Cr(CO)_3$

Investigations into the photochemistry of (η^6-arene)$Cr(CO)_3$ showed CO-loss to be independent of irradiation wavelength between 436 nm (22935 cm^{-1}) and 313nm (31948 cm^{-1}). This is consistent with population of the lowest energy excited state.

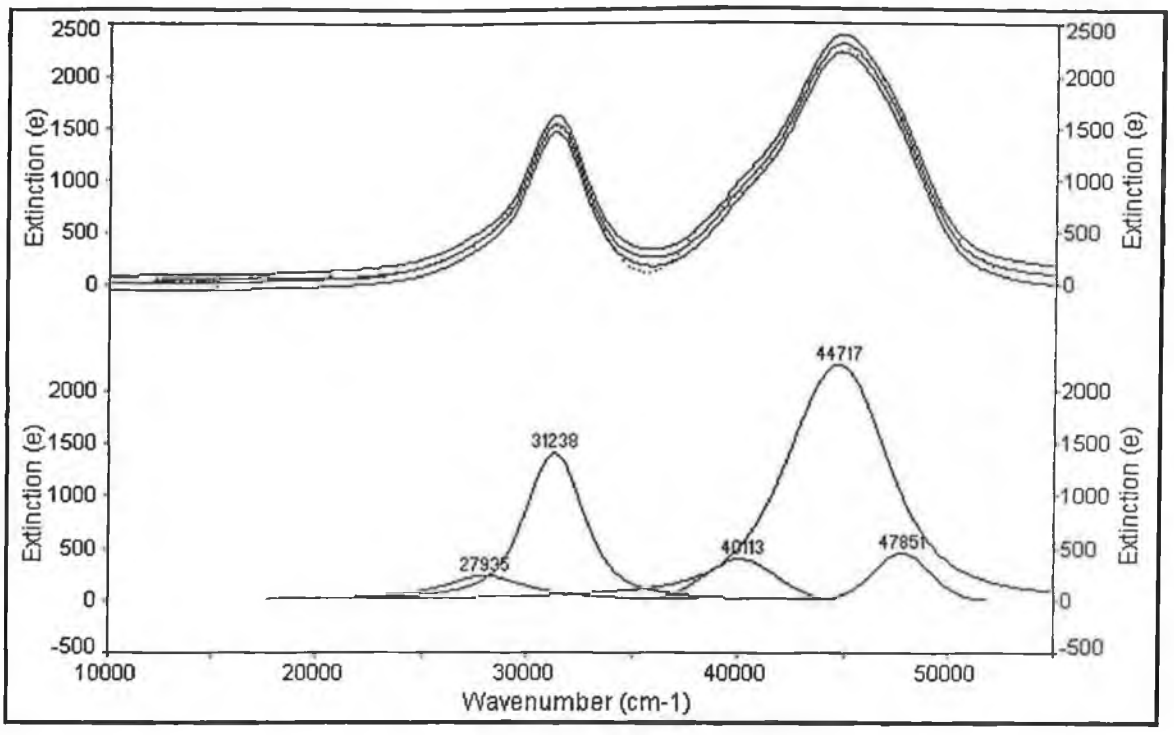

Figure 2.5 PeakPick analysis of the UV/vis spectrum of (η^6-mesitylene)$Cr(CO)_3$ in cyclohexane (1 x 10^{-4}M)

The PeakPick analysis of the analogous Mo system is presented in Figure 2.6. Deconvolution of the spectrum reveals 6 components in the UV/vis region of the spectrum. The proposed assignments for some of the transitions are presented in Table 2.4. The most striking feature in the deconvoluted spectrum is the absorbance band at 35412 nm (282 nm). This feature is absent in the spectrum of the Cr system. Both the shape and intensity of this band matches well with the lowest energy transition of the Cr system (Figure 2.4), and so is assigned to a LF transition. This assignment correlates well with the trend in the $\Phi_{CO\text{-}loss}$; efficient population of this LF state would be reduced by population of the intervening lower energy MLCT transitions. A proposed comparison of the variation in energy of the excited states in (η^6-arene)$Cr(CO)_3$ and (η^6-arene)$Mo(CO)_3$ is presented in Figure 2.7.

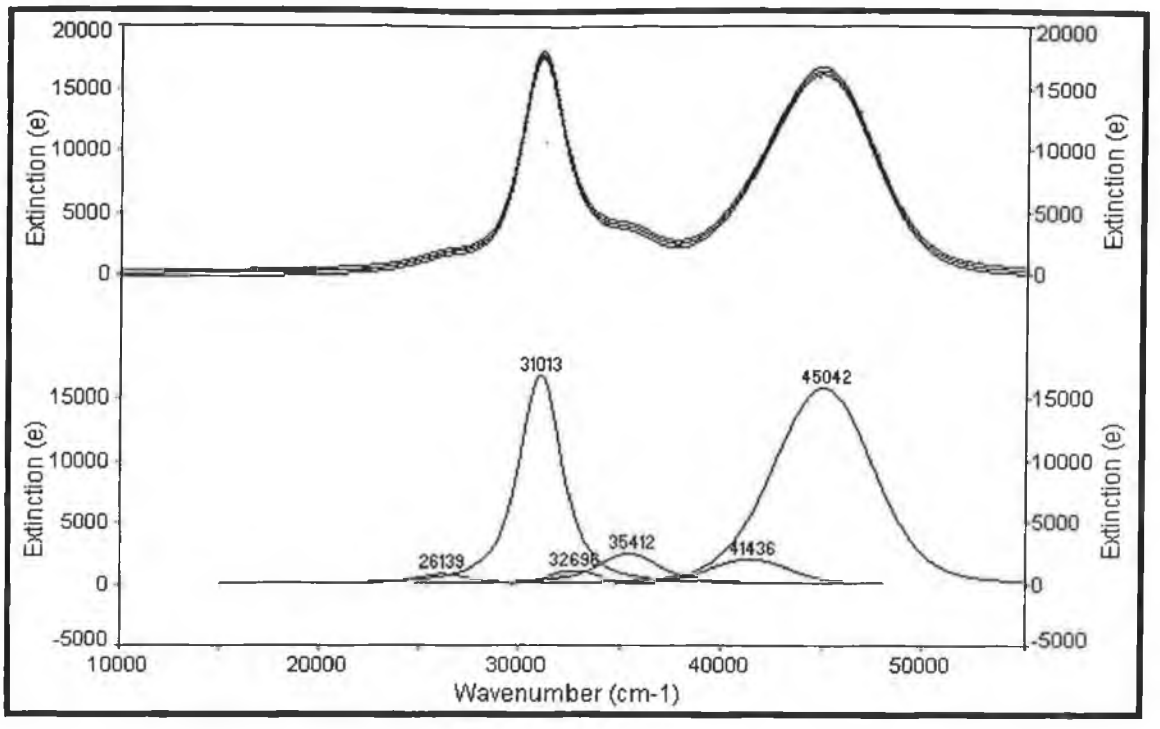

Figure 2.6 PeakPick analysis of the UV/vis spectrum of (η^6-mesitylene)$Mo(CO)_3$ in cyclohexane (1 x 10^{-4}M)

Wavenumber(cm^{-1})	Assignment
26139	MLCT?
31013	M→π*CO CT
35412	LF
45043	M→arene π* CT

Table 2.4 Proposed assignments for the electronic transition in (η^6-mesitylene) $Mo(CO)_3$

Strohmeier and co-workers[1(a)] studied the percentage photoinduced arene exchange in (η^6-toluene)$M(CO)_3$ (M = Cr or Mo). Upon photolysis at 366 nm arene exchange was twice as efficient in the Mo complex compared to the Cr complex. The results for CO-loss in the Mo system show that CO-loss at 366 nm is very inefficient. Together these results would suggest that upon irradiation into the low energy region of the molybdenum spectrum (proposed to be due to a MLCT transition), arene loss occurs possibly *via* a ring-slip intermediate. However it is possible that Strohmeier's observations were due to a thermal rather than a photochemical process.

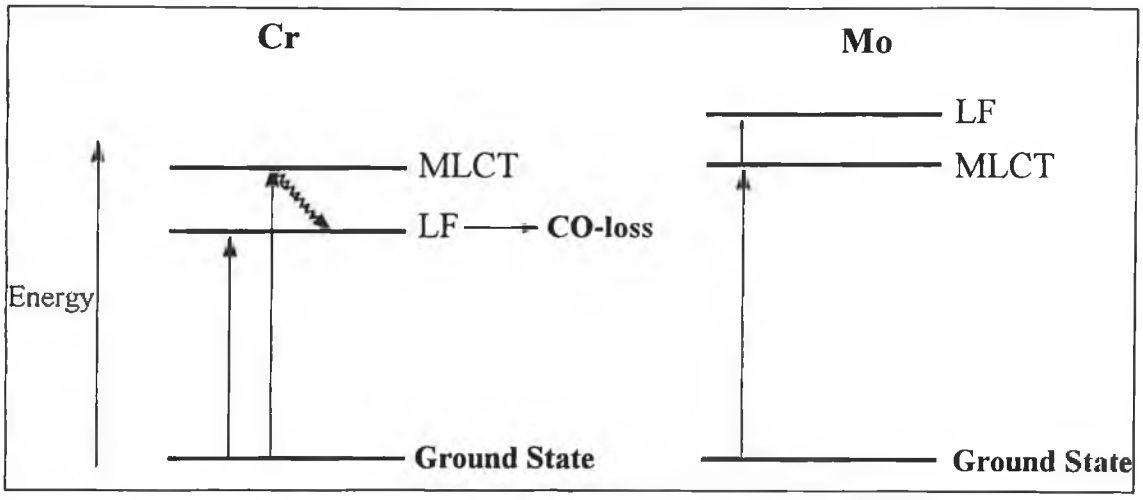

Figure 2.7 Representation of the variation in energy of the excited states in (η^6-arene) $Cr(CO)_3$ and (η^6-arene)$Mo(CO)_3$.

2.22 Electronic structure of (η^6-mesitylene)$W(CO)_3$

Figure 2.8 presents the peak analysis of the UV/vis spectrum of (η^6-mesitylene) $W(CO)_3$ in cyclohexane. As previously mentioned a low energy feature is particularly evident in the spectrum of the W complex; 27464 cm^{-1}. This has been assigned to a singlet to triplet spin-forbidden transition.[21] Spin orbital coupling in the W would be sufficient to relax selection rules for such a transition to occur. This was confirmed by PES studies on $W(CO)_6$.[24] As is the case in the (η^6-mesitylene)$Mo(CO)_3$ complex, the LF transition appears to lie at higher energy relative to the Cr analogue. The transition at 35454 cm^{-1} is assigned to a LF transition.(η^6-Arene)$W(CO)_3$ complexes are accepted as being photochemically inert. It is possible that the triplet state is very efficiently populated upon irradiation, but it does not lead to M-CO lability. Nesmeyanov *et al*[25] reported on the formation of a chelated dicarbonyl upon photolysis of (η^6-alkenylarene)$W(CO)_3$, where the double bond is separated from the arene ring by $(CH_2)_2$ or $(CH_3)_2$. This suggests that altering the nature of the ligand may "switch on" the photochemistry of the tungsten tricarbonyl systems.

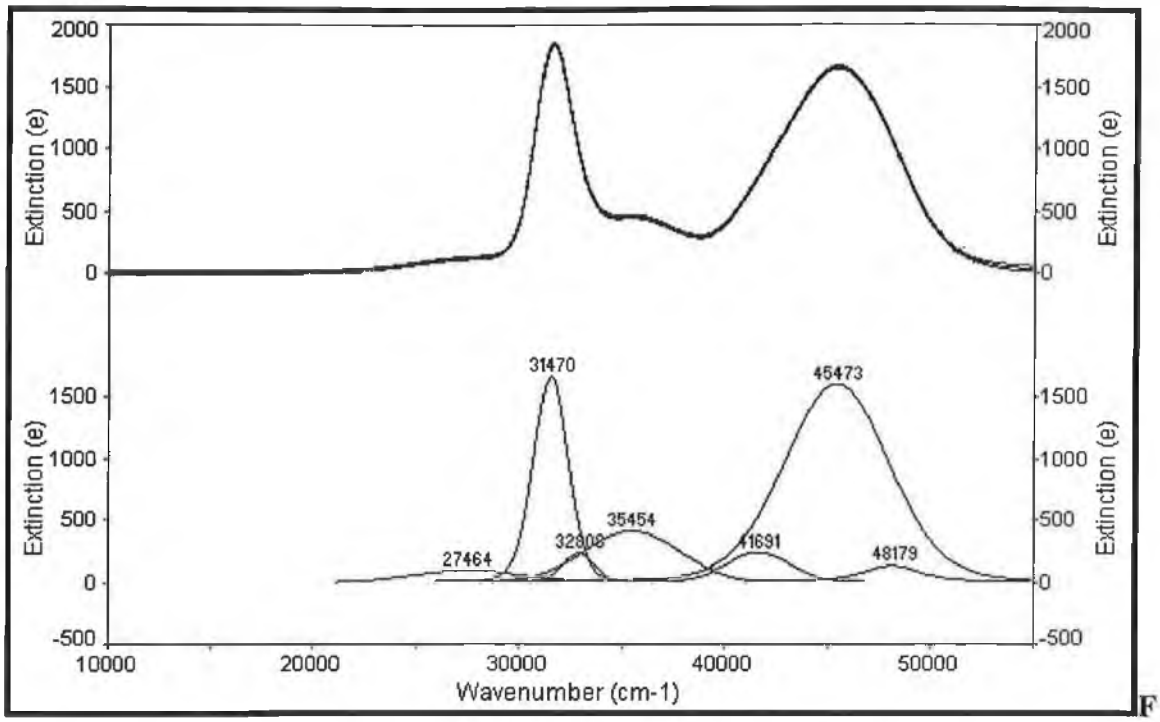

igure 2.8 Peak pick analysis of the UV/vis spectrum of (η^6-mesitylene)$W(CO)_3$ in cyclohexane(1 x 10^{-4}M)

2.23 Luminescence in (η^6-mesitylene)$W(CO)_3$

The earliest report of emission for metal carbonyl complexes involved $W(CO)_5L$ species as pure solids or in rigid glass matrices at 77 K, (L = N-donor ligand).[26] The emission was assigned to a spin-forbidden LF transition; $^3E(e^3b_2{}^2a_1{}^1) \rightarrow {}^1A_1(e^4b_2{}^2)$. The luminescence life-times were in the range 10^{-6} - 10^{-7}s, typical of emissions of spin-forbidden character. [27,28] The analogous Cr and Mo complexes displayed no luminescence properties under identical conditions, and this was associated with the lack of an observable singlet to triplet transition. When L = pyridine with a highly electron withdrawing substituent, then the lowest energy excited state was identified as a M $\rightarrow \pi^*$ pyridine CT. Emission from these complexes was identified as a MLCT emission.[29,30]

The emission spectrum for (η^6-mesitylene)$W(CO)_3$ was recorded in an ethanol:methanol 4:1 glass at 77K, λ_{exc} = 350 nm. Three emission bands can be seen at 391, 411, and 432 nm as presented in Figure 2.9. It is the excitation spectrum presented in Figure 2.10 which is particularly significant. The λ of irradiation absorbed for the emission process is in the range ~290 to 340 nm. This absorption corresponds to the

electronic transition centred at 31470 cm^{-1} (317 nm), which is assigned to a MLCT transition. No emission is observed from the transition centred at 35454 cm^{-1} (282 nm), which would further support it's assignment to a LF transition. This shows that there is no communication between the LF and the MLCT excited states.

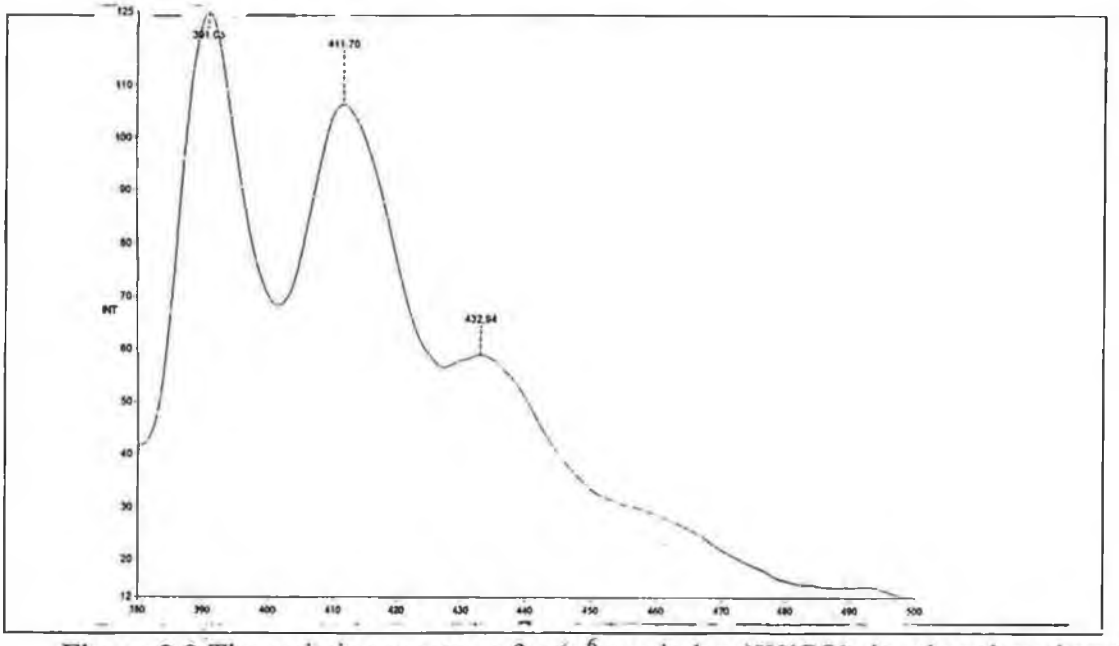

Figure 2.9 The emission spectrum for (η^6-mesitylene)$W(CO)_3$ in ethanol:methanol 4:1, λ_{exc} = 350 nm.

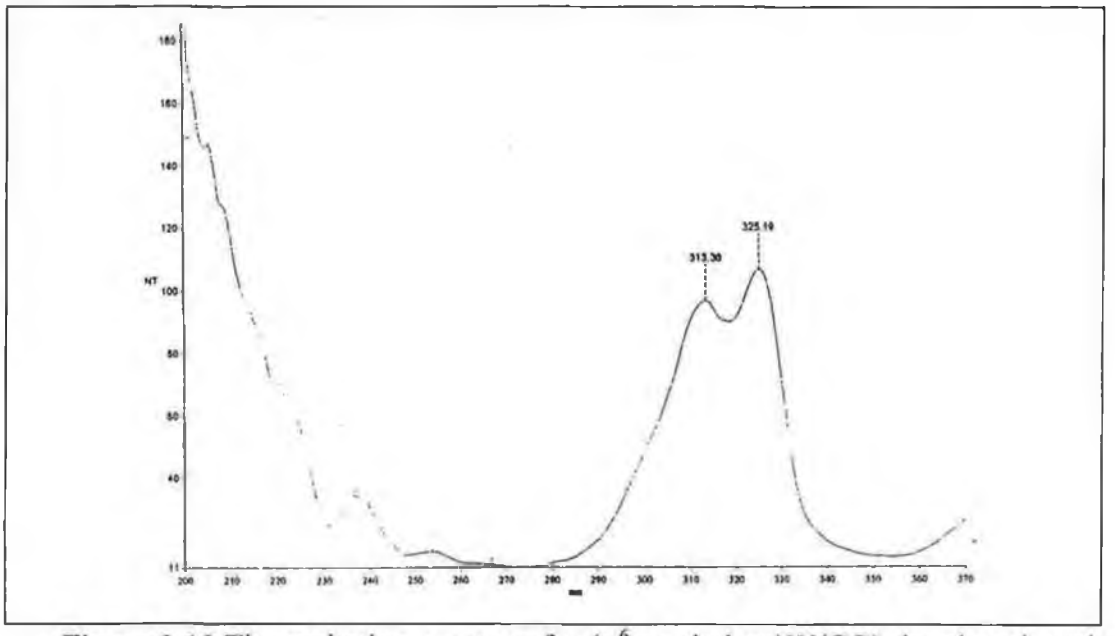

Figure 2.10 The excitation spectrum for (η^6-mesitylene)$W(CO)_3$ in ethanol:methanol 4:1, λ_{emm} = 410.

2.24 The effect of symmetry on the electronic structure of half sandwich complexes

The photochemistry of (η^6-naphthalene)$Cr(CO)_3$[31] and (η^6-pyridine) $Cr(CO)_3$[12,32] has been studied in detail. In both instances the photochemistry was found to be wavelength dependent; low energy photolysis resulted in arene-loss *via* ring-slip processes while higher energy photolysis was required to cause CO expulsion. These photochemical trends can be rationalised in terms of the change in the electronic structure of the complexes on moving from C_{3v} to C_s symmetry.

As discussed in the literature survey the electronic structure of (η^6-arene) $Cr(CO)_3$ complexes of C_{3v} symmetry has been elucidated, by a combination of theoretical calculations and experimental methods.[22,33,34 23] The low energy band in the UV/vis spectrum of (η^6-mesitylene)$Cr(CO)_3$ as presented in Figure 2.5, has been shown to be LF in nature. However PES studies and Fenske-Hall molecular orbital calculations[22] have shown that there are two accessible LF transitions; $(2e^4\ 1a_1^2\ 3e^0) \rightarrow (2e^4\ 1a_1^1\ 3e^1)$ and $(2e^4\ 1a_1^2\ 3e^0) \rightarrow (2e^3\ 1a_1^2\ 3e^1)$. The HOMO in (η^6-arene)$Cr(CO)_3$ complexes with C_{3v} structure is the $1a_1$ orbital, so the poorly resolved lowest energy absorption band in Figure 2.5 can be assigned to the $1a_1 \rightarrow 3e$ transition. The second LF transition is not observed. The PES studies of Byers *et al.*[22] found an energy difference in the two LF transitions of ~ 0.3 eV, and so the higher energy transition would be expected at ~ 30300 cm^{-1}, which is overlapped by the intense MLCT transition.

The $1a_1$ orbital has been confirmed to be mainly metal d_z^2 in character with some bonding interaction with respect to the Cr-CO bond [34] but nonbonding interaction with respect to the Cr-arene bond.[22] So depopulation of the $1a_1$ would result in CO expulsion. Conversely the 2e orbital has been confirmed to be the main contributor to the metal-arene bond, and so depopulation of this would have implications for the metal arene bond. In the chromium half sandwich complexes of C_{3v} symmetry the $2e \rightarrow 3e$ transition is obscured by the intense $M \rightarrow \pi^*$ CO absorbance at ~31000 cm^{-1}, thus in these complexes CO loss would be expected to be the dominant photoprocess independent of wavelength.

Figure 2.11 and 2.12 present the peak analysis for the UV/vis spectra of (η^6-naphthalene)$Cr(CO)_3$ and (η^6- pyridine)$Cr(CO)_3$ respectively. The low energy features are particular evident here as compared to the spectrum of the mesitylene analogue (Figure 2.4). The lowest energy feature is unaffected by changes in the solvent polarity typical of a LF transition. Arene-loss was observed from both of these systems upon low energy irradiation, while high energy irradiation resulted in both CO-loss and arene-loss.[23, 32, 12] These results imply that population of the lowest energy excited state in both of these complexes may labilise the metal-arene bond.

The photochemistry can be rationalised in terms of symmetry. Figure 2.10 portrays the changes in the molecular orbitals on moving from a complex of C_{3v} symmetry to one of $C_{s,}$ as occurs on changing the arene ligand from benzene to naphthalene or pyridine. The degeneracy of the e-type orbitals is lifted and the orbital of d_{xy} character is destabilised now lying at higher energy to the orbital of d_z^2 character.[35] So in the unsymmetric complex the HOMO originates from the d_{xy} orbital which is of the correct symmetry to be bonding with respect to the metal arene bond. The lowest energy LF transition should then correspond to the $a^{II} \rightarrow a^{II}$ transition which would effect the metal-arene bond. It is proposed that the transitions at 22433 and 26444 cm^{-1} in the naphthalene and pyridine complexes respectively can be assigned to the $a^{II} \rightarrow a^{II}$ transition. The higher energy $a^{I} \rightarrow a^{II}$ transition (as indicated in Figure 2.10) would effect the metal-CO bond as previously described. This analysis of the electronic transitions in the C_s complexes explains the wavelength dependence of their photochemistry.

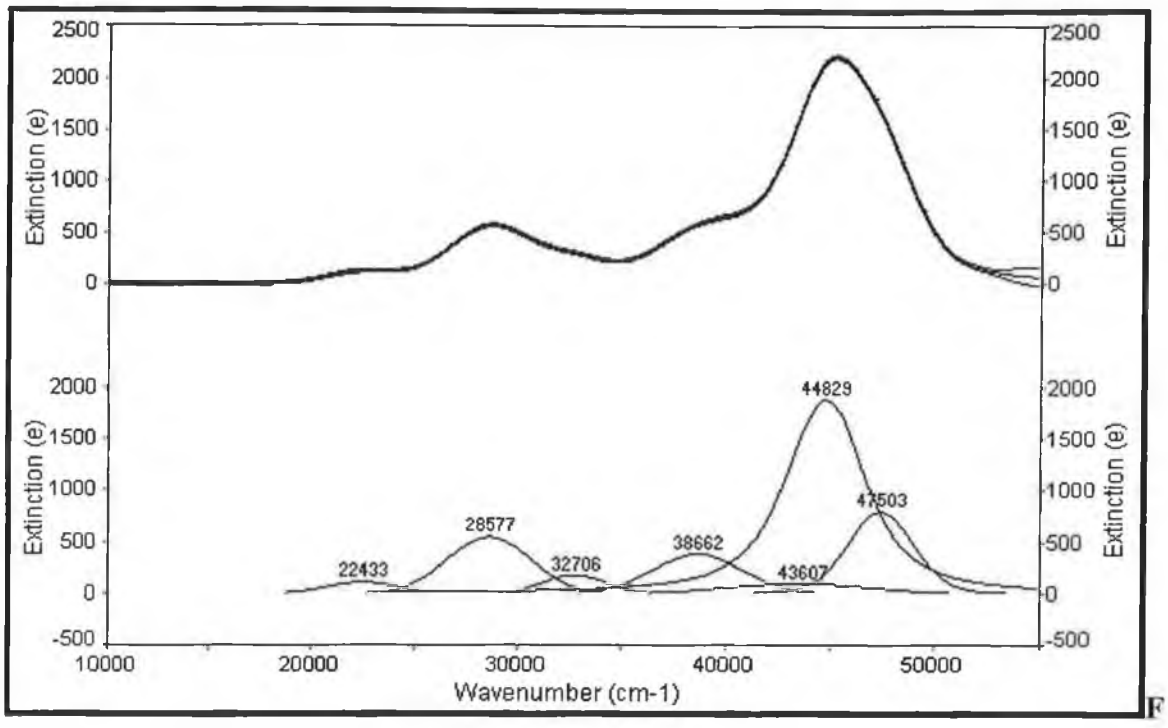

igure 2.11 PeakPick analysis of the UV/vis spectrum of (η^6-naphthalene)$Cr(CO)_3$ in cyclohexane(1 x 10^{-4}M)

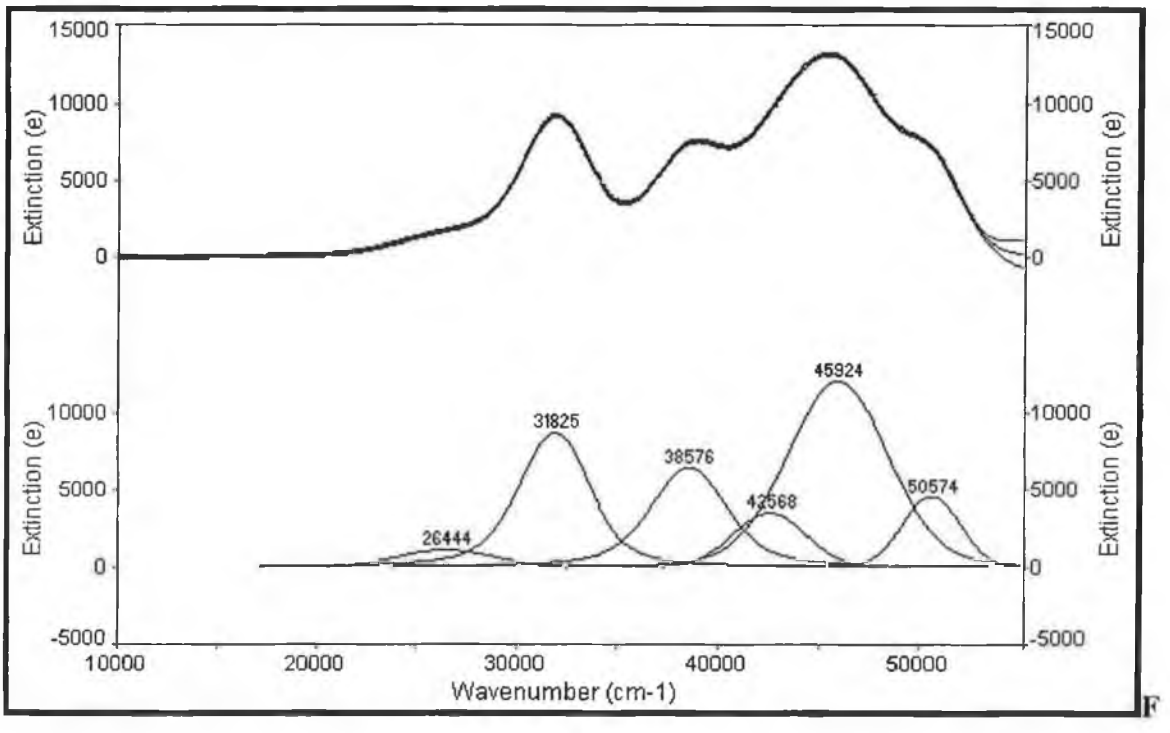

igure 2.12 PeakPick analysis of the UV/vis spectrum of (η^6-pyridine)$Cr(CO)_3$ in cyclohexane(1 x 10^{-4}M)

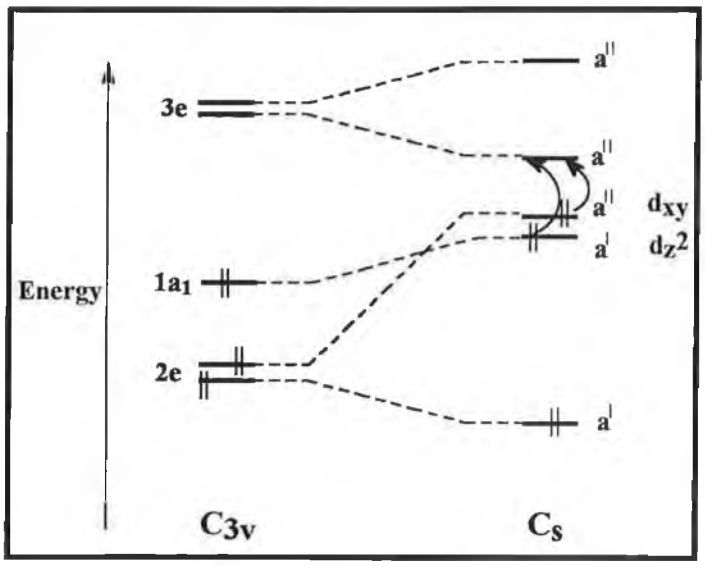

Figure 2.13 Comparison of the molecular orbital diagrams for (η^6-arene)$Cr(CO)_3$ complexes of C_{3v} and C_s symmetry.

2.3 Investigations into the Trapping of Ring-Slip Intermediates

(η^6-Allylbenzene)M(CO)$_3$ (M = Cr and Mo), were studied in an attempt to identify ring-slip intermediates. Previous investigations into the photochemistry of the Cr species proposed that irradiation resulted in a hapticity change in the metal arene bond from $\eta^6 \rightarrow \eta^4$, maintaining the tricarbonyl.[31] This is depicted in Reaction 2.4.

Reaction 2.4

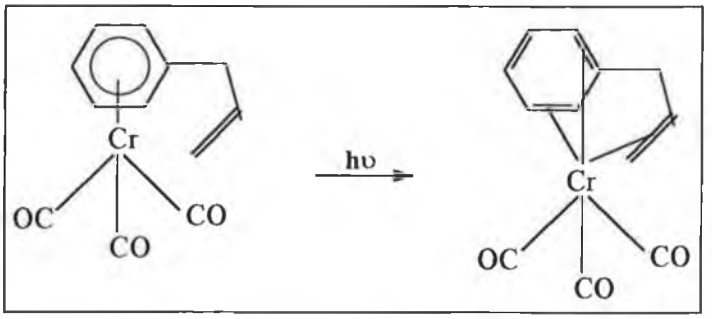

(η^6-Allylbenzene)Cr(CO)$_3$ was incorporated into a polyethylene disk and its photolysis monitored by IR, at room temperature and 223K.

2.31 Room temperature IR monitored photolysis of (η^6-allylbenzene)Cr(CO)$_3$

The IR of (η^6-allylbenzene)Cr(CO)$_3$ in polyethylene displayed two intense carbonyl absorption bands at 1908 and 1976 cm^{-1}. Upon photolysis at >340 nm a depletion of the parent absorption's was observed along with the formation of a photoproduct at 1985 cm^{-1} (Figure 2.14). Also the polyethylene disk was observed to change in colour from bright yellow to a pale yellow colour. The absorption of the photoproduct is consistent with the CO stretching frequency of Cr(CO)$_6$. The photolysis was carried out in an out gassed environment, so no CO was present to interfere with the photoreaction. The formation of Cr(CO)$_6$ upon photolysis of (η^6-arene)Cr(CO)$_3$ has been rationalised in a study by Setkina *et al.*[36] Both IR and NMR monitored photolysis experiments were interpreted as indicating the formation of a multicentre complex, as presented in Figure 2.15. Photolysis of this complex was proposed to yield Cr(CO)$_6$ by labilisation of the Cr-CO bridging bond. Alternatively it is plausible that if photolysis of

(η^6-allylbenzene)$Cr(CO)_3$ resulted in arene loss the $Cr(CO)_3$ moiety would rapidly scavenge CO molecules to form $Cr(CO)_6$.

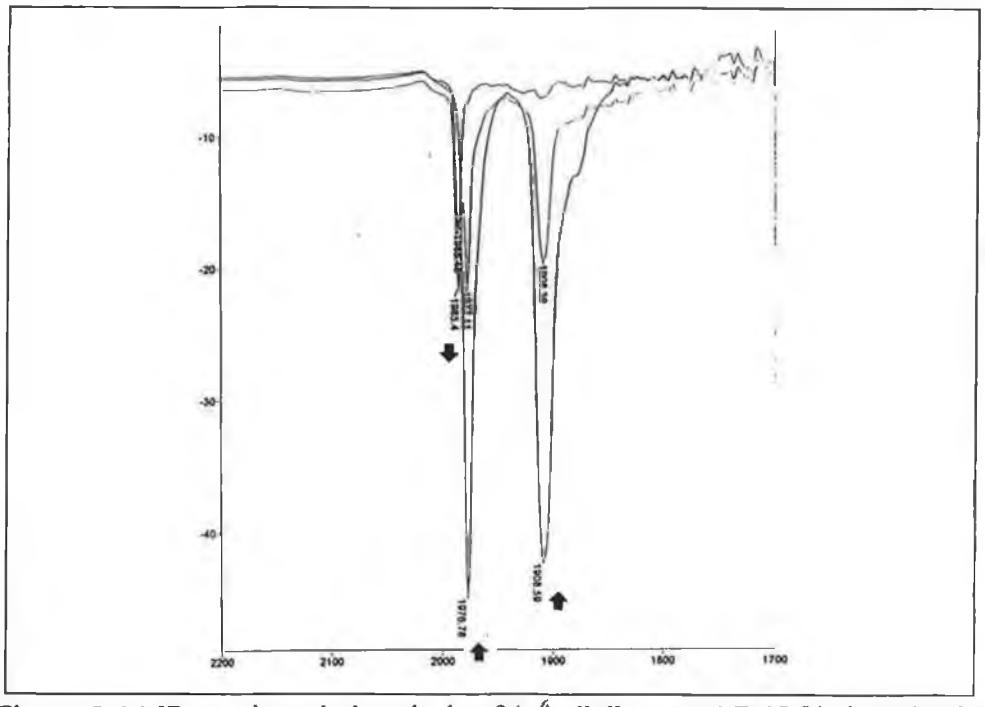

Figure 2.14 IR monitored photolysis of (η^6-allylbenzene)$Cr(CO)_3$ in polyethylene, λ_{irrad} > 340nm, Temperature = 295K

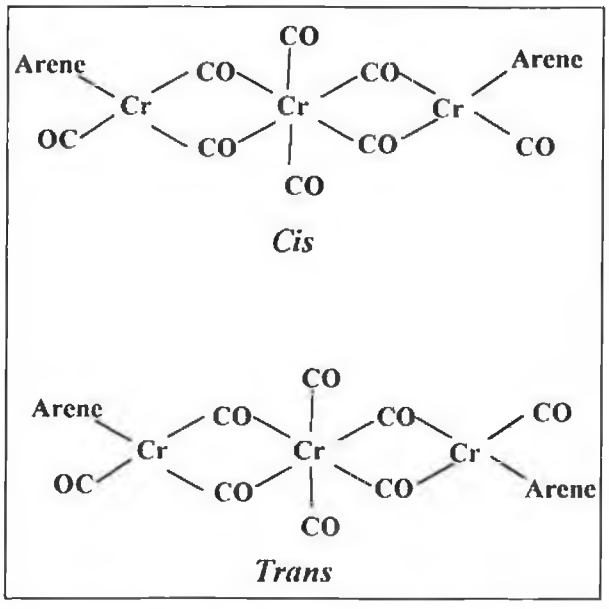

Figure 2.15 Proposed multicentre intermediate complex formed upon photolysis of (η^6-arene)$Cr(CO)_3$.

2.32 Low temperature IR monitored photolysis of(η^6-allylbenzene)$Cr(CO)_3$

The low temperature apparatus was out gassed prior to photolysis. Photolysis and monitoring was carried out at 223K. Upon photolysis depletion of the parent bands coincided with the formation of a photoproduct at 1934 and 1877 cm^{-1} as presented in Figure 2.16. Prolonged photolysis did not lead to any other product formation. Upon allowing the sample to return to room temperature the parent bands were regenerated.

Nesmeyanov *et al.*[25] reported on the photochemical generation of chelate alkenylarenedicarbonylmetal complexes (metal = Cr, Mo, and W). Irradiation of the tricarbonyl complex in which the double bond was separated from the arene moiety by $(CH_2)_2$ or $(CH_2)_3$ resulted in stable chelate dicarbonyl complexes. When the bridge between the arene was only CH_2, as in allylbenzene, irradiation of the tricarbonyl complex only resulted in its decomposition. It would not be sterically feasible for a dicarbonyl chelate to for in the allylbenzene complex, so it is proposed that the new carbonyl stretching frequencies observed upon photolysis are due to a ring slip complex stabilised by the vinylic bond, as depicted in reaction 2.4.

2.33 UV/vis monitored steady state photolysis of (η^6-allylbenzene)$Mo(CO)_3$

A sample of the Mo complex was prepared in cyclohexane and degassed by purging with argon for 20 minutes prior to photolysis. Figure 2.17 presents the changes in the UV/vis spectrum upon irradiation at $\lambda > 340$ nm. A depletion of the parent absorption's at ~ 335 nm coincides with an increase in absorbance at ~280 nm and a further absorbance beyond 360 nm. Similar results were observed when the sample was purged with CO prior to photolysis. The increase in absorption at ~280 nm can be assigned to the uncomplexed allylbenzene.

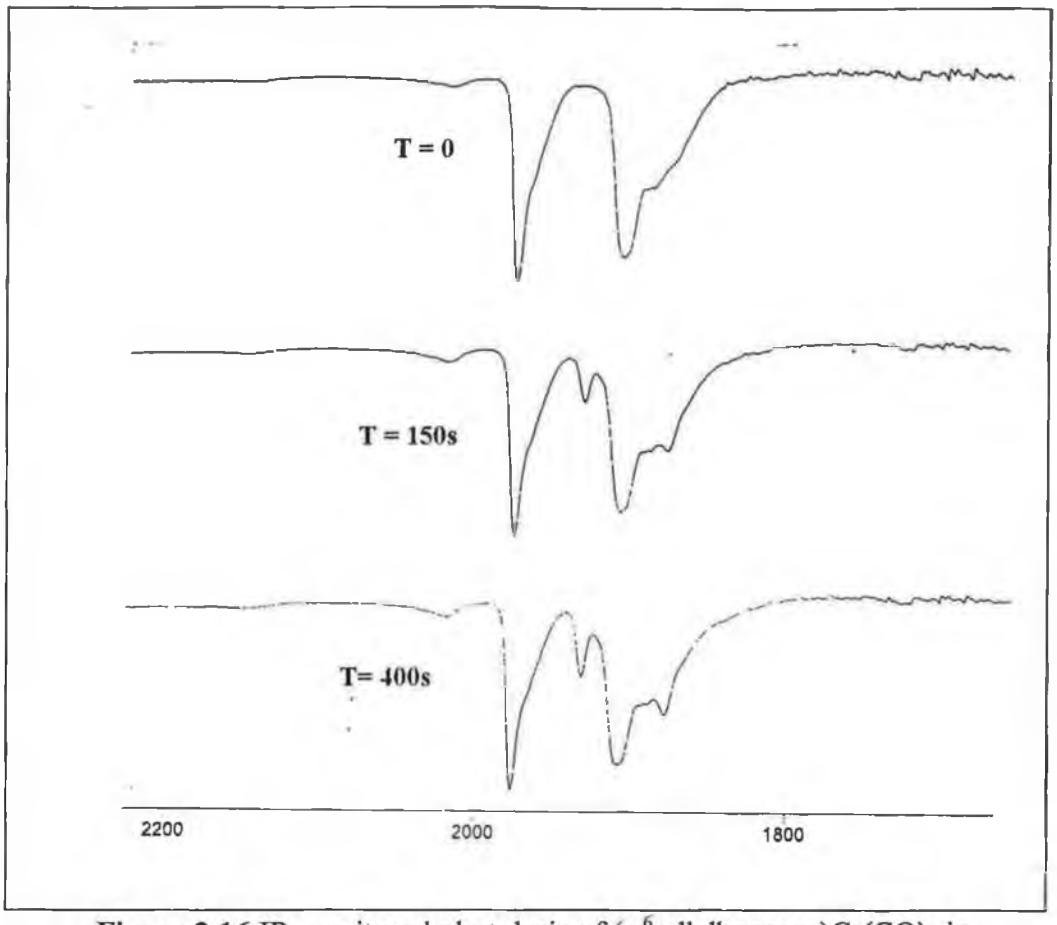

Figure 2.16 IR monitored photolysis of (η^6-allylbenzene)$Cr(CO)_3$ in polyethylene, $\lambda_{irrad} > 340nm$, Temperature = 223K

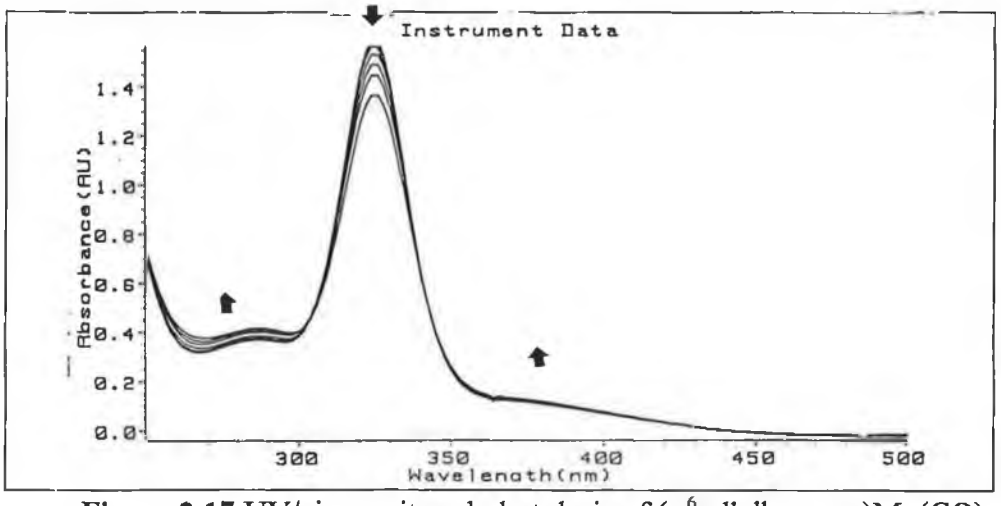

Figure 2.17 UV/vis monitored photolysis of (η^6-allylbenzene)$Mo(CO)_3$ in argon degassed cyclohexane.

2.34 IR monitored photolysis of (η^6-Allylbenzene)Mo(CO)$_3$

The IR monitored photolysis was carried out in the IR cells on an argon degassed sample of the Mo species. Upon photolysis at $\lambda > 340$ nm a depletion of the parent bands was observed at 1981, and 1911 cm^{-1}. This depletion coincided with the growin of a number of product bands; 1935, 1934, 1971, 1987, and 2043 cm^{-1}. These changes in the IR spectrum are presented in Figure 2.18. As was suggested from the UV/vis monitored photolysis results a single clean reaction is not observed. The band at 1987 cm^{-1} is typical of Cr(CO)$_6$. It is difficult to elucidate the identity of the other product(s), however the results upon photolysis of (η^6-ethylbenzene)Cr(CO)$_3$ under identical conditions do yield some clues. Figure 2.119 presents the IR changes observed in the ethylbenzene system (the product bands are indicated by arrows).

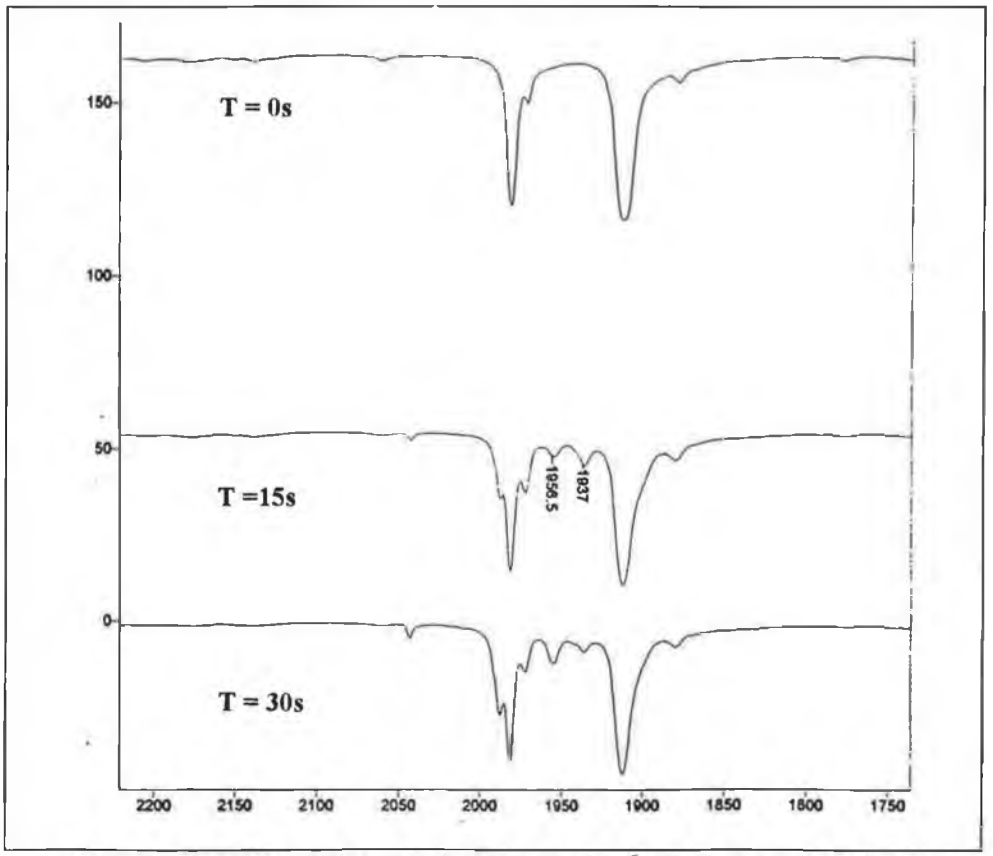

Figure 2.18 IR monitored photolysis of (η^6-allylbenzene)Mo(CO)$_3$ in argon degassed cyclohexane, $\lambda_{exc} > 340$nm.

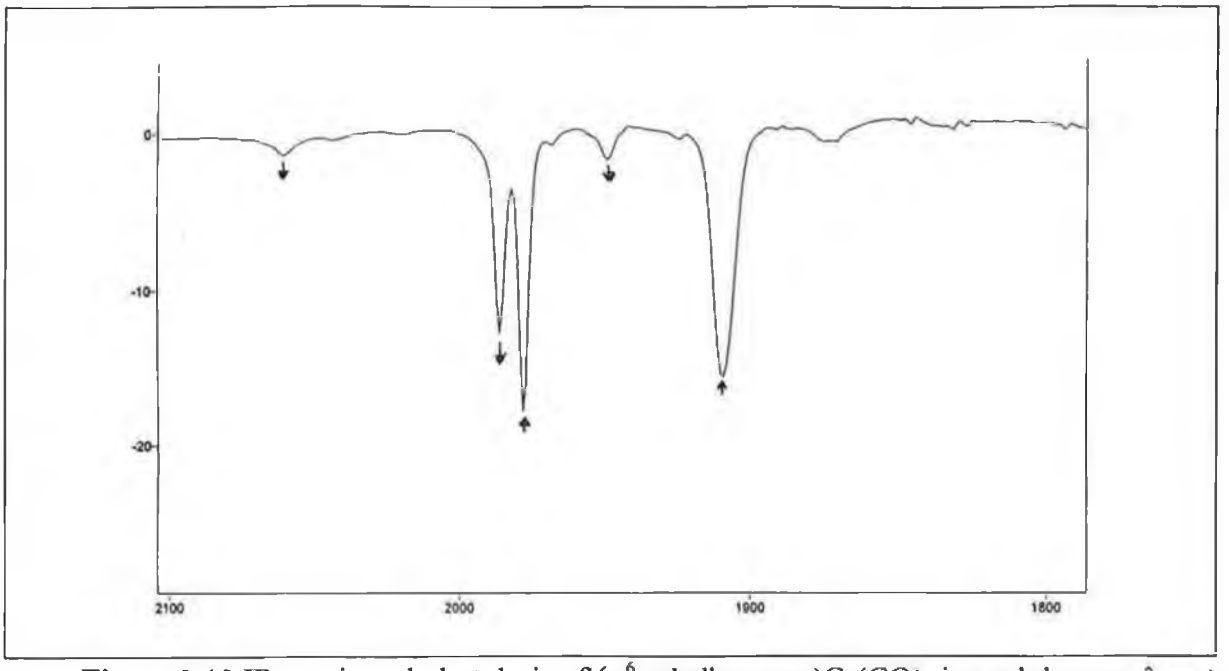

Figure 2.19 IR monitored photolysis of (η^6-ethylbenzene)$Cr(CO)_3$ in cyclohexane λ_{irrad} > 340nm.

Investigations into the photochemistry of (η^6-hexaethylbenzene)$Cr(CO)_3$ proposed the formation of a dinuclear species during laser flash photolysis experiments.[31] It is possible that along with the formation of $Cr(CO)_6$ a binuclear species; (η^6-ethylbenzene)$_2Cr_2(CO)_5$ is formed, the $Cr(CO)_2$ fragment being bound to the $Cr(CO)_3$ fragment *via* a Cr-Cr interaction and a bridging carbonyl group. The CO-stretching frequencies for the photoproduct(s) upon photolysis of (η^6-allylbenzene)$Mo(CO)_3$ are similar to those of (η^6-ethylbenzene)$Cr(CO)_3$ and so are tentatively be assigned to a binuclear species.

2.4 Conclusion

The $\Phi_{co\text{-}loss}$ in (η^6-mesitylene)$Mo(CO)_3$ has been shown to decrease with increasing irradiation wavelength, this is in contrast to its Cr analogue. The decrease in the efficiency of CO-loss in the molybdenum species is attributed to its photoreactive LF transition lying at higher energy as compared with the equivalent LF transition in the Cr system. Lower energy MLCT transitions (probably nonphotoreactive) may be efficiently populated and so reduce population of the higher energy LF state. In the Cr system the LF transition is accepted to be populated either directly or *via* a radiationless decay from a higher energy MLCT transition. There is evidence from the excitation spectrum for (η^6-mesitylene)$W(CO)_3$ that there is no communication between the LF and the MLCT transition, this may explain the lack of efficient CO-loss in the Mo system and the lack of photochemistry in the (η^6-arene)$W(CO)_3$.

The reported photochemistry of (η^6-naphthalene)$Cr(CO)_3$ and (η^6-pyridine)$Cr(CO)_3$ can be explained in terms of symmetry. Two accessible photoreactive LF transitions are involved in the photochemistry. Low energy photolysis results in depopulation of a d-orbital which is bonding with respect to the arene, while higher energy photolysis results in depopulation of a d-orbital which is bonding with respect to the CO ligands. These conclusions suggest that the arene-loss cannot occur *via* the dicarbonyl intermediate, as was previously proposed.[4] Instead CO-loss and arene loss occur *via* two separate LF excited states.

The results of the IR monitored photolysis of (η^6-allylbenzene)$Cr(CO)_3$ are consistent with the formation of a ring slip intermediate, further supporting the theory that arene loss occurs *via* a haptotropic rearrangement of the metal-arene bond rather than the dicarbonyl intermediate. the studies on the (η^6-allylbenzene)$Mo(CO)_3$ complex are at present inconclusive, however they show that the photochemisty of the tricarbonyl systems may be as straightforward as was initially believed.

References

[1] (a) Strohmeier, W; von Hobe, D.; *Z. Naturforsch.* **18b**, 981,1963.

(b) Strohmeier, W; Hellmann, H; *Chem. Ber.*, **96**, 2859, 1963.

(c) Strohmeier, W; von Hobe; D, *Z. Naturforsch.* **18b**, 770, 1963.

[2] Wrighton, M.S.; Haverty, J. L.; *Z.Naturforsch.* **30b**, 254, 1974.

[3] Nasielski, J; Denisoff, O.; *J. Organomet. Chem.* **102**, 65, 1975.

[4] Gilbert, A.; Kelly, J.M.; Budzwait, M.; von Gustorf, E.K.; *Z. Naturforsch.* **31b**, 1091, 1976.

[5] Trembovler, V. N.; Baranetskaya, N. K.; Fok. N.V.; Zaslavskaya, G.B.; Yavorski, B. M.; Setkina, V. N.; *J. Organomet. Chem.* **117**, 39, 1976.

[6] Bamford, C. H.; Allamee, K. G.; Konstaninov, C. J.; *J. Chem. Soc. Faraday Trans. I*, **73**, 1406, 1977.

[7] Rest A. J.; Sordeau, J. R.; Taylor, D. J.; *J. Chem. Soc., Dalton Trans.* 651, 1978.

[8] Bitterwolf, T.; Colt, K. A.; Rest A. J.; Mascetti, J.; *J. Organomet. Chem.* **419**, 113, 1991.

[9] Wang, W.; Jin,P.; Liu, Y.; Yongbo, S.; Fu, K-J; *J Phys Chem.* **96**, 1278, 1992

[10] Hill, R. H.; Wrighton, M. S.; *Organometallics* **6**, 632, 1987.

[11] Zheng, Y.; Wang, W.; Lin, J.; She, Y.; Fu K-J.; *J. Phys. Chem.* **96,** 9821, 1992.

[12] Breheny C. J.; Draper, S. M.; Grevels, F-W; Klotzbücher, W.. E.; Long, C.; Pryce, M T.; Russell G.; *Organometallics* **15**, 3679, 1996.

[13] (a) Strohmeier, W.; Mittnacht, H; *Z. Phys. Chem.* **29**, 339, 1961.

(b) Strohmeier, W.; Starricho, E.H.; *Z. Phys. Chem.* **38**, 315, 1963.

(c) Strohmeier, W.; Muller, M.; *Z.Phys. Chem.* **40**, 85, 1964.

[14] (a) Mahaffy, C.A. L.; Pauson, P. L.; *J. Chem. Res. (S)* 126, 1979.
(b) Mahaffy, C. A. L.; Pauson, P. L.; *J. Chem. Res. (M)* 1752, 1979.

[15] Zimmerman, C. L.; Pauson, P. L.; Roth, S.A.; Willeford, B. R.; *J. Chem. Res. (S)* 108, 1980.

[16] (a) Traylor, T. G.; Stewart, K. J.; Goldberg, M. J.; *J. Amer. Chem. Soc.* **106**, 4445, 1984.

(b) Traylor, T. G.; Stewart, K. J.; *Organometallics* **3**, 325, 1984.

(c) Traylor, T. G.; Stewart, K. J.; Goldberg, M. J.; *Organometallics* **5**, 2062, 1986.

(d) Traylor, T. G.; Stewart, J. S.; *J. Amer. Chem. Soc.* **108**, 6977, 1986.

(e) Traylor, T. G.; Goldberg, M. J.; *J. Amer. Chem. Soc.* **109**, 3968, 1987.

(f) Traylor, T. G.; Goldberg, M. J.; *Organometallics* **6**, 2413, 1987.

(g) Traylor, T. G.; Goldberg, M. J.; *Organometallics* **6**, 2531, 1987.

[17] Albright T. A.; Hofmann, P.; Hoffmann, R.; Lillya, C.; Dobosh, P. A.; *J. Amer. Chem. Soc.* **105**, 3396, 1983.

[18] Cunningham, S. D.; Ofele, K.; Willeford, B. R.; *J. Amer. Chem. Soc.*; **108**, 193, 1983.

[19] Kriss, R. V.; Treichel, P. M.; *J. Amer. Chem. Soc.* **108**, 853, 1986.

[20] Howell, J .A. S.; Ashford, N. F.; Dixon D.T.; Kola, J. C.; Albright, T. A.; Kang S. K.; *Organometallics* **10**, 1852, 1991.

[21] Geoffroy, G. L.; Wrighton, M. S.; *Organometallic Photochemistry*, Academic Press, New York, 1979.

[22] Byers, B. P.; Hall, M. P.; *Organometallics,* **6**, 2319, 1986.

[23] Carroll, D. G.; McGlynn S. P.; *Inorg. Chem.* 7, 1285, 1968.

[24] Lichtenberger, D. L.; Kellog, G. E.; *Acc. Chem. Res.* **20**, 379, 1987.

[25] Nesmeyanov, A. N.; Krivykh, V. V.; Petrovskii, P. V.; Kaganovich, V. S.; Rybinskaya, M. I.; *J. Organomet. Chem.* **162**, 323, 1978.

[26] Wrighton, M.; Hammond, G. S.; Gray, H. B.; *J. Amer Chem. Soc.* **93**, 4336, 1971.

[27] Demas, J. N.; Crosby, G. A.; *J. Amer. Chem. Soc.* **92**, 7262, 1970.

[28] Watts, R. J.; Crosby, G. R.; *J.Amer. Soc.* **94**, 2606, 1972.

[29] Wrighton, M.; Hammond, G. S.; Gray, H. B.; *Mol, Photochem.* **5,** 179, 1973.

[30] Wrighton, M.S.; Abrahamson, H. B.; Morse, D. L.; *J. Amer. Chem. Soc.* **98,** 4105, 1976.

[31] Pryce, M. T.; *Ph.D. Thesis* Dublin City Univerrsity, 1994.

[32] Breheny, C. J.; *Ph.D. Thesis* Dublin City University, 1996.

[33] Guest, J. C.; Hillier, H. I.; Higinson, B. R.; Llyod, B. R.; *Mol. Phys.* **29**, 113, 1975.

[34] Elian, M.; Hoffman, R.; Hoffman, R. J.; *J. Amer. Chem. Soc.* **99,** 7546, 1977.

[35] Albright, T. A.; Hofmann, P.; Hoffmann, R.; Lillya, C. P.; Dobosh, P. A.; *J. Amer. Chem. Soc.* **105**, 3396, 1983.

[36] Domogatskaya, E. A.; Setkina, V. N.; Baranetskaya, N. K.; Trembolver,V. N.; Yavorskii, B. M.; Shteinshneider, A. Ya.; Petrovskii, P. V.; *J. Organomet. Chem.* **248,** 161, 1983.

CHAPTER 3

The Photochemistry of $[(\eta^6\text{-Benzene})_2Cr]^+$

3.1 Introduction

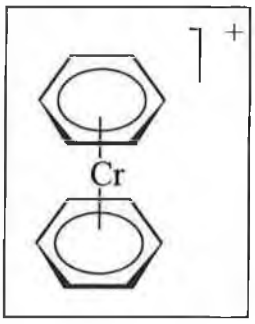

The neutral [(η^6-benzene)$_2$chromium] (DBC) compound is photoinert in hydrocarbon solution.[1] By contrast the corresponding cation DBC^+ has an extensive photochemistry. The only mechanistic work on DBC^+ to date was carried out by Traverso and his co-workers.[2] The photochemistry of the salt (DBC^+Cl^-) in aqueous solution was found to be qualitatively the same upon irradiation at 254, 334, 365, or 404 nm, but did depend on whether the solution was degassed or aerated. Photolysis in a nitrogen gas saturated solution resulted in a depletion of the bands assigned to the salt and the formation of a band characteristic of free benzene and a precipitate confirmed to be the neutral species (DBC). Photolysis in an aerated solution resulted only in the formation of free benzene with no evidence for the formation of the neutral species. The following mechanism was proposed;

Reaction 3.1

Excitation	$Cr(C_6H_6)_2^+ \rightarrow {}^*Cr(C_6H_6)_2^+$	(1)
Deactivation	${}^*Cr(C_6H_6)_2^+ \rightarrow Cr(C_6H_6)_2^+$	(2)
1° Photoprocess	${}^*Cr(C_6H_6)_2^+ \rightarrow Cr^+ + 2C_6H_6$	(3)
2° Thermal rxns	$Cr(C_6H_6)_2^+ + Cr^+ \rightarrow Cr(C_6H_6)_2 + Cr_2^+$	(4)
	$Cr^+ + 1/2\ O_2 + H_2O \rightarrow Cr^{2+} + OH^-$	(5)

The Cr^+ ions are scavenged by oxygen so no DBC is formed in the aerated system

The photochemistry was not equally efficient over the range of irradiation wavelengths. Table 3.1 shows the variation in quantum yields with wavelength. The UV/vis spectrum of $DBC^+ I^-$ in water is presented in Figure 3.1. Weber and his co-workers[3] have assigned the intense absorption band at 272 nm to a MLCT transition and the absorption at 334 nm to a LMCT transition. A MLCT transition has also been assigned to an absorption at 395 nm lying under the LMCT band. These assignments may explain the effect of wavelength on the quantum yields. There is a weak absorbance at 1160 nm in the electronic absorbance spectrum of DBC^+ which was assigned to a LF transition[3]. No photochemistry was observed upon irradiation into this low energy band. From these results Wrighton proposed that a CT excited state probably an MLCT state is responsible for the observed photochemistry.[4]

To our knowledge the work by Traverso *et al.*[2] represents the only account of the photochemistry of DBC^+, however many investigation have been reported for the related $[(\eta^5\text{-cyclopentadiene})\ M\ (\eta^6\text{-arene})]^+$ system (M = Fe or Ru).[5,6,7,8,9] In the presence of Lewis acids such as acetonitrile, photolytic arene loss was observed. The mechanism of this arene loss was proposed to involve either solvent-assisted steps in polar, nucleophilic solvents or anion-assisted steps in non-polar, weakly nucleophilic solvents.[6] Experimental results lead to the conclusion that the ligand field excited state was the photoactive excited state[7]. More recently investigations into the photochemistry of $[Fe(\eta^6\text{-mesitylene})_2]^{2+}$ proposed that photoinduced loss of both mesitylene rings occured from both LF and mesitylene $\rightarrow$ Fe CT excited states.[10]

In the case of $[(\eta^6\text{-arene}_1)\text{-Ru-}(\eta^6\text{-arene}_2)]^{2+}$, irradiation in co-ordinating solvents lead to the formation of the fully solvated complex$[Ru(solvent)_6]^{2+}$ via the half sandwich intermediate $[(\eta^6\text{-arene})Ru(solvent)_3]^{2+}$, as depicted in Reaction 3.2.[11] Similar observations were made following irradiation of the $[(\eta^6\text{- toluene})Cr]^+$ complex, but the quantum yield for the disappearance of the toluene species was only 0.04 [12] compared with up to 0.18 for the DBC^+ complex.[2]

This chapter presents the results of investigations into the photochemistry of DBC^+ providing further elucidation of the intermediates involved. This work is a continuation of research carried out by Dr. Charles Gordon during his post doctoral research at DCU.

	Wavelengths of Irradiation (nm)			
	254	313	365	404
Aerated				
$\Phi Cr(bz)_2^+$(disappearance)	0.10	0.064	0.055	0.075
Φbz(formation)	0.21	0.10	0.12	0.15
Deaerated				
$\Phi Cr(bz)_2^+$(disappearance)	0.18	0.10	0.094	0.14
Φbz(formation)	0.21	0.13	0.11	0.15
$\Phi Cr(bz)_2$(formation)	0.08	0.04	0.04	0.06

Table 3.1 Quantum Yields for the Irradiation of DBC^+ in Aqueous Solution

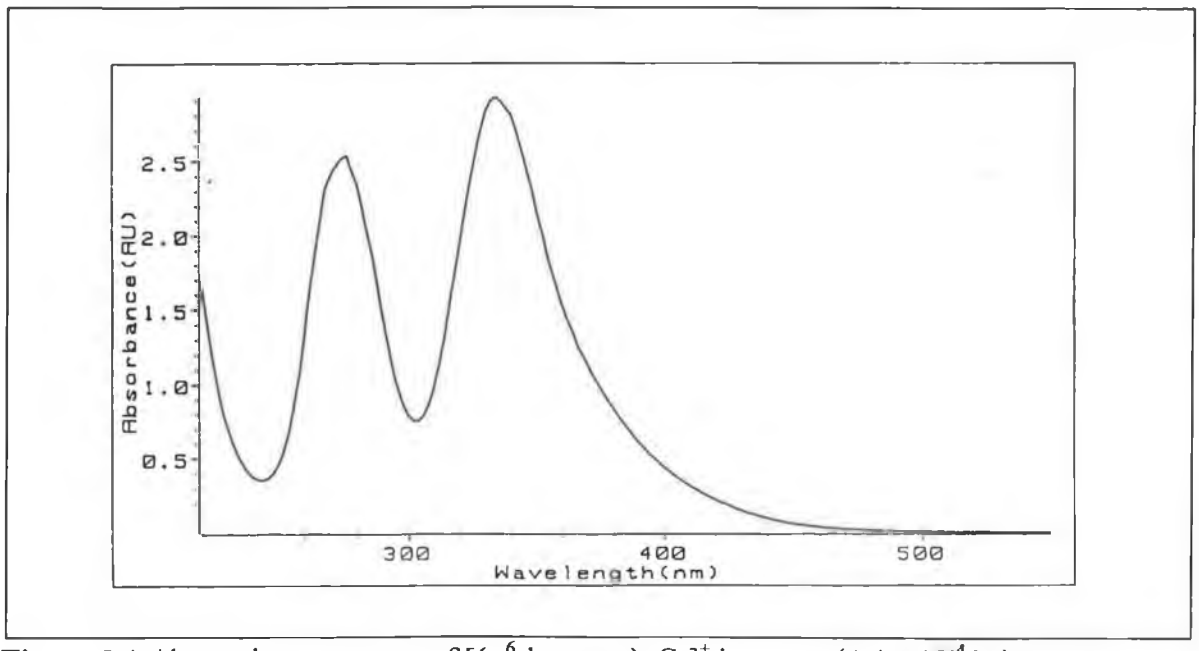

Figure 3.1 Absorption spectrum of $[(\eta^6\text{-benzene})_2 Cr]^+$ in water (4.4×10^{-4} M)

Reaction 3.2

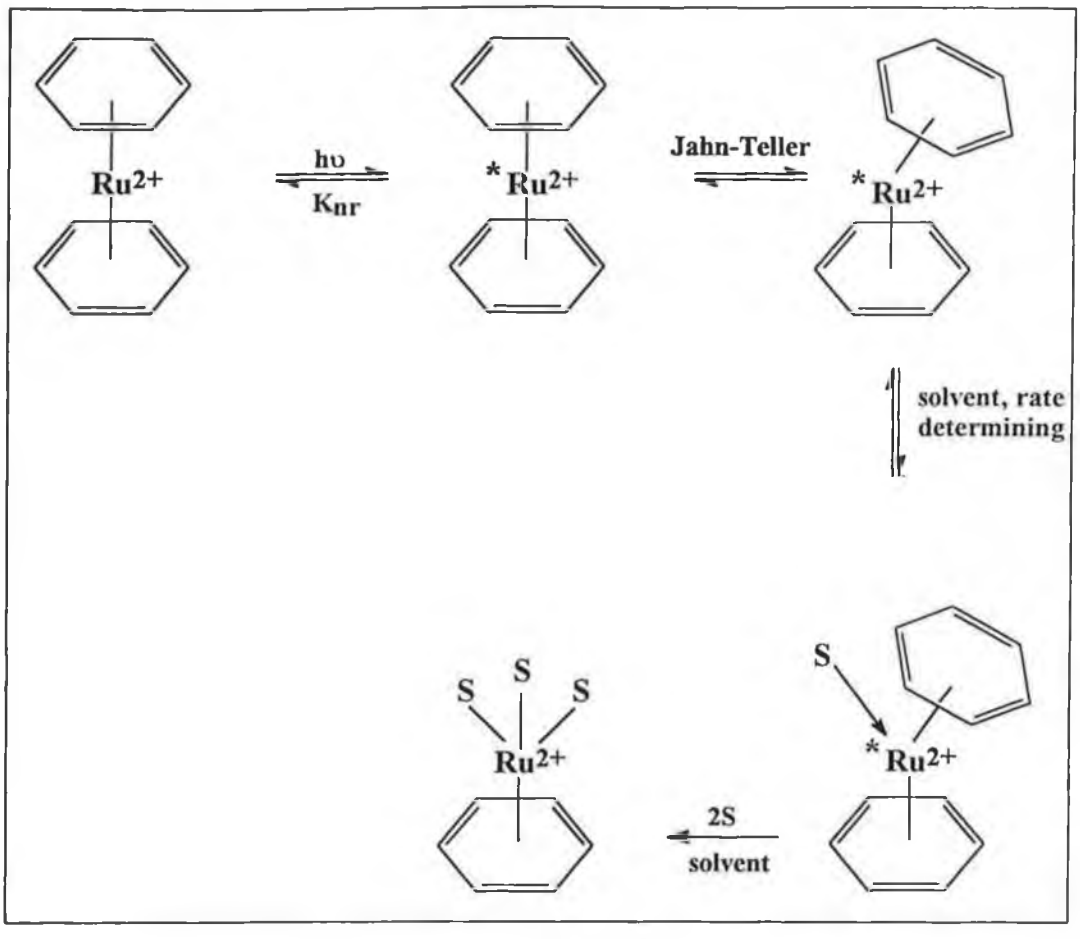
Ru2+
hυ
Knr
*Ru2+
Jahn-Teller
*Ru2+
solvent, rate
determining
S
S
S
Ru2+
S
*Ru2+
2S
solvent

3.2 UV/vis Monitored Steady State Photolysis of $[(\eta^6\text{-benzene})_2Cr]^+$

As in previous work on this system initial studies were conducted using UV/vis monitored photolysis of the complex. The samples were irradiated at a variety of wavelengths ($\lambda > 400$ nm, $\lambda > 340$ nm, or $\lambda > 270$ nm). The results were qualitatively the same for each of these wavelengths. The result of irradiation of DBC^+ with either chloride or iodide as the counterion is shown in Figure 3.2. The depleted bands are those of the parent complex while the increase in absorbance at 254 nm coincides with the absorption spectrum of uncoordinated benzene. The spectra obtained in both degassed and aerated systems are identical. Presumably any formation of the neutral species (DBC) is not observed in degassed solution due to its insolubility in water. In order to check that the neutral species was indeed formed a range of similar experiments were carried out in acetonitrile.

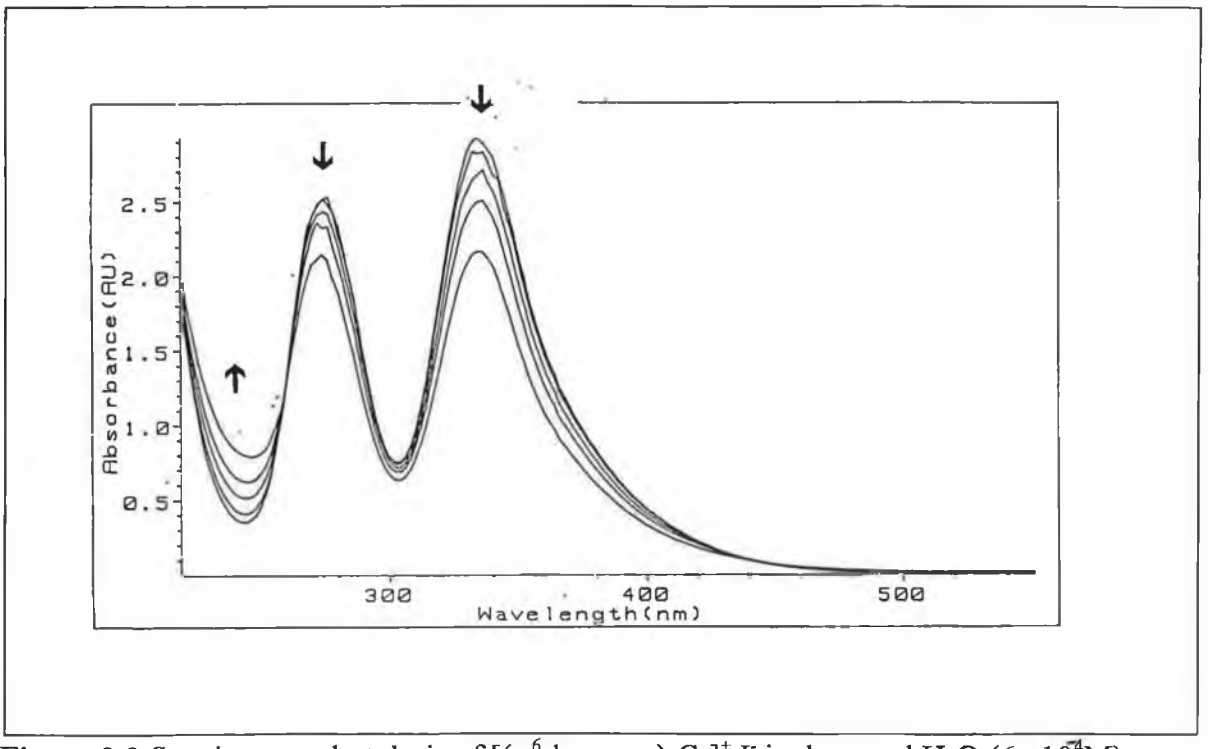

Figure 3.2 Steady state photolysis of $[(\eta^6\text{-benzene})_2Cr]^+ I^-$ in degassed H_2O (6×10^{-4}M) $\lambda_{irrad} > 340$ nm

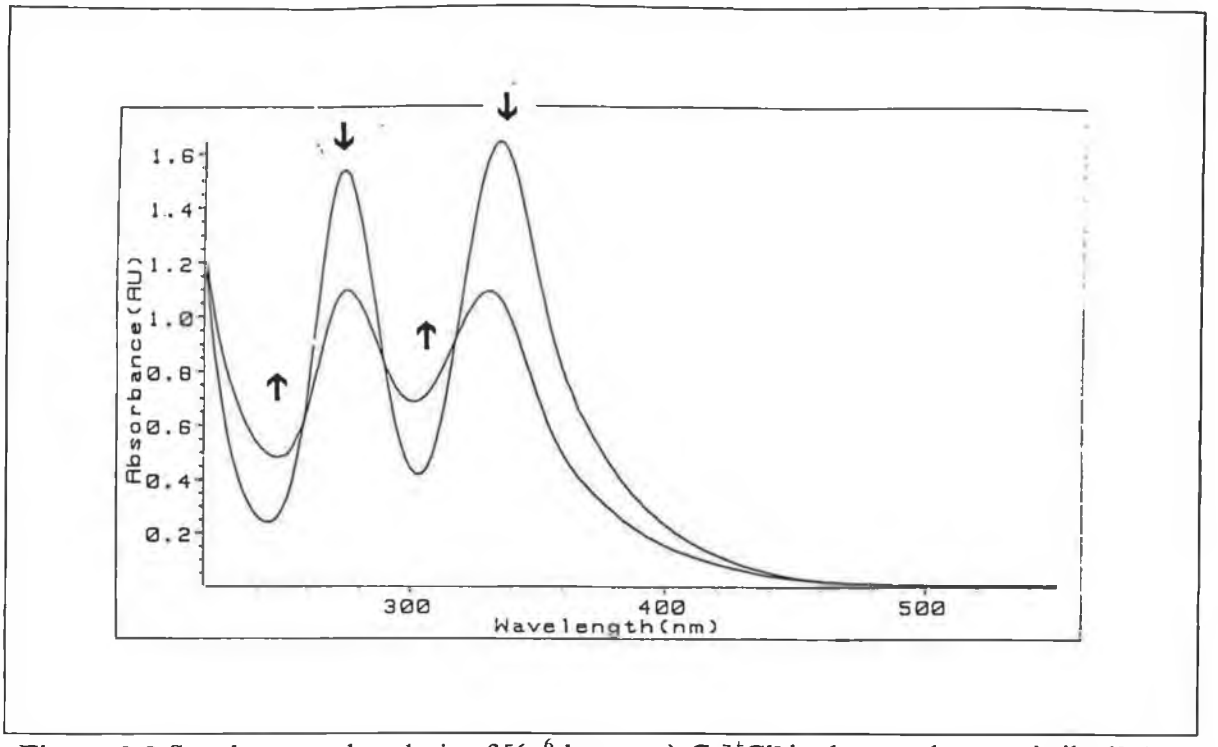

Figure 3.3 Steady state photolysis of $[(\eta^6\text{-benzene})_2Cr]^+Cl^-$ in degassed acetonitrile (2.9 x 10^{-4}M), $\lambda_{irrad} > 340$nm.

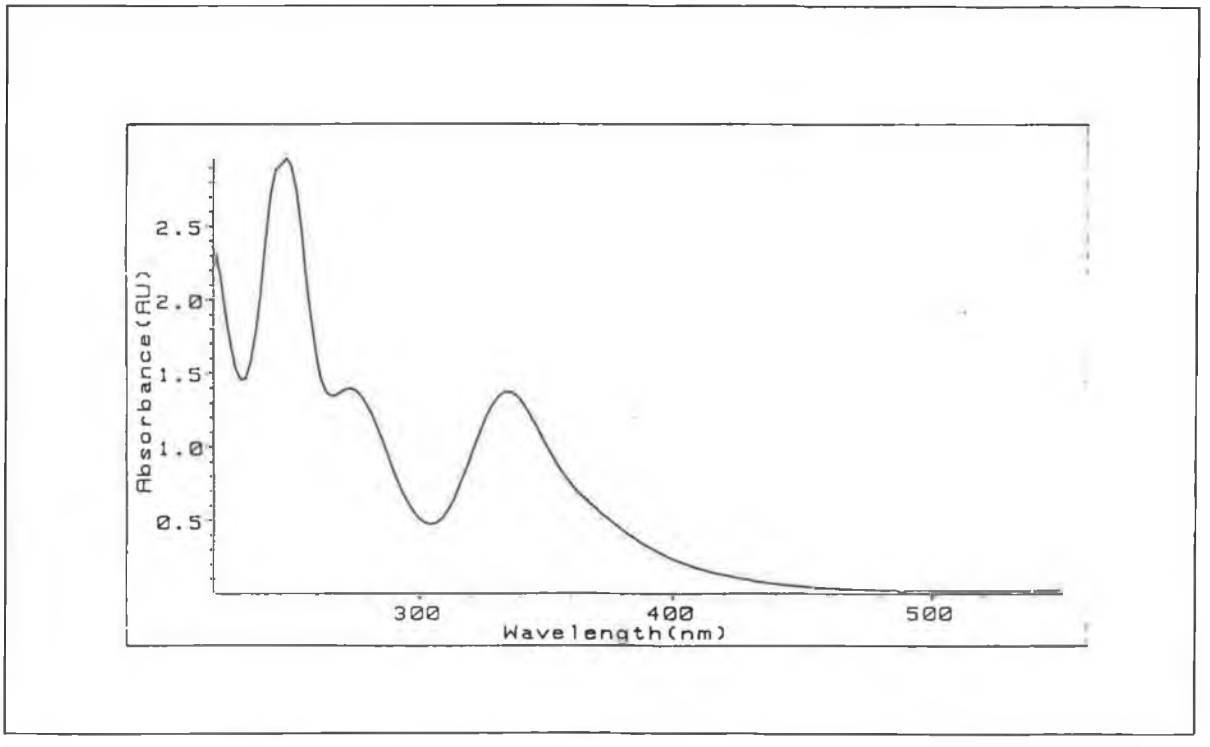

Figure 3.4 UV/vis Spectrum of $[(\eta^6\text{-benzene})_2Cr]^+I^-$ in acetonitrile (~4 x 10^{-4}M)

Figure 3.3 presents the spectra obtained on irradiation of $DBC^+ Cl^-$ in degassed acetonitrile. Again the parent bands are depleted and the formation of benzene is observed by production of a band at 254 nm. The production of a band at 310 nm is consistent with the generation of the neutral species. In aqueous solution the spectra of the chloride and the iodide salt are almost identical, however in acetonitrile the spectrum of DBC^+ is dependent on the nature of the anion. Figure 3.4 shows the absorption spectrum of DBC^+I^- in acetonitrile. There is a slight shift in the λ_{max} absorbances to lower energy in the acetonitrile as compared with aqueous solution. The new absorbance seen at 250 nm is assigned to the iodide ion. Upon photolysis of DBC^+I^- in degassed acetonitrile (Figure 3.5) formation of benzene is obscured by the absorbance of the counterion, however the DBC formation can be monitored under these conditions.

The results of the photolysis of $DBC^+ I^-$ in aerated acetonitrile are surprising however. From Figure 3.6 a complete shift to lower energy is observed in the spectra of the irradiated salt. The photoproduct(s) absorb at around 290 nm and 368 nm with an absorbance tail stretching out beyond 400 nm. Also the absorption band of the iodide ion reduces in intensity. The product under these conditions appears to be I_2 as the absorption bands at 290 and 368 nm correspond exactrly to those of I_2 (Figure 3.7) Reaction 3.3 presents a suggested route for the irradiated DBC^+I^- in aerated acetonitrile. The formation of the neutral species is obscured by the absorption of the iodine. The quantum yield for the formation of I_2 at 254 nm is 0.29 in water and 0.75 in acetonitrile[15] which explains thereduced significance of iodine formation in the aqueous solution. In the presence of oxygen the solvated electron is scavenged and I_2 formed. In the absence of oxygen the process is reversible.

Reaction 3.3

$$I^- \xrightarrow{h\upsilon} I^\circ + e^-_{MeCN}$$

$$I^\circ + I^\circ \longrightarrow I_2$$

$$DBC^+ + e^-_{MeCN} \longrightarrow DBC$$

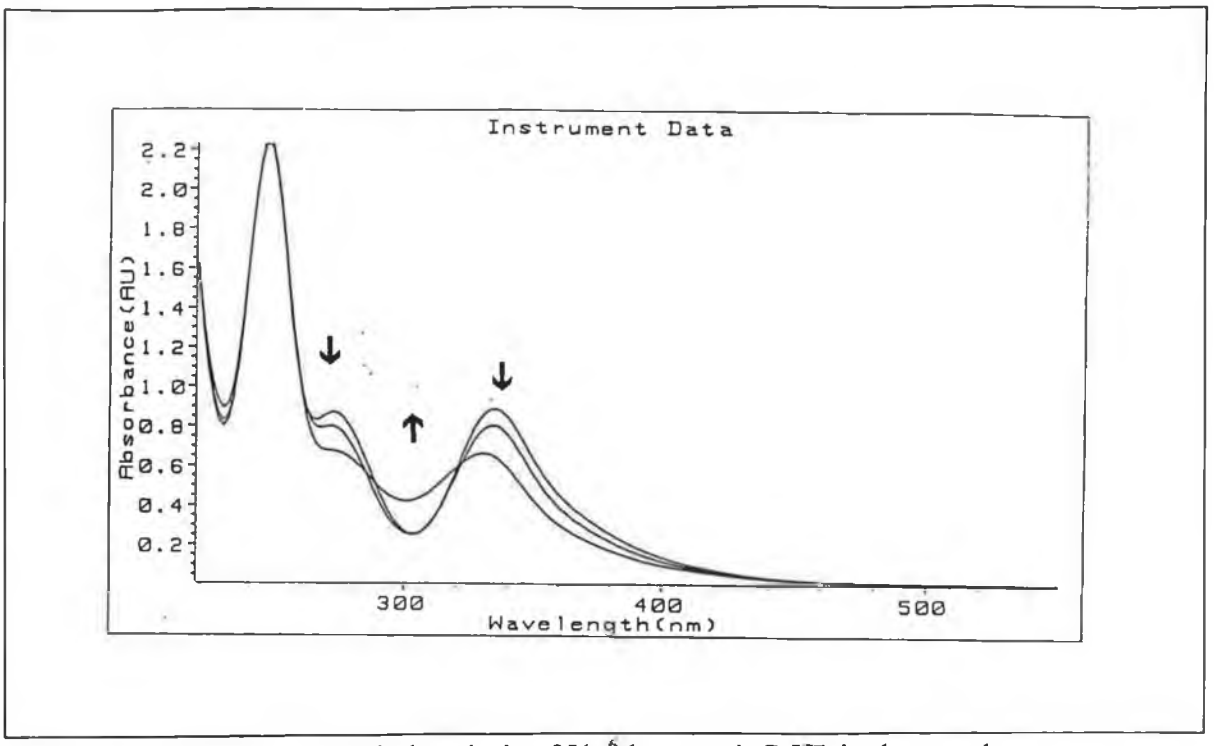

Figure 3.5 UV/vis monitored photolysis of $[(\eta^6\text{-benzene})_2Cr]^+I^-$ in degassed acetonitrile (~3 x 10^{-4} M), λ_{irrad} >340nm

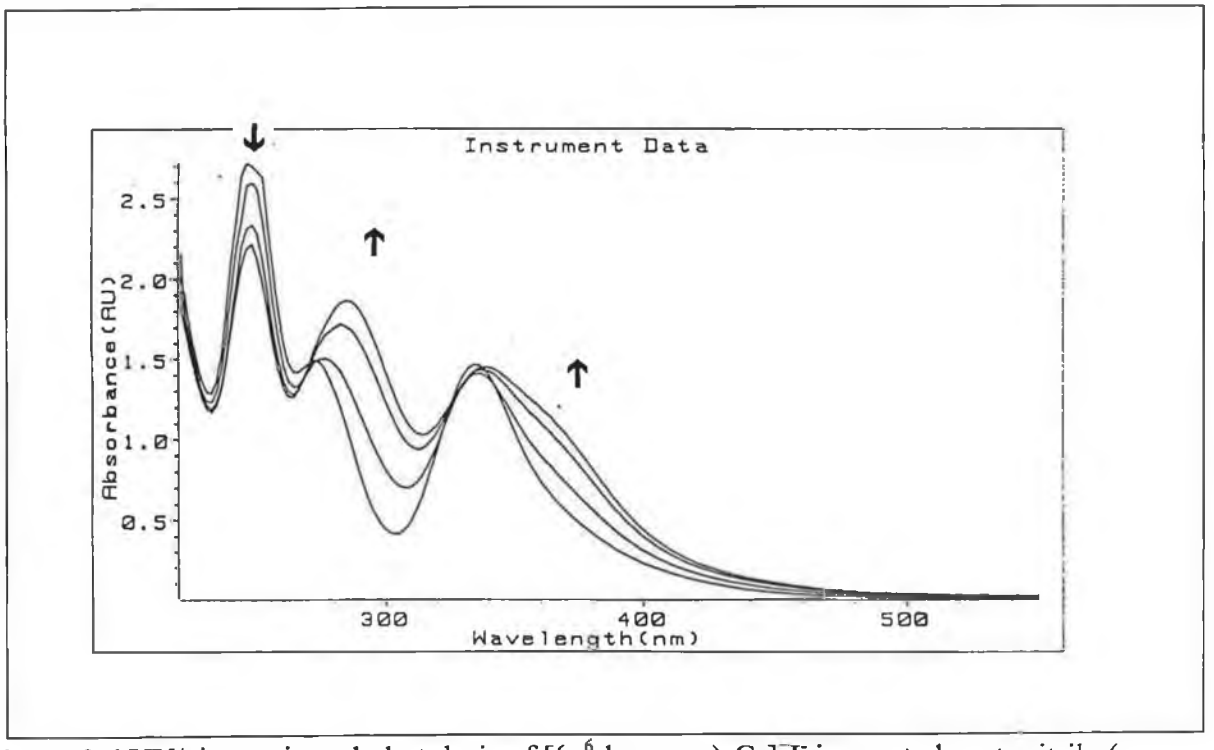

Figure 3.6 UV/vis monitored photolysis of $[(\eta^6\text{-benzene})_2Cr]^+I^-$ in aerated acetonitrile (~ 4 x 10^{-4}M), λ_{irrad} >340nm

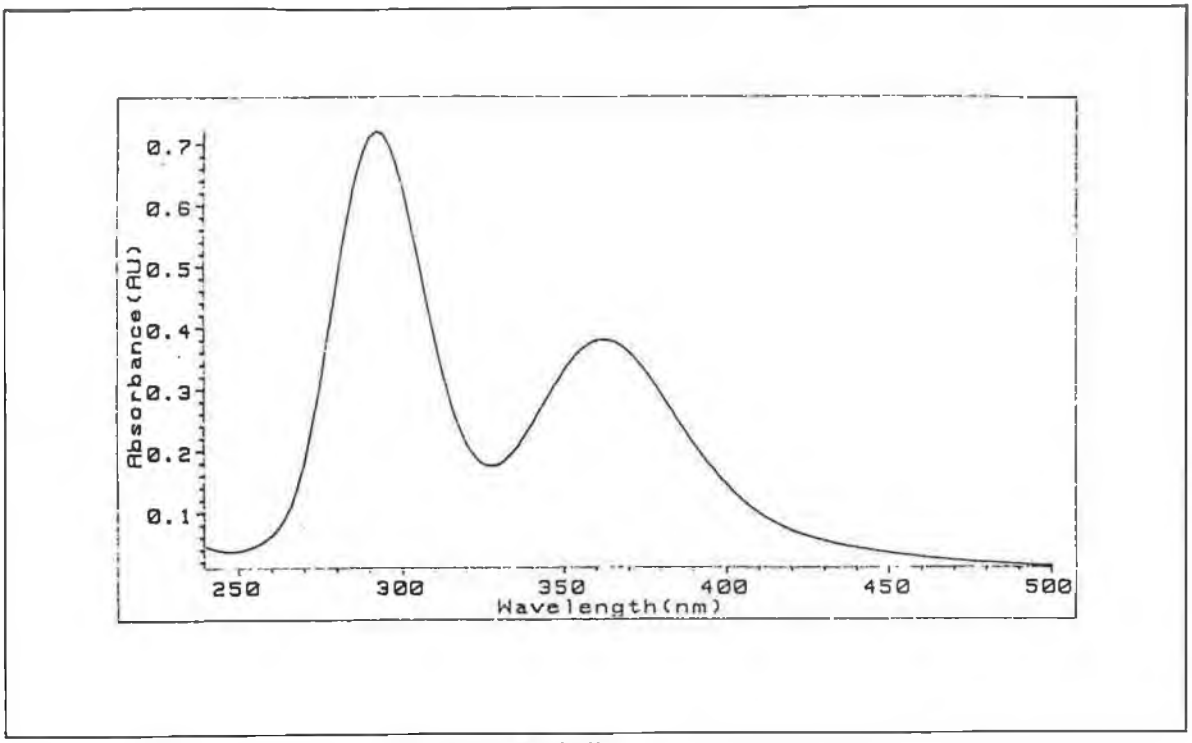

Figure 3.7 UV/vis spectrum of I_2 in acetonitrile.

3.3 Laser Flash Photolysis of $[(\eta^6\text{-Benzene})_2Cr]^+ I^-$

3.31 Flash photolysis of DBC^+I^- in degassed aqueous solution

The excitation of degassed aqueous solutions of DBC^+I^- with 355 nm photons resulted in a number of changes in the UV/vis absorbance of the sample in the range 300 nm to 400nm. A weak transient absorption is observed at 400 nm which decays to baseline as presented in Figure 3.8. The extinction of the transient decreases as the as the monitoring energy increases, so that at 340 nm (Figure 3.9) a step depletion of the parent (DBC^+) is observed immediately after the laser pulse followed by the slower decay of the intermediate. The decay of the intermediate is rapid ~ 6.5 μs. There is an increase in intensity centred at 310 nm as presented in Figure 3.10. The formation of this photoproduct is of the same time scale as the decay of the intermediate (~6.5μs). This increased intensity remains during the time scale of the experiment. From the results of the steady state photolysis experiments the long-lived photoproduct seen at 310 nm can be assigned to the neutral species (DBC). Traverso *et al.*[2] provided evidence for the formation of the Cr^+ ion upon photolysis using 2,2,bipyridine as a trapping ligand. It is plausible that the intermediate observed at 410 nm is the solvated Cr^+ ion. These results support the formation of DBC via a disproportionation reaction between DBC^+ and Cr^+ as shown in Reaction (4) of Reaction 3.1.

Using the 355 nm line of the laser should induce photochemistry from MLCT excited state consequently the excitation wavelength was changed to 266 nm to see if the photochemistry differed on excitation into the LMCT band. The transient signals obtained were more intense as would be expected because of the increased energy of the pulse and the increase in photochemical yields quantum yields at this wavelength. No change in the nature transient species was observed however. Unfortunately luminescence occurs at monitoring wavelengths below 330 nm when exciting with 266 nm and so results at the lower wavelengths were unavailable.

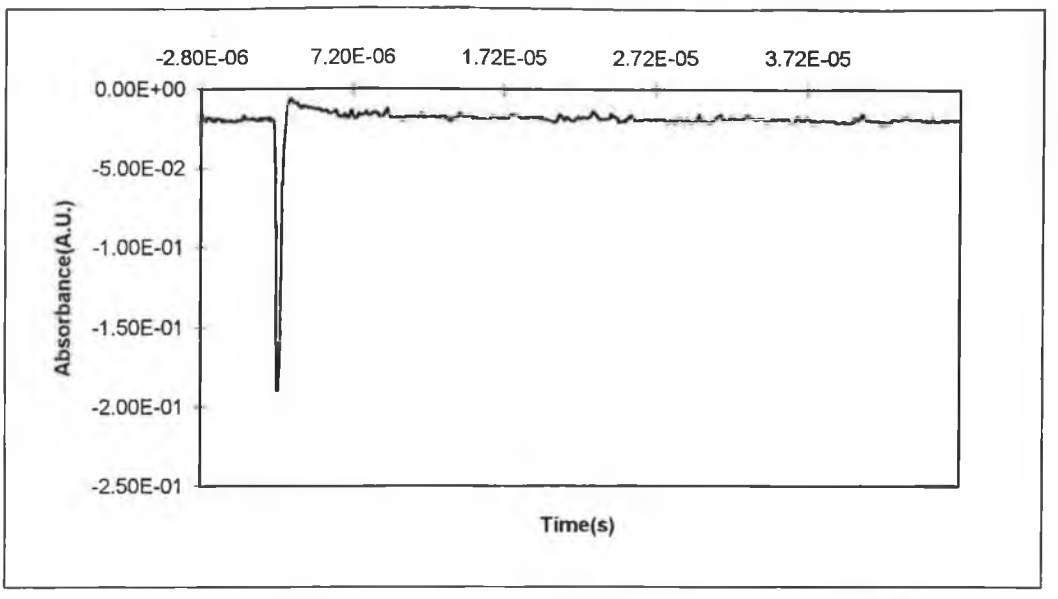

Figure 3.8 Transient observed at 400nm (λ_{exc} = 355 nm) for $DBC^{-}I^{-}$ in degassed acetonitrile.

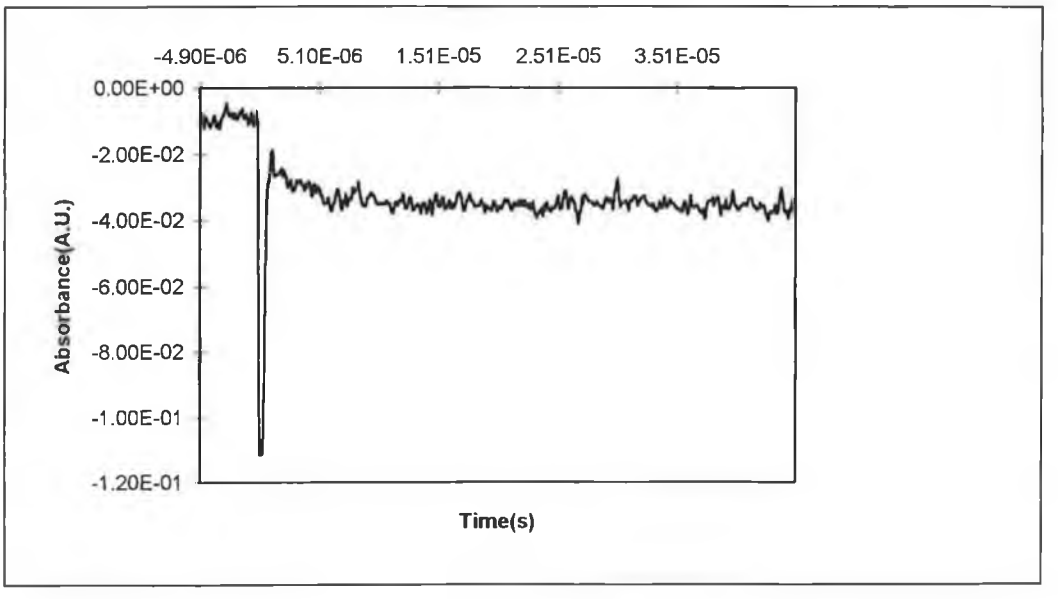

Figure 3.9 Trace at monitoring wavelength 340nm(λ_{exc} = 355 nm.) for DBC^{+} in degassed aqueous solution

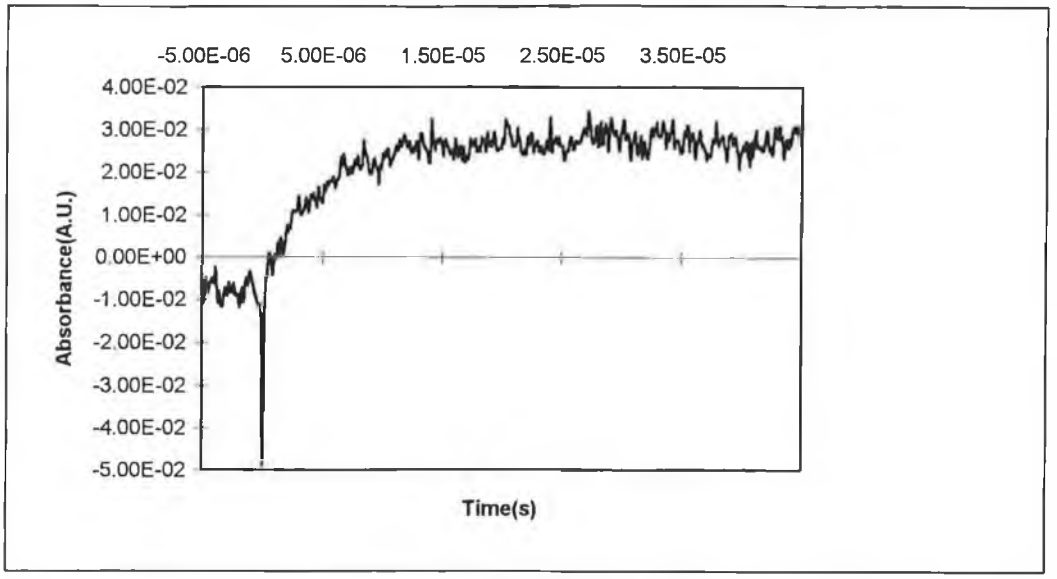

Figure 3.10 Trace at monitoring wavelength 310 nm(λ_{exc} = 355 nm) for DBC^+I^- in aqueous solution.

3.32 Flash photolysis of DBC^+I^- in aerated aqueous solution

The Proposed intermediate; Cr^+, is oxidised in the presence of oxygen and so flash photolysis experiments were carried out in aerated aqueous solution. A transient signal was observed in the monitoring region 400 nm to 330 nm. Figure 3.11 shows an example of this signal at monitoring wavelength 370 nm. The decay of the intermediate is slower than in the degassed aqueous system; ~22μs compared with ~ 6.5μs. This decay can be assigned to the oxidation of the intermediate species. Surprisingly DBC formation is also observed in the aerated system. At 310 nm monitoring wavelength a transient formation was observed (Figure 3.12) with a decay of ~19μs. Presumably this decay results from the oxidation of the neutral species to the cation DBC^+. The fact that DBC is formed in the aerated sample suggests that the DBC^+ competes with the O_2 for reaction with the intermediate.

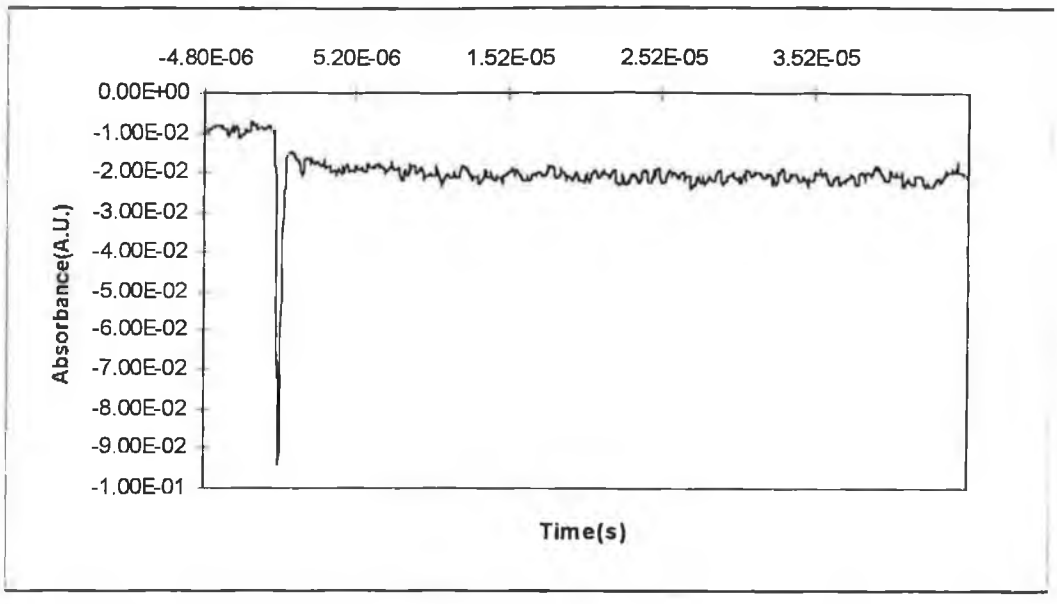

Figure 3.11 Trace at monitoring $\lambda = 370$ nm ($\lambda_{exc} = 355$ nm) DBC^{+} in aerated aqueous solution.

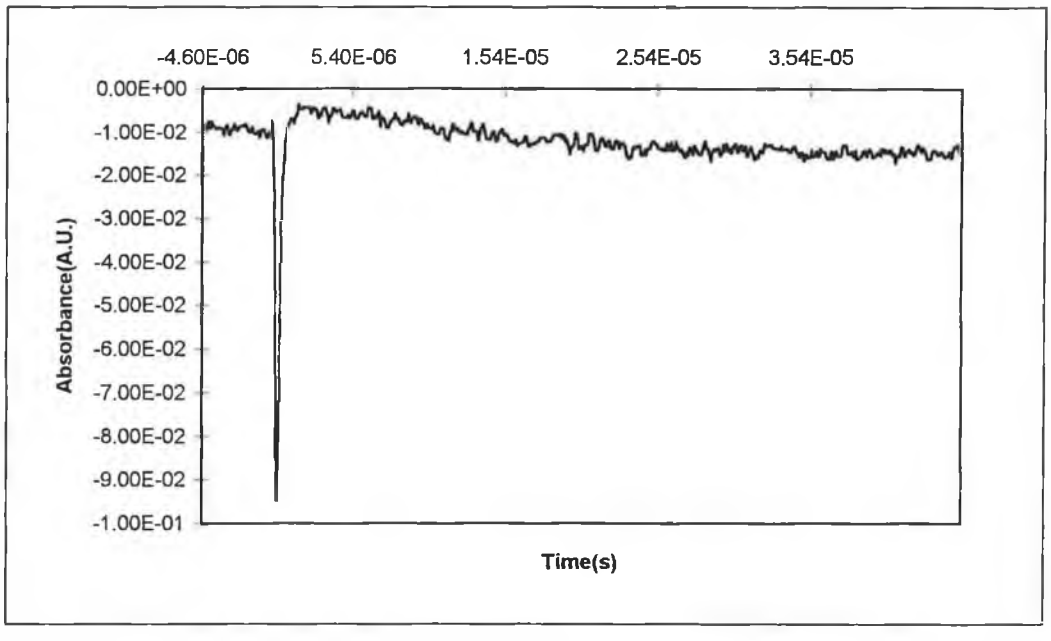

Figure 3.12 Transient at monitoring wavelength 310 nm ($\lambda_{exc} = 355$ nm) for $DBC^{\cdot}I^{-}$ in aerated aqueous solution.

3.33 Flash photolysis of DBC^+I^- in degassed acetonitrile solutions

The excitation of a degassed acetonitrile solution of DBC^+I^- resulted in transient signals which differed from those in aqueous solution. As for the degassed aqueous system a transient intermediate can be observed at 400nm as presented in Figure 3.13. At 370 nm (Figure 3.14) the extinction coefficient of the intermediate in the presence of acetonitrile is greater than that of the intermediate in aqueous solution, as no step depletion of the parent salt is observed here. The changes in the UV/vis spectrum of the solution were monitored regularly during the experiment and showed DBC^+ to be significantly more photosensitive in acetonitrile solution. This may explain the overall bleaching observed here. Centred at monitoring wavelength 310 nm (Figure 3.15) is a step increase in intensity immediately after the laser pulse, as in the degassed aqueous experiment this can be assigned to the formation of the neutral species. There is a further slower increase in intensity after the initial step formation which is not observed in the degassed aqueous solution. It is possible that the intermediate absorbs in this region of the spectrum also.

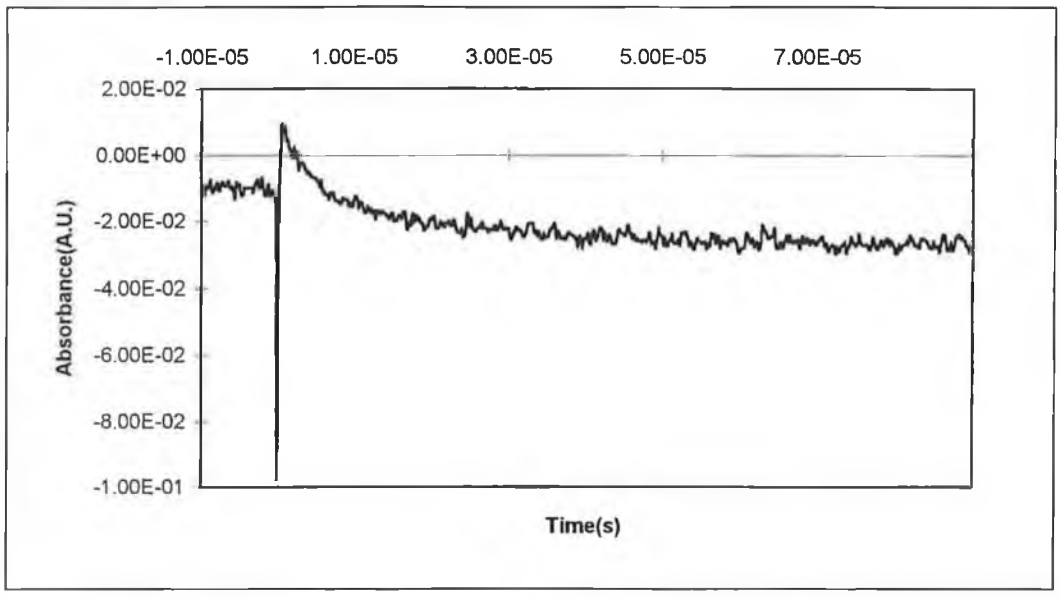

Figure 3.13 Transient at monitoring wavelength 400 nm (λ_{exc} = 355 nm) for DBC^+I^- in degassed acetonitrile.

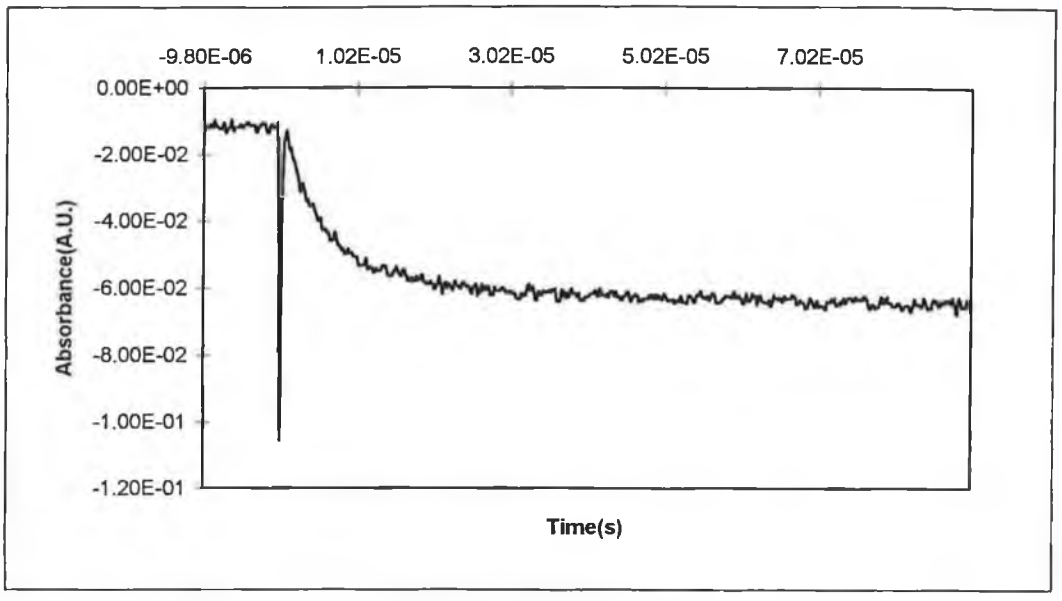

Figure 3.14 Trace at monitoring wavelength 370 nm (λ_{exc} = 355 nm) for DBC^+I^- in degassed acetonitrile

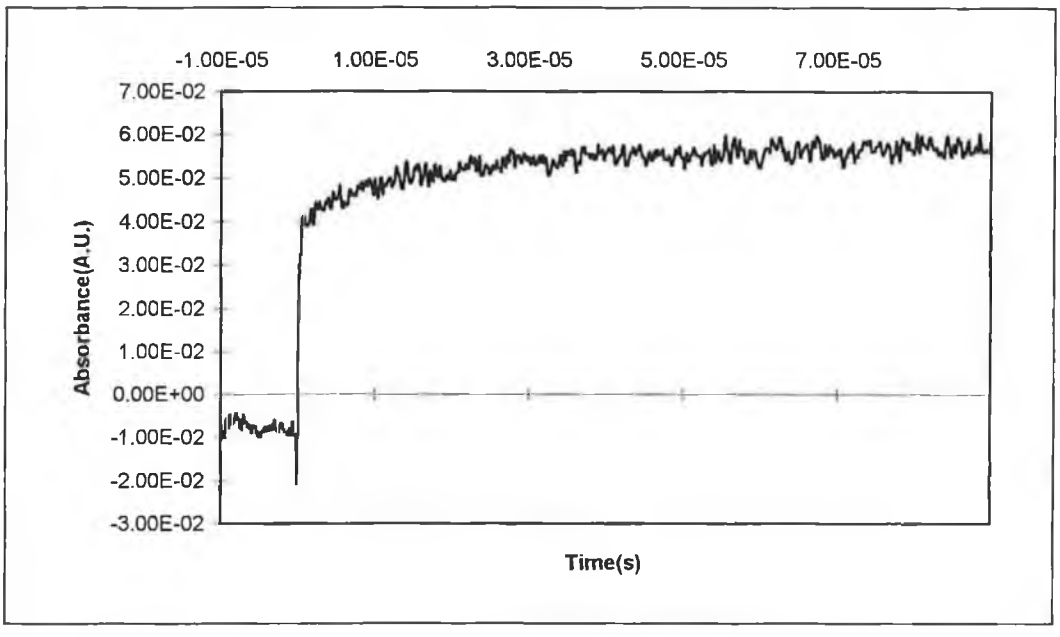

Figure 3.15 Trace at monitoring wavelength 310 nm (λ_{exc} = 355 nm) for DBC^+I^- in degassed acetonitrile.

These results suggest that the intermediate in the acetonitrile system differs from that in the aqueous system. This is further supported by the fact that, while in aqueous solution the k_{obs} for the decay of the intermediate does not vary with the concentration of the parent, the k_{obs} increases linearly with increasing DBC^- concentration. These results are presented in Table 3.2, and a graph of the relationship is shown in Figure 3.16

Acetonitrile		Water	
Conc. (10^{-4}M)	K_{obs} (10^4)	Conc. (10^{-4}M)	K_{obs} (10^4)
1.8	2.1	2.1	1.5
2.9	3.2	1.8	1.4
3.5	4.1	3.4	1.6
4.5	9.1	4.5	1.6

Table 3.2 Variation of K_{obs} with concentration of DBC^+ in degassed acetonitrile and degassed water.(λ_{exc} = 355 nm, $\lambda_{monitoring}$ = 400nm)

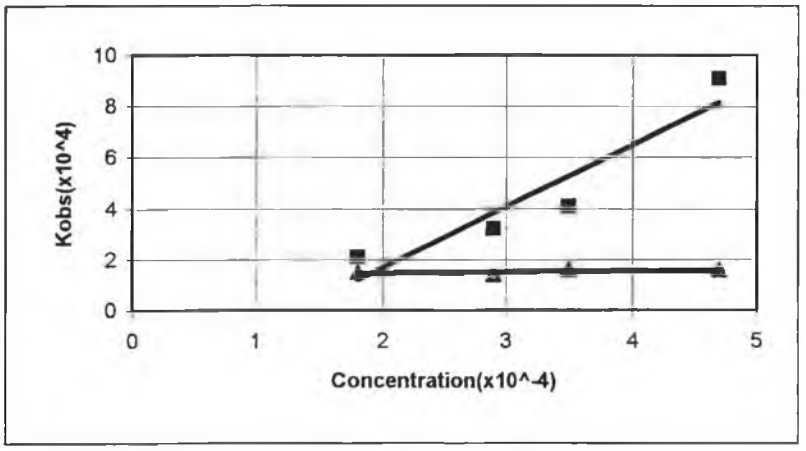

Figure 3.16 Graph of Concentration vs k_{obs} for DBC^+I^- (λ_{exc} = 355 nm, $\lambda_{monitoring}$ = 400 nm) .□ = Acetonitrile. Δ = Water

Again the 266 nm line of the laser was also employed for the experiments in acetonitrile solution. From Figure 3.17; the transient species monitored at 370 nm, it can be seen that the transient signal absorbs intensely. The decay of the transient signal appeared to follow a combination of first and second order decays.

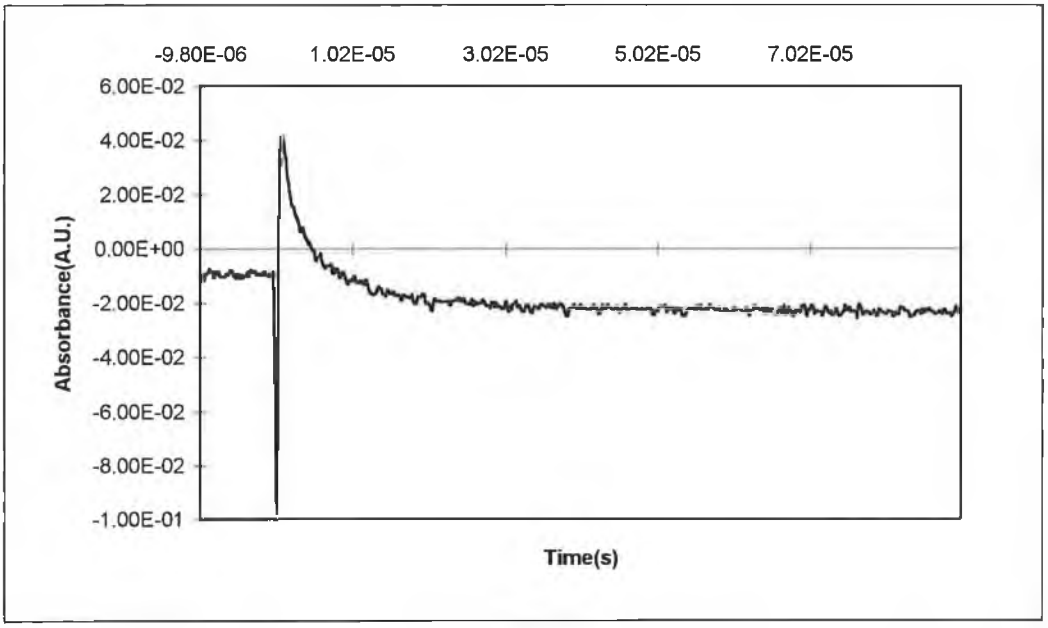

Figure 3.17 Transient at monitoring wavelength 370 nm (λ_{exc} = 266 nm) for $DBC^{+}I^{-}$ in degassed acetonitrile

The iodide ion absorbs in the region of 266 nm in acetonitrile, so its photochemistry needed to be considered under these conditions. To assess any iodide photochemistry a degassed acetonitrile solution of potassium iodide was excited with 266 nm photons and monitored between 400nm and 340nm. The results of this are presented in Figure 3.18. Analysis of the transient showed the decay to follow second order kinetics with a very rapid decay of 0.6μs. By comparison with the literature the transient species may be assigned to the iodide radical.[12] In the degassed system the formation of I° and a solvated electron is reversible.

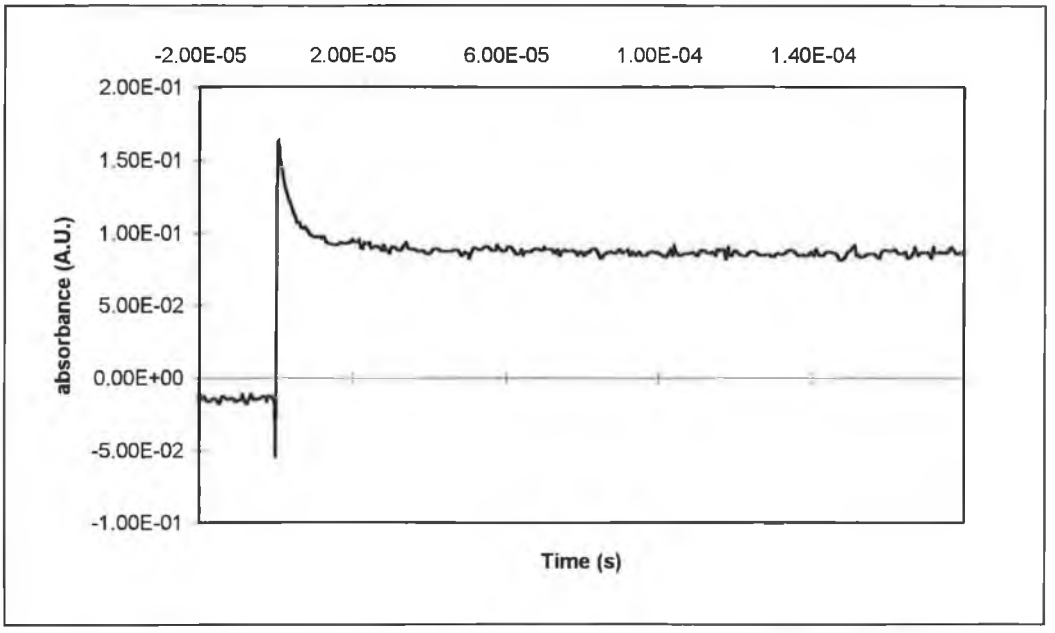

Figure 3.18 Transient at monitoring wavelength 370 nm (λ_{exc} = 266 nm) for potassium iodide in degassed acetonitrile.

3.34 Flash photolysis of DBC^+I^- in aerated acetonitrile solutions

The results of the flash photolysis experiment in aerated acetonitrile λ_{exc} = 355 showed the decay of a transient intermediate in a similar time scale to the decay observed in aerated aqueous solution. The transient decay time was ~ 21 μs and was not fully reversible as can be seen from the signal at 370 nm in Figure 3.19. No evidence for the formation of DBC is seen anywhere in the region of 300 nm. This is in contrast to the aqueous samples which showed a transient formation of the DBC. In the acetonitrile it would seem that the DBC^+ does not compete with the O_2 for reaction with the Cr^+. These results further support the proposal that the mechanism of the photochemistry of the DBC^+ in acetonitrile differs from that in aqueous solution.

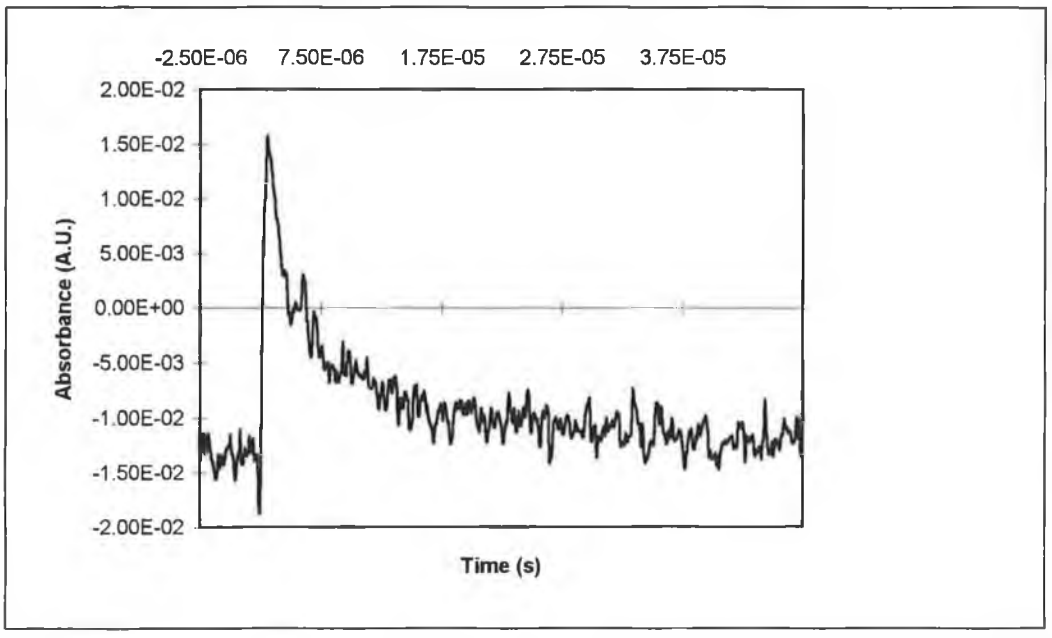

Figure 3.19 Transient at monitoring wavelength 370 nm (λ_{exc} = 355 nm) for $DBC^{+}I^{-}$ in aerated acetonitrile.

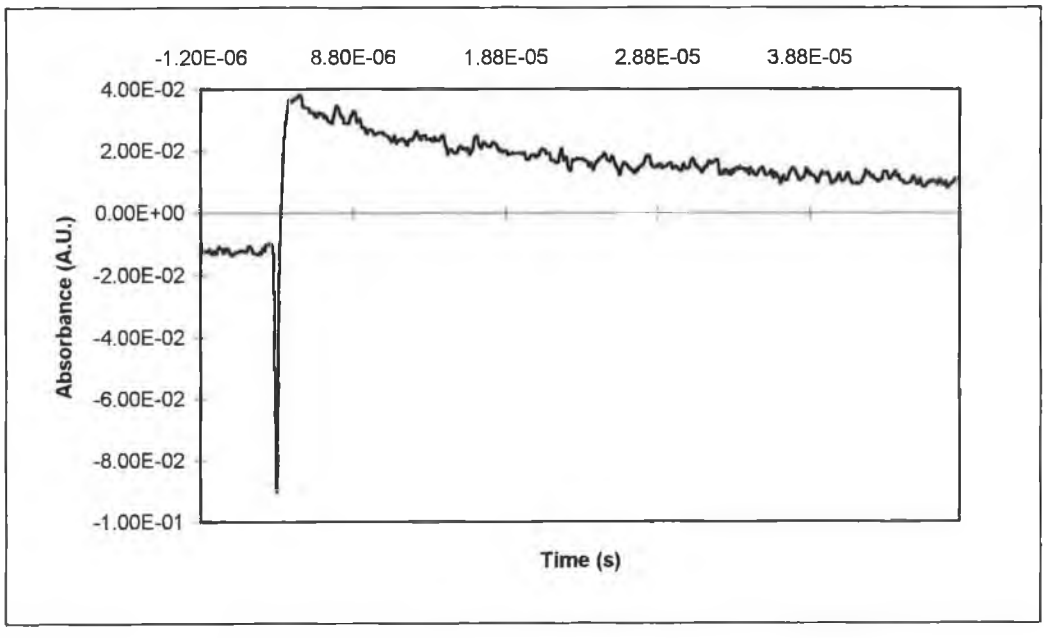

Figure 3.20 Transient at monitoring wavelength 370 nm (λ_{exc} = 266 nm) for $DBC^{+}I^{-}$ in aerated acetonitrile.

When this experiment was repeated with λ_{exc} = 266 nm a transient was observed which decayed but did not return to baseline in the time base of the experiment. This transient is seen at monitoring wavelengths between 400nm and 330 nm (Figure 3.20). These signals can be explained by the formation of a transient intermediate and it's decay overlaid with the formation of a long-lived photoproduct;

I_2.

3.4 Flash Photolysis of $[(\eta^6\text{-benzene})_2Cr]^+ Cl^-$

Preliminary laser flash photolysis experiments were carried out on the chloride salt. Degassed aqueous solutions were studied at λ_{exc} = 266 nm and λ_{exc} = 355 nm. Both excitation wavelengths yield similar results. The transients observed for the intermediate between 400 nm and ~ 340 nm were weak and it was not possible to establish kinetic data for the decay. As for the iodide salt the formation of the neutral species was observed at 310 nm (Figure 3.21). The accurate determination of the rate of formation was not possible from the transients obtained.

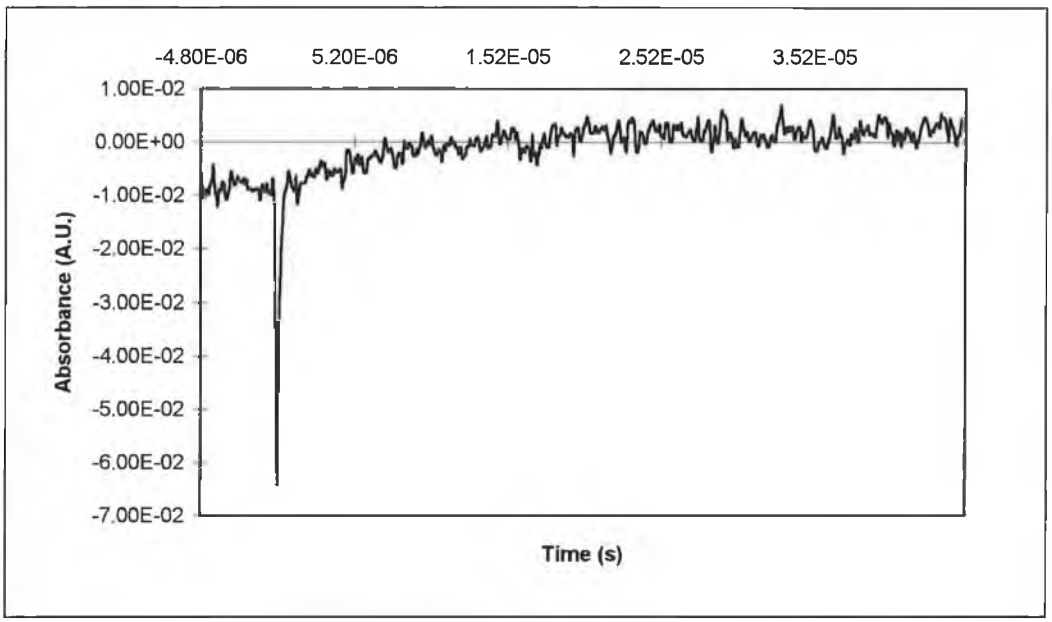

Figure 3.21 Transient at monitoring wavelength 310 nm (λ_{exc} = 355 nm) for $DBC^+ Cl^-$ in degassed acetonitrile.

DBC^+Cl^- was also studied in degassed acetonitrile λ_{exc} = 355 and 266 nm. In the acetonitrile medium the transient for the intermediate(s) was more intense and is presented in Figure 3.22. Again the decay of the intermediate appeared to be dependent on the concentration of the parent, however further concentration studies are necessary to confirm this. The transient presented in Figure 3.22 shows the formation of the neutral species as monitored at 310 nm. The transient is characteristics are similar to those of the iodide sample, probably due to the absorbance of the DBC being overlaid with the absorbance of the intermediate.

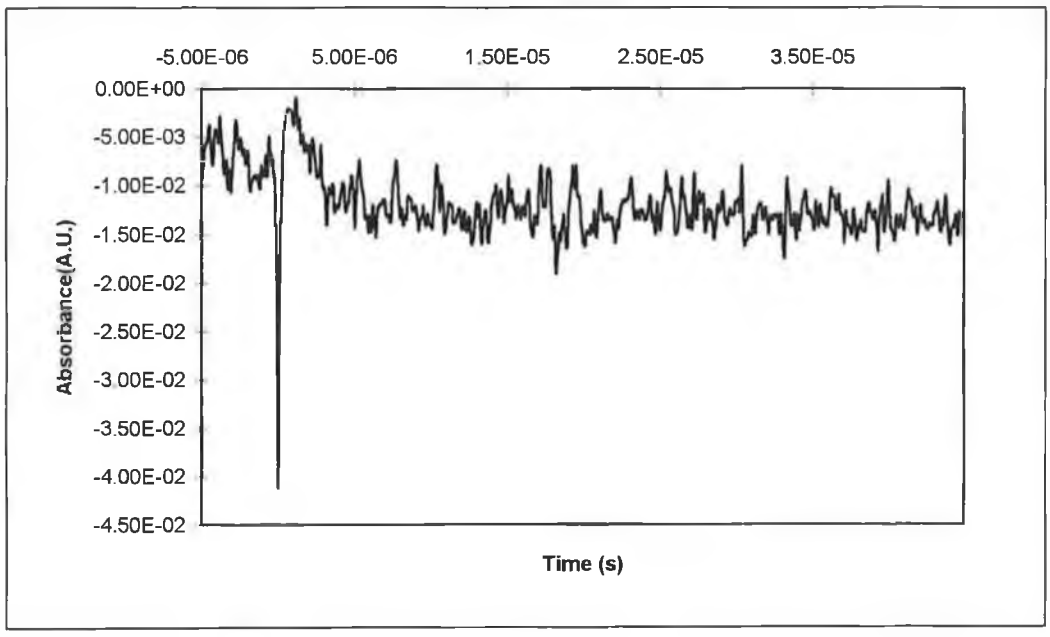

Figure 3.22 transient monitored at 400 nm (λ_{exc} = 355 nm) for DBC^+Cl^- in degassed acetonitrile.

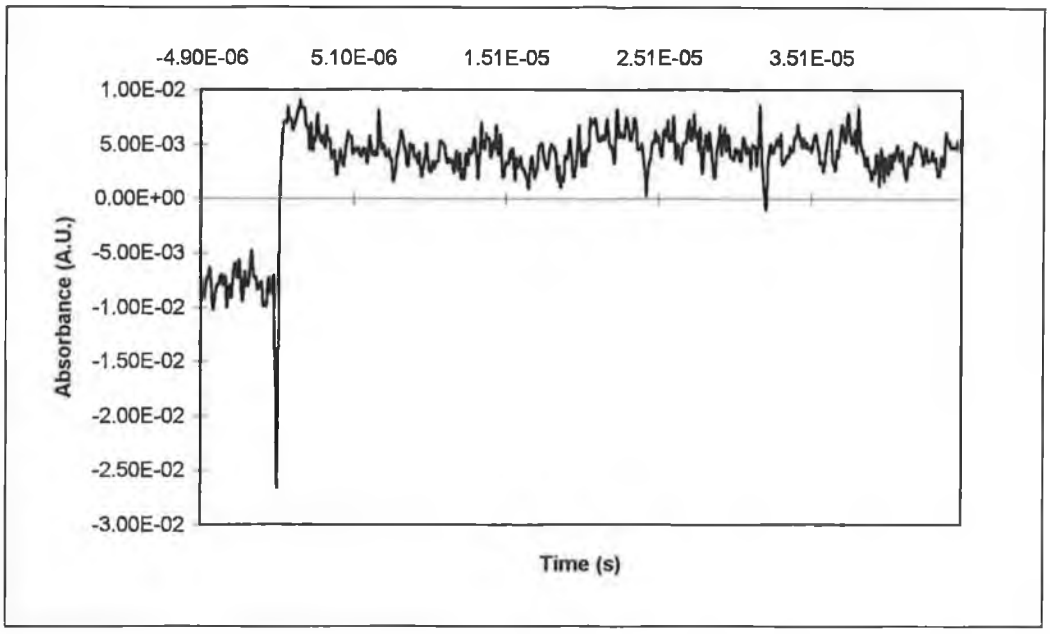

Figure 3.23 Transient monitored at 310 nm (λ_{exc} = 355) for $DBC^{+}Cl^{-}$ in degassed acetonitrile.

3.5 Conclusion

The results of steady state photolysis of DBC^+ in water and acetonitrile showed free benzene and the neutral species to be the dominant photoproducts. This results coincide with those proposed by Traverso *et al.*, however they provide no evidence as to the identity of the intermediate(s). In the case of $DBC^+ I^-$, irradiation in acetonitrile in the presence of oxygen resulted in the formation of I_2.

Traverso *et al.*[2] displayed the presence of the Cr^+ ion upon photolysis of DBC^+ in aqueous; the addition of 2,2-bipyridine prior to photolysis resulted in the formation of the violet $[Cr(bipy)_3]^+$ complex. The Cr^+ ion has also been established to occur upon photolysis of $[(\eta^6\text{-toluene})_2Cr]^+$ in acetonitrile.[12] Whether the arene deligation is associative or dissociative has not been established. The variation in the nature of the transient(s) on changing the solvent from water to acetonitrile shows the mechanism to be solvent dependent. Arene deligation has been attributed to nucleophilic attack of the metal centre by the solvent molecule.[11,14] The results here reflect a varying ability of the H_2O and the MeCN molecules to interact with the excited state.

Ludi *et al.* [11] proposed a reaction scheme for the photochemically induced solvation of sandwich compounds, as depicted in Reaction 3.2. As the decay of the transient in aqueous solution was independent of the concentration of the parent complex it is plausible that the solvation of the DBC^+ is the rate determining step as depicted in the proposed mechanism in Reaction 3.4. In the case of the acetonitrile system the decay of the intermediate is dependent on the concentration of the parent complex. The second order rate constant for the photolysis of $(\eta^6\text{-arene})_2Ru^{2+}$ in acetonitrile was 10 times greater than that in H_2O, so the solvation of the Cr centre would in more rapid in the acetonitrile system than in the aqueous system. It is proposed that the acetonitrile solvated intermediate is more stable than the aqueous intermediate and so parent concentration would be influential in the disproportionation reaction.

The solvated Cr^+ ion has been identified as a photoproduct following steady state photolysis of Cr^+ sandwich complexes in both aqueous[2] and acetonitrile[12] solution. It is possible however, that the intermediate is the half sandwich solvated ion, with only one

arene ring being lost upon excitation. Upon LF excitation the metal- arene bond would be expected to lengthen and so it must also be considered that deligation of the arene rings may be dissociative with the rate limiting step being the solvation of a half sandwich intermediate. In the analogous ruthenium systems $^1H_1$ NMR monitored photolysis showed the formation of $(\eta^6\text{-arene})Ru(solvent)_3^{2+}$ initially, further photolysis yielded the hexasolvated ion. The DBC^+ complex is paramagnetic so NMR cannot be employed in elucidation of the intermediates. The identity of the intermediate still remains unknown, however a proposed reaction mechanism is presented in Reaction 3.4.

Reaction 3.4

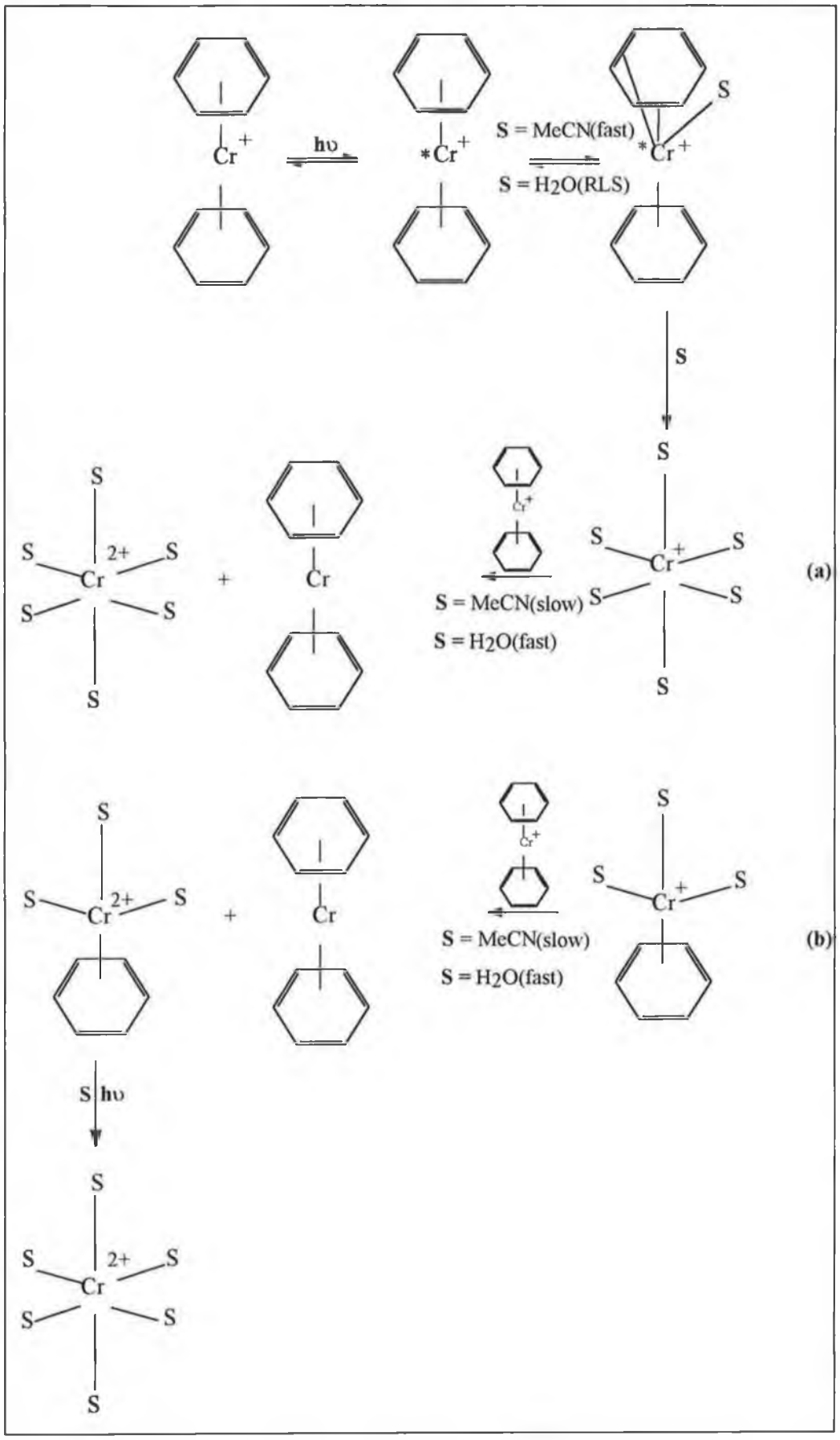

3.6 Relationship Between the Ground State Electronic Structure and the Photochemistry of DBC and DBC^+

The elucidation of the ground and excited states for both DBC and DBC^+ has been discussed in the literature survey. While DBC^+ has an extensive photochemistry the neutral species exhibits no photochemistry.[2] The photochemistry of DBC^+ has been presumed to originate from a CT transition[4], as irradiation into the low energy LF absorption resulted in no observable photochemistry. However DBC also displays CT transitions in the visible region of UV/vis region of the spectrum. The arrangement of the molecular orbitals is the same in both molecules, but the cation is stabilised by ~ 5-6 eV for each level.[3] The population of the MO can be summarised in Figure 3.25.

The $a_1 \rightarrow e_1$ LF transition in the neutral species which is observed at ~ 640 nm involves both depopulation and population of orbitals which are nonbonding with respect to the metal arene bond, and so would have no influence on the bonding characteristics. A second LF transition ($e_2 \rightarrow e_1$) has been calculated by Weber[3] to occur in the region of 400 nm. However this is in the region of more intense CT transitions, so it is possible that while the CT excited states are efficiently populated the LF transition is not. In the case of the cation, the LF transition from $e_2 \rightarrow a_1$, is the lowest energy absorption feature (~ 1180 nm), and is not obscured by other transitions. Both theoretical calculations and PES [3,15] studies have shown that the e_2 orbital is the main contributor to the metal arene bond, and so depopulation of this energy level would have implications for the metal arene bond. It is plausible that the LF excited state is populated *via* an internal conversion from a higher energy MLCT excited state, ultimately resulting in arene loss. This would rationalise the differences in the photochemistry between the neutral and the cationic species.

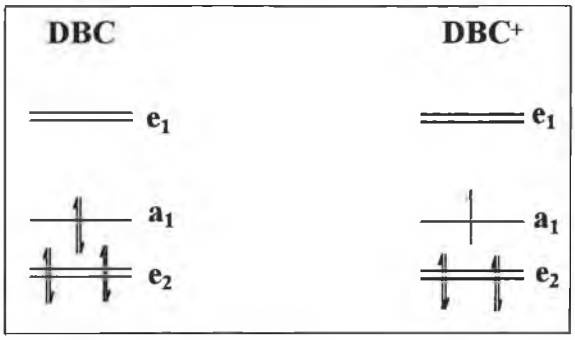

Figure 3.25 Ground-state configurations for $(\eta^6\text{-benzene})_2Cr$ and $(\eta^6\text{-benzene})_2Cr^+$

References

[1] Gilbert, A.; Kelly, J. M.; Budzwait, M.; Koerner von Gustorf , E.; *Z. Naturforsch* **31b**, 1091, 1976.

[2] Traverso, O.; Scandola, F.; Balzani, V.; Valcher, S.; *Mol. Photochem.* **1**, 289, 1969.

[3] Weber, J.; Geoffroy, M.; Goursot, A.; Penigault, E. J.; *Amer. Chem. Soc.* **100**, 3995, 1978.

[4] Geoffroy, G. L.; Wrighton, M. S.; *Organometallic Photochemistry*, Academic Press, New York, 1979.

[5] Gill, T. P.; Mann, K. R.; *Organometallics* **1**, 485, 1982.

[6] Schrenk, J. L.; Palazzotto, M.C.; Mann, K.R.; *Inorg. Chem.* **22**, 4047, 1983.

[7] McNair, A. M.; Schrenk, J. L.; Mann, K. R.; *Inorg. Chem.* **23**, 2633, 1984.

[8] Schrenk, J. L.; Mann, K.R.; *Inorg. Chem.* **25**, 1906, 1986.

[9] Schrenk, J. L.; McNair, A. M.; McCormack, F. B.; Mann, K. R.; *Inorg. Chem.* **25**, 3501, 1986.

[10] Gamble, G.; Grutsch, P. A.; Ferraudi, G.; Kutal, C.; *Inorg. Chim. Acta.* **247**, 5, 1996.

[11] Karlen,T.; Hauser, A.; Ludi, A.; *Inorg. Chem.* **3**, 2213, 1994.

[12] Gamble, G. Kutal C.; *Polymers for Advanced Tech.*, **5**, 63, 1994.

[13] Adamson, A. W.; Fleischauer P. D.; *Concepts of Inorganic Photochemistry,* Wiley and Sons, New York, 1975.

[14] Weber, W. Ford, P. S.; *Inorg. Chem.*, **25,** 1088, 1986.

[15] Guest, J. C.; Hillier, I. H.; Higginson, B. R.; Llyod, B. R.; *Mol. Phys.* **29**, 113, 1975.

CHAPTER 4

The Photochemistry of [(η^6-*cis* and *trans*-1,2-diphenyl ethene)($Cr(CO)_3)_2$]

4.1 Introduction

In the pentaammineruthenium (II) complexes of pyridine and its analogues Ford *et al.*[1] assigned the absorption in the visible region of the UV/vis spectrum to a metal to ligand charge transfer (MLCT) transition. This initiated an interest in compounds exhibiting low-lying MLCT excited states, in particular complexes of the type $[W(CO)_5L]$, where L is a Lewis base.[2] If L has low lying π acceptor orbitals then a low energy MLCT transition is possible.

Photoreaction studies of $[W(CO)_5(pyridine)]$ at room temperature showed the quantum yields for the reactions 4.1 and 4.2 to be wavelength dependent.[3] (Φ_{CO} = 0.002 at 436 nm and 0.04 at 254 nm; Φ_L = 0.34 at 254 nm and 0.63 at 436 nm). Irradiation at lower energy causes more efficient ligand loss but less efficient CO loss. The photochemistry of $[W(CO)_5(pyridine)]$ and $[W(CO)_5(3,bromopyridine)]$ was investigated in an argon matrix at 12 K.[4] Upon irradiation at 320 nm < λ < 390 nm the photoproduct was $W(CO)_5$. Further irradiation at longer wavelengths resulted in regeneration of the parent complex and depletion of the photoproduct. Unfiltered irradiation resulted in free CO along with lower order metal carbonyl fragments. These results were consistent with reactions observed in solution.[3]

Reaction 4.1

$$[W(CO)_5L] \xrightarrow{h\nu} [W(CO)_4L] + CO$$

Reaction 4.2

$$[W(CO)_5L] \xrightarrow{h\nu} [W(CO)_5] + L$$

Wrighton *et al.* showed how variation of the substituents on the pyridine ring could be used to "fine tune" the excited states and the photochemical properties of the $[W(CO)_5L]$ systems. Spectral data showed that the tungsten to pyridine CT state moved to lower energy as the electron withdrawing nature of the substituents increased. The quantum yield for pyridine displacement upon irradiation into the lowest lying absorption

band was a function of the nature of the lowest energy excited state be it LF or MLCT in character.

While $[W(CO)_5(pyridine)]$ undergoes efficient photoinduced pyridine-loss, the analogous *trans*-4-styrylpyridine complex has a far less efficient ligand loss.[3] This reduced quantum yield for pyridine loss is because of competing *cis* to *trans* isomerisation of the ligand. Upon irradiation at 436 nm the quantum yields were; $\Phi_{pyr\text{-}loss} = 0.16$, $\Phi_{cis \rightarrow trans} = 0.31$. The isomerization was proposed to occur from an IL triplet state, arising from internal conversion from the lowest lying LF excited state.

The photochemistry of $(\eta^6$-*cis* and *trans*-1,2-diphenylethene$)Cr(CO)_3$ has been investigated previously.[5] The primary photoprocess for the *cis* isomer was found to be *cis* to *trans* isomerisation. The photochemistry of the *trans* isomer was found to be wavelength dependent; long wavelength irradiation resulted in unique ligand loss while short wavelength irradiation resulted in CO loss.

4.2 Results and Discussion

4.21 NMR characterisation of [(η^6-*cis* and *trans*-1,2-diphenylethene) ($Cr(CO)_3)_2$]

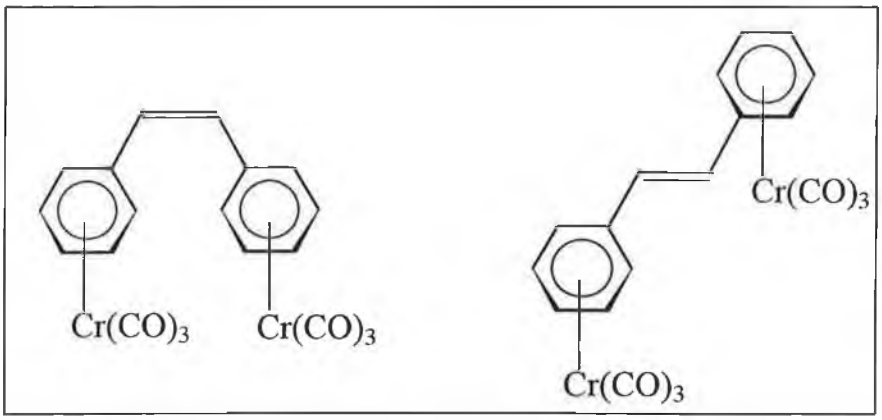

[(η^6-*cis* and *trans*-1,2-Diphenylethene)($Cr(CO)_3)_2$]

The proton ^1H NMR for the *trans* and *cis* complexes are presented in Figures 4.1 and 4.2 respectively. The low solubility of the *trans* complex-isomer explains the poor quality of the spectrum in Figure 4.1. In the *trans* isomer resonances for the phenyl rings appear between 5.6 and 5.9 ppm, these are assigned as being the protons ortho(o) meta(m) and para(p) to the vinylic group. The singlet at 6.9 ppm is attributed to the vinylic protons. Similar assignments are made for the *cis* isomer, however the protons ortho and meta to the vinylic group are equivalent in this instance.

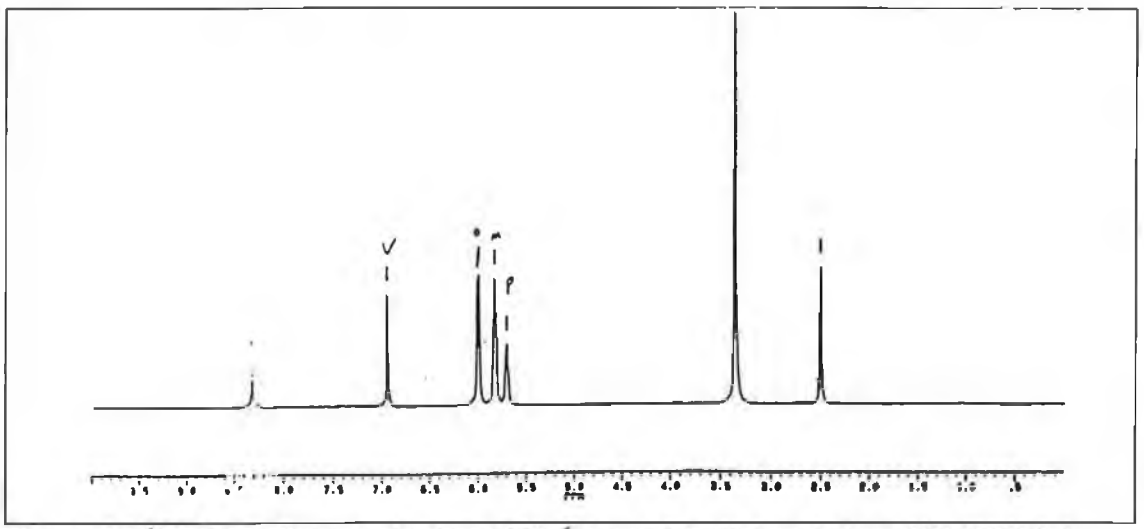

Figure 4.1 ^1H NMR Characterisation of [(η^6-*trans*-1,2-diphenylethene)($Cr(CO)_3)_2$]

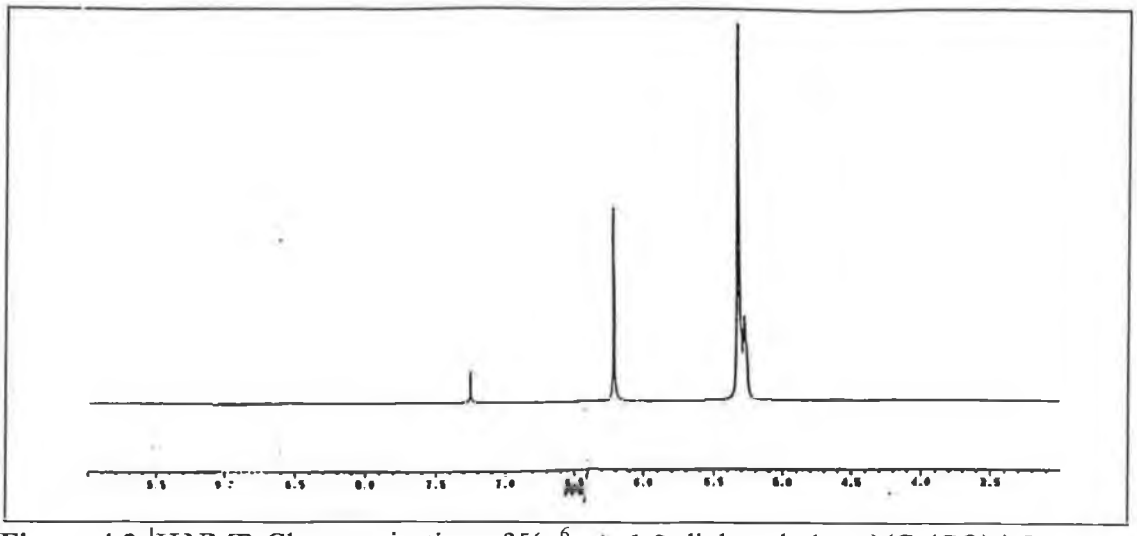

Figure 4.2 ^{1}H NMR Characterisation of [(η^6-*cis*-1,2-diphenylethene)($Cr(CO)_3)_2$]

4.22 Electronic absorbance spectrum of [(η^6-*cis* and *trans*-1,2-diphenylethene) ($Cr(CO)_3)_2$]

The UV/vis spectra for [(η^6-*cis* and *trans*-1,2-diphenylethene)($Cr(CO)_3)_2$] are presented in Figure 4.1. The *trans* complex exhibits a λ_{max} at ~290 nm, which can be assigned to the chromium → arene CT transition with some chromium → π^* CO CT character.[6] This is not typical of (η^6-arene)$Cr(CO)_3$ type complexes as they usually have a window in the 300 nm region of the absorbance spectrum. The *cis* complex does have this window at 300 nm , the λ_{max} shifting to longer wavelength. This is also assigned to a chromium → arene transition with some chromium → π^* CO character.

The *cis* isomer has a shoulder at ~260 nm which is assigned to a M —> π^* CO CT transition. This is not observed in the *trans* isomer, however the shoulder on the high energy side of the λ_{max} may be attributed to this. The absorbance of both these isomers, particularly the *trans* isomer stretches well into the visible region of the spectrum. The electron withdrawing nature of the vinylic group between the phenyl in the *cis* and *trans* ligands results in low-lying acceptor orbitals in the ligand, and so a low energy MLCT excited state is expected. The absorption maxima at ~430 nm and ~460 nm for the *cis* and *trans* isomer respectively are thought to be MLCT transitions.

MLCT excited states are known to be solvent sensitive[7], and increasing the solvent polarity caused a blue shift in these low energy absorption bands, as depicted for the *cis* isomer in Figure 4.5

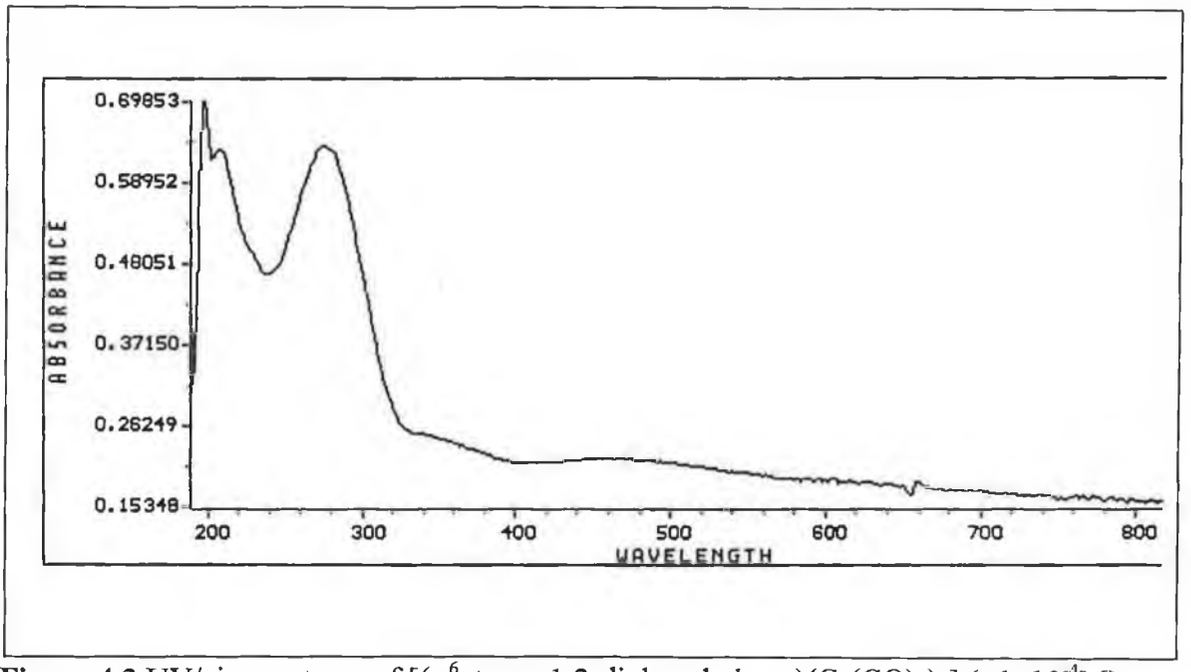

Figure 4.3 UV/vis spectrum of [(η^6-*trans*-1,2-diphenylethene)($Cr(CO)_3)_2$] (~$1x10^{-4}$M)

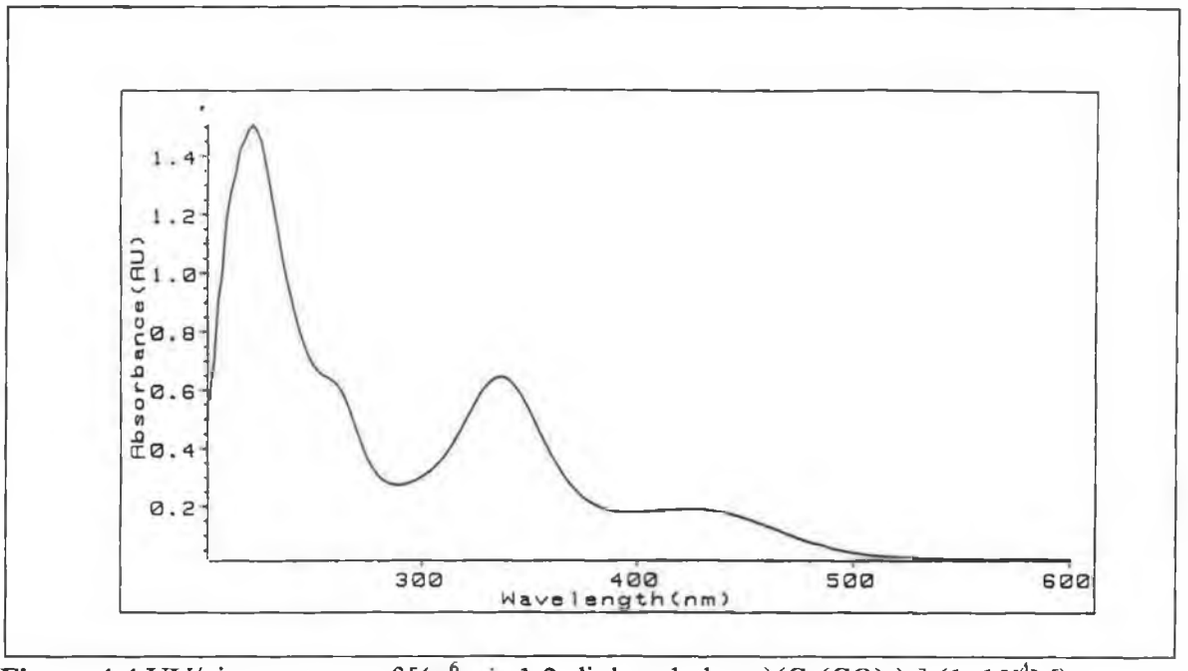

Figure 4.4 UV/vis spectrum of [(η^6-*cis*-1,2-diphenylethene)($Cr(CO)_3)_2$] ($1x10^{-4}$M)

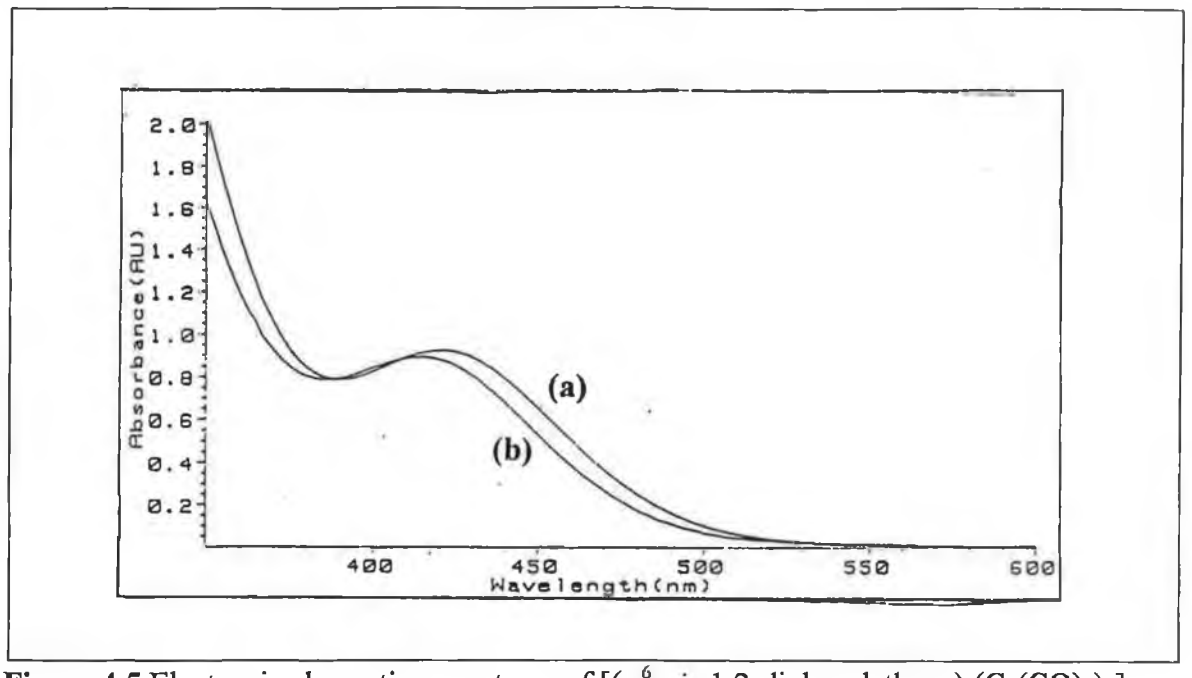

Figure 4.5 Electronic absorption spectrum of [(η^6-*cis*-1,2-diphenylethene) ($Cr(CO)_3)_2$] in (a)hexane (b) ethanol

4.23 UV/vis Monitored Steady State Photolysis of [(η^6-*trans*-1,2-diphenylethene) ($Cr(CO)_3)_2$]

A CO degassed sample of the *trans* isomer was irradiated with λ_{exc} > 400nm. The changes in the UV/vis spectrum are presented in Figure 4.5. A reduction in the absorption of the parent coincides with an increase in absorption at ~ 300 nm. This can be assigned to the formation of free ligand. The low energy deligation of the ligand implies that the arene-loss originates from the low-lying LF transition.

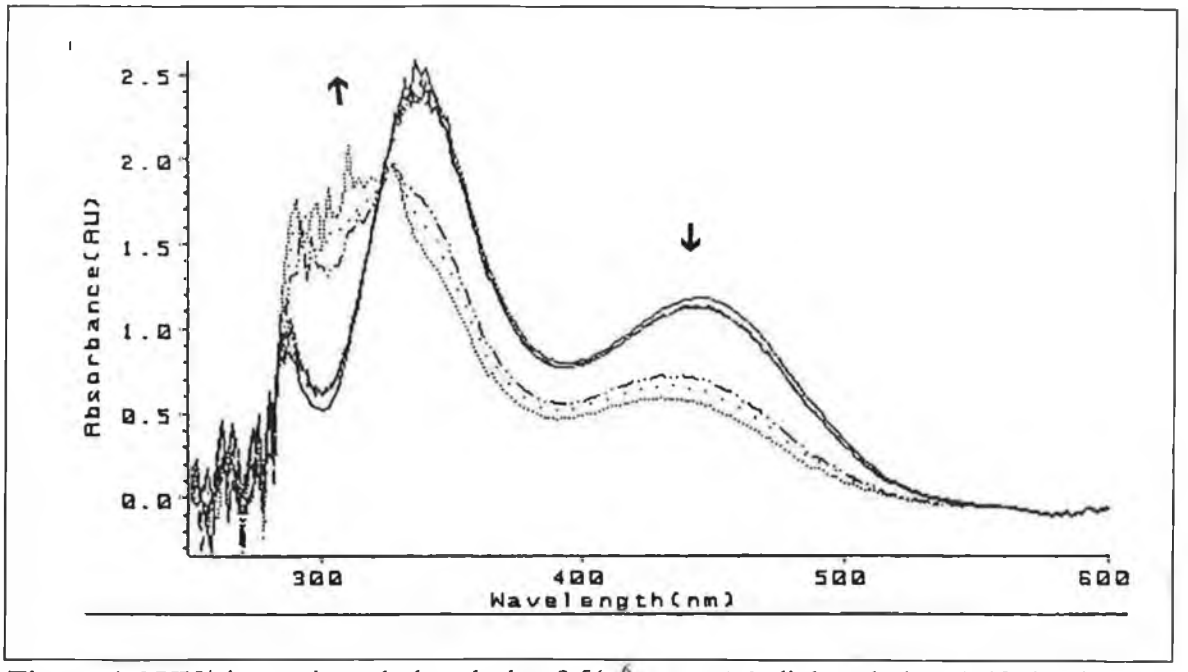

Figure 4.6 UV/vis monitored photolysis of [(η^6-*trans*-1,2-diphenylethene) ($Cr(CO)_3)_2$] in toluene, λ_{irrad} > 400 nm.

4.24 Laser Flash Photolysis of [(η^6-*trans*-1,2-diphenylethene) ($Cr(CO)_3)_2$]

Samples were prepared as described in the experimental section. Experiments were carried out in toluene under 1 atm of CO. A plethora of transients were observed at monitoring wavelengths ranging from 530 to 320 nm (the toluene absorbed below ~300 nm). Figure 4.6 presents the transient centred at 500 nm. The intermediate followed a first order decay with a decay time of 989 μs. There was a residual absorption which did not return to base-line during the time-scale of the experiment. A shorter lived transient is presented in Figure 4.7. This transient is centred at 330 nm, with a decay time of ~ 200 μs. The intermediate can tentatively be assigned to a dicarbonyl intermediate. The

transient decays below the absorption of the intermediate, implying that the system is not reversible. Changes in the UV/vis spectrum of the sample were checked at intervals during the experiment, some formation of free ligand was observed which explains the bleaching observed in the transients. If photoinduced carbonyl loss was occurring then a transient decay of the parent would be expected, however, no evidence for this was observed. It must be considered though that any decay of the parent may be overlapped by a photoproduct absorption. The amount of transients observed suggests a complicated series of intermediate products.

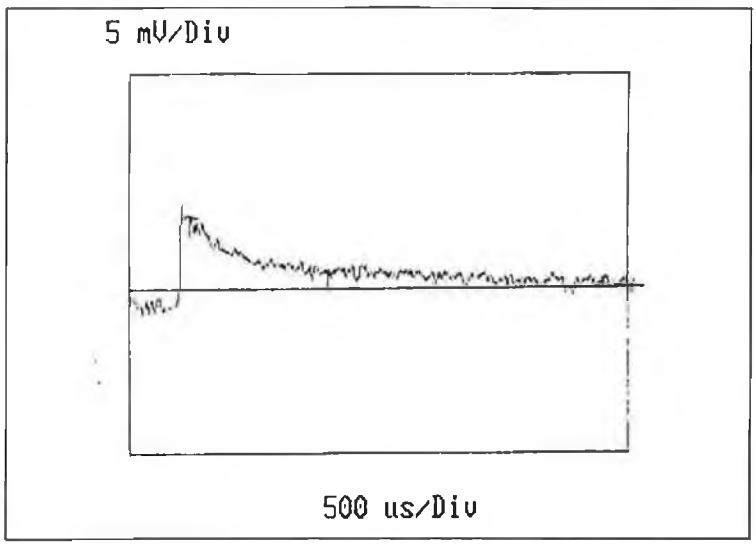

Figure 4.7 Transient observed at monitoring wavelength 500 nm, λ_{exc} = 355 nm, for [(η^6-*trans*-1,2-diphenylethene) ($Cr(CO)_3)_2$] in toluene.

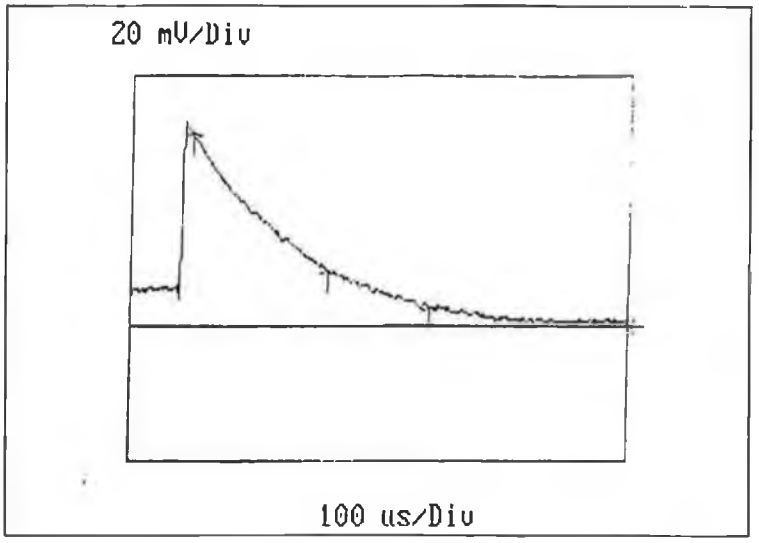

Figure 4.8 Transient observed at monitoring wavelength 330 nm, λ_{exc} = 355 nm, for [(η^6-*trans*-1,2-diphenylethene) ($Cr(CO)_3)_2$] in toluene.

4.25 IR Monitored Photolysis of [(η^6-*trans*-1,2-diphenylethene) ($Cr(CO)_3)_2$]

In order to investigate whether CO loss was a significant photoprocess following photolysis of the *trans* species IR monitored photolysis was carried in argon degassed toluene in the presence of pyridine. Upon photolysis at $\lambda > 400$ nm a decay in the parent CO stretching frequencies was observed, however no new carbonyl stretching frequency were observed. Figure 4.9 presents the changes in the IR spectrum upon photolysis at $\lambda_{exc} > 340$ nm. The decay of the parent bands at 1966 and 1900 cm^{-1} coincides with new band formation at 1943, 1872, 1858, 1803 cm^{-1}. These bands can only be tentatively assigned. The bands at 1858 and 1803 cm^{-1} are consistent with the shift to lower wavenumber upon carbonyl loss and the separation of 55 cm^{-1} is typical of a metal dicarbonyl complex. The proposed reaction is depicted in Reaction scheme 4.3. The bands at 1872 and 1943 cm^{-1} are of typical separation for a tricarbonyl species. This would imply that only one carbonyl has been displaced by the pyridine.

The *trans* isomer was also photolysed in a KBr disk, however prolonged photolysis did not show any significant changes in the IR spectrum.

Reaction 4.3

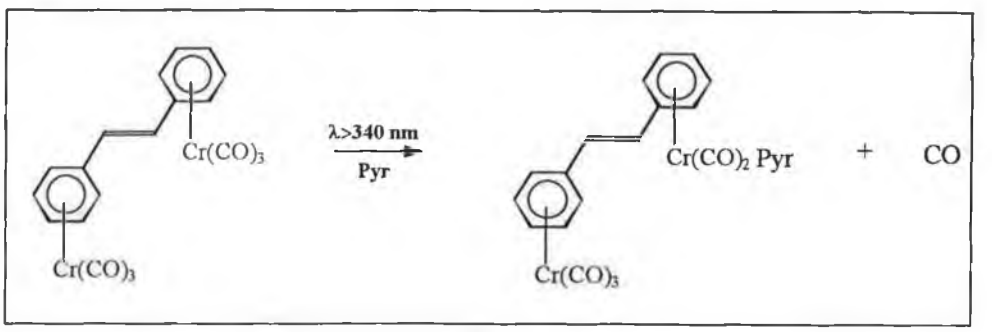

4.26 UV/vis monitored Steady State Photolysis of [(η^6-*cis*-1,2 diphenylethene)($Cr(CO)_3)_2$]

Initial steady state photolysis experiments were carried out in CO purged cyclohexane. This resulted in a depletion of the parent bands and a broad product band at ~270 nm. The product absorbance is consistent with that of either *cis* or *trans*-1,2-diphenylethene. No evidence for isomerisation of the complex from the *cis* to the *trans* species was observed. The *trans* complex however is very insoluble in non polar solvents. The experiment was repeated in toluene and the result of photolysis at λ_{irrad} > 400nm is presented in Figure 4.10. An isobestic point is seen at 450 nm as the parent decays and the photoproduct(s) absorb at ~280 nm and ~550 nm. These changes are consistent with the formation of [(η^6-*trans*-1,2-diphenylethene) ($Cr(CO)_3)_2$]. Continued photolysis resulted in the formation of free ligand as was observed in cyclohexane.

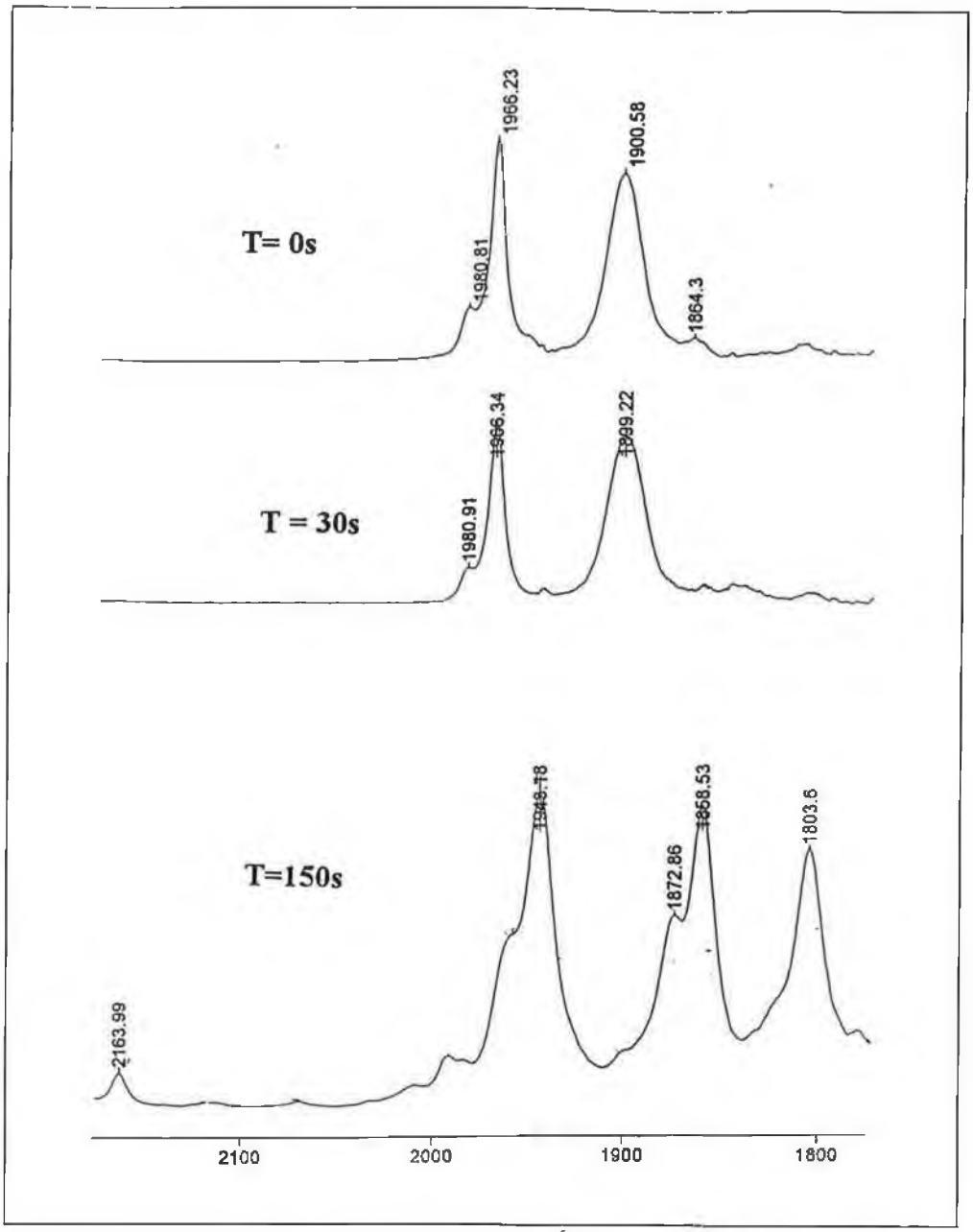

Figure 4.9 IR monitored photolysis of [(η^6-*trans*-1,2-diphenylethene) $(Cr(CO)_3)_2$] in toluene, $\lambda_{irrad} > 340$ nm.

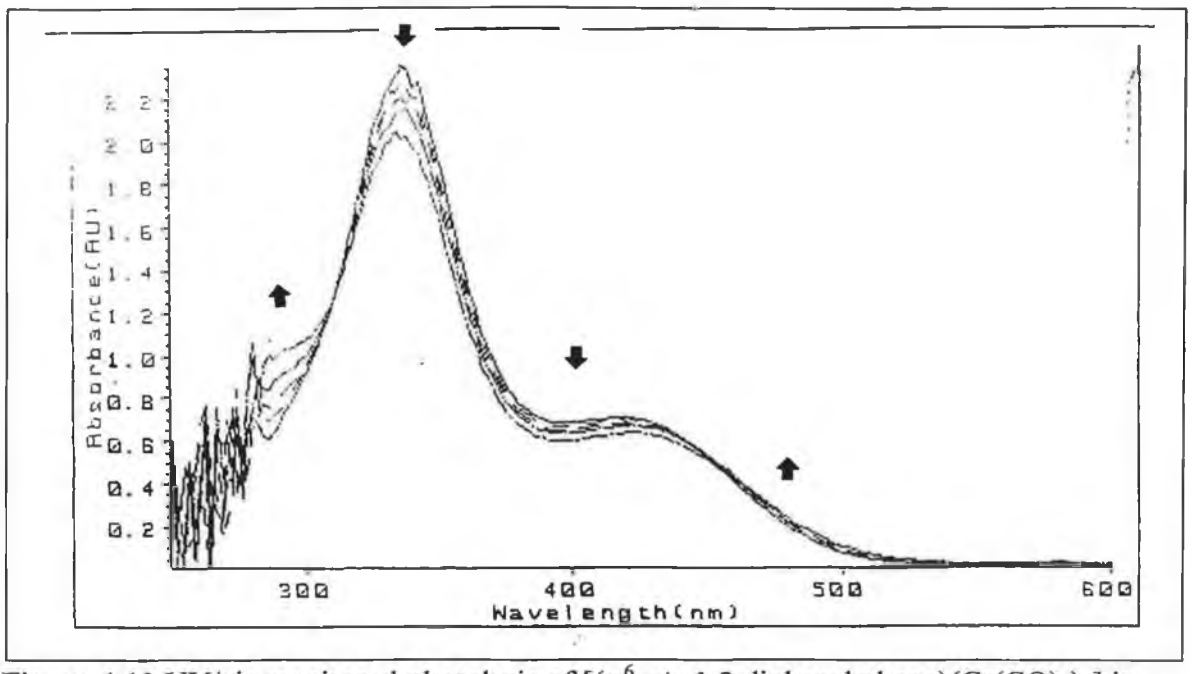

Figure 4.10 UV/vis monitored photolysis of [(η^6-*cis*-1,2 diphenylethene)($Cr(CO)_3)_2$] in toluene, $\lambda_{irrad} > 400$ nm.

4.27 Laser Flash Photolysis of [(η^6-*cis* -1,2 diphenylethene)($Cr(CO)_3)_2$]

A sample of the *cis* isomer was prepared in cyclohexane under 1 atm of CO. The sample was flashed at 355 nm. A transient decay of the parent is observed centred at 430 nm with a regeneration time of ~160 μs (Figure 4.11). No evidence for a carbonyl-loss intermediate was observed. The decay and regeneration of the parent under an atmosphere of CO is typical of CO dissociation process. Dicarbonyl intermediates are typically observed in the region of 290 nm, however it is proposed that only one carbonyl ligand is lost per molecule. The pentacarbonyl intermediate may absorb in the region of the parent and so no formation is observed.

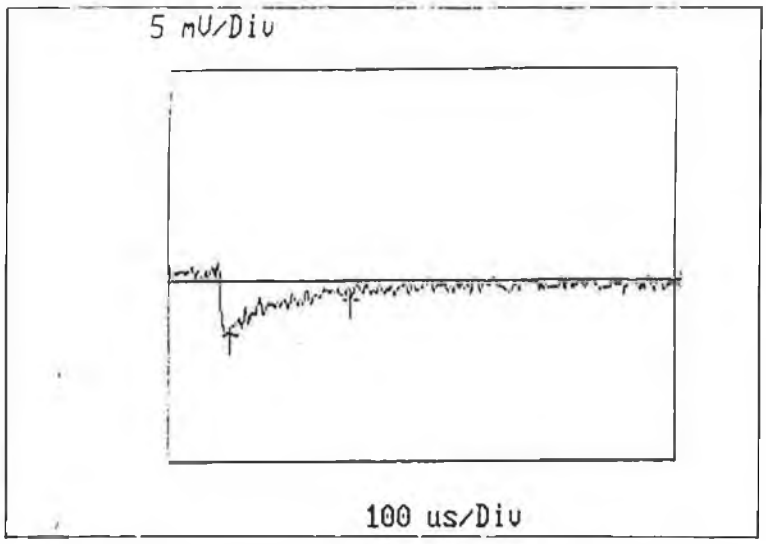

Figure 4.11 Transient decay at monitoring wavelength 430 nm, λ_{exc} = 355 nm.

4.28 NMR monitored photolysis of [(η^6-*cis*-1,2-diphenylethene) ($Cr(CO)_3)_2$]

Photolysis of the *cis* isomer was followed by proton NMR in order to elucidate the photoproducts. The sample was prepared in C_6D_6 under 1 atm of CO as described in the experimental section. The photoproducts were qualitatively the same upon photolysis at $\lambda > 400$nm and $\lambda > 340$nm, however the product formation was faster upon short wavelength irradiation. Figure 4.12 presents the NMR of the *cis* isomer prior to photolysis. After 30 minutes of irradiation a number of changes were observed in the spectrum (Figure 4.13). The new resonance bands at ~ 7.1, 7.0, 5.8, and 4.5 ppm are assigned to the mononuclear species; (η^6-*cis*-1,2-diphenylethene) $Cr(CO)_3$, as depicted in Figure 4.14. In particular the band at ~ 4.9 ppm is indicative of a complexed arene, which would discount the loss of both $Cr(CO)_3$ moieties. The physical changes to the sample were particularly significant; red crystals precipitated from the sample during photolysis. These were removed from the NMR tube under argon. Their insolubility in most solvents and physical appearance was coincident with the properties of [(η^6-*trans*-1,2-diphenylethene)($Cr(CO)_3)_2$)]. The UV/vis spectrum of the crystals presented in Figure 4.15 confirms them as being [(η^6-*trans*-1,2-diphenylethene($Cr(CO)_3)_2$]. The solution was dried under argon to yield a yellow solid. The IR spectrum of the solid is presented in Figure 4.16 and is typical of a tricarbonyl complex. No evidence for the

formation of $Cr(CO)_6$, which would be expected in the region of $1985cm^{-1}$ is seen in the spectrum.

Solubility problems hampered any NMR monitored photolysis of the *trans* isomer.

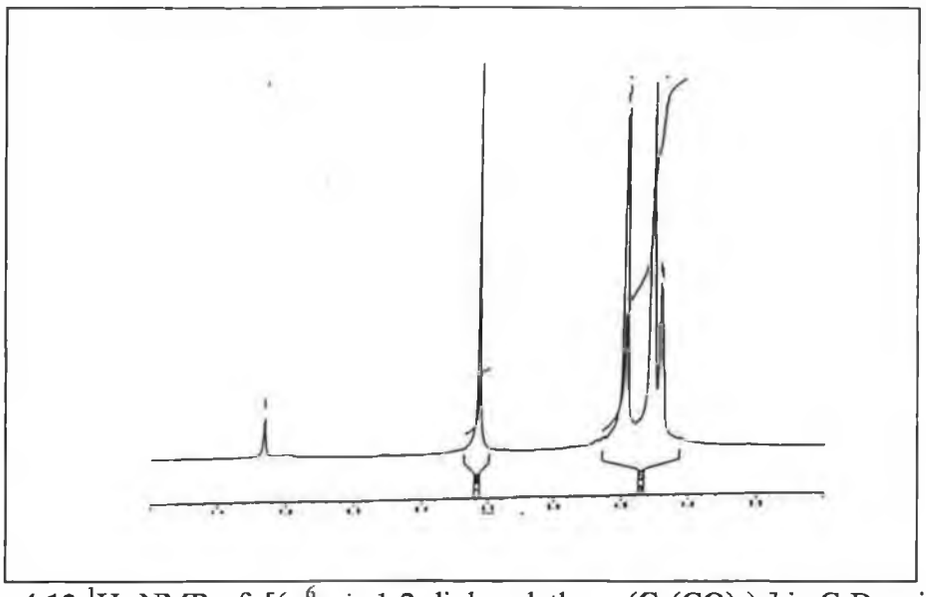

Figure 4.12 $^1H_1$ NMR of [(η^6-*cis*-1,2-diphenylethene ($Cr(CO)_3)_2$] in C_6D_6 prior to photolysis.

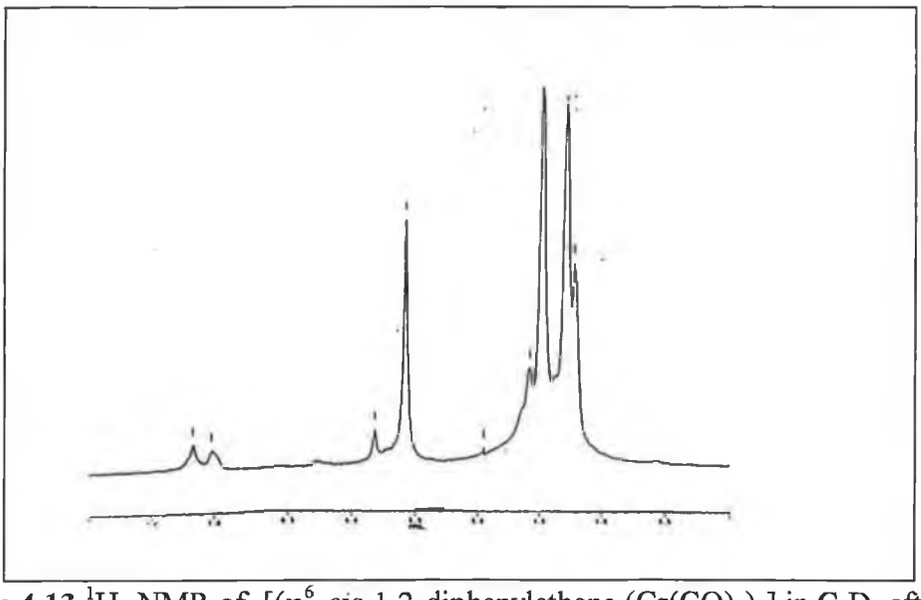

Figure 4.13 $^1H_1$ NMR of [(η^6-*cis*-1,2-diphenylethene ($Cr(CO)_3)_2$] in C_6D_6 after 30 minutes photolysis.

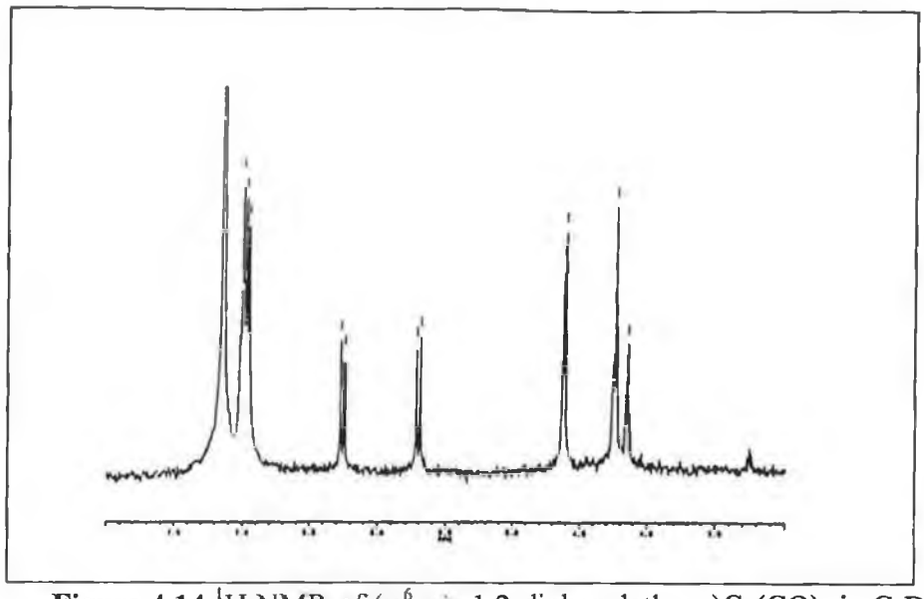

Figure 4.14 ^{1}H NMR of (η^6-*cis*-1,2-diphenylethene)Cr(CO)$_3$ in C_6D_6

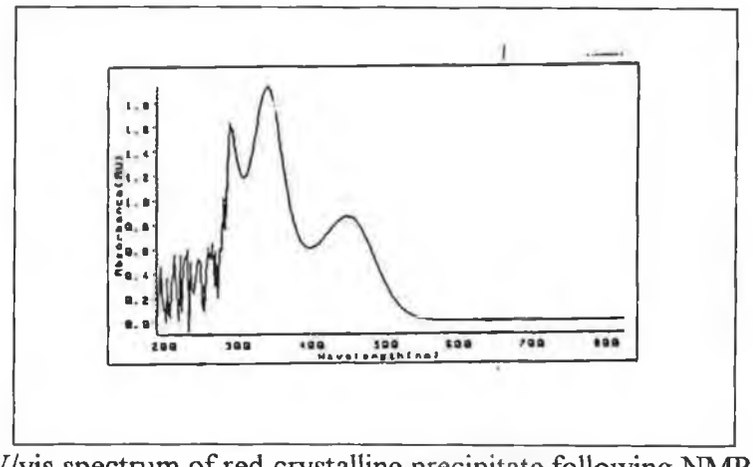

Figure 4.15 UV/vis spectrum of red crystalline precipitate following NMR monitored photolysis, $\lambda_{irrad} > 400$ nm.

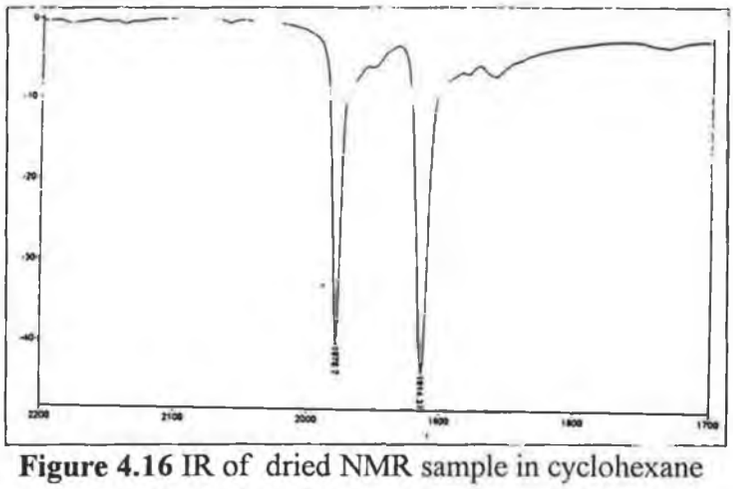

Figure 4.16 IR of dried NMR sample in cyclohexane

4.3 Preliminary Studies on [(η^1:η^6-4-phenylpyridine)($W(CO)_5$) ($Cr(CO)_3$)]

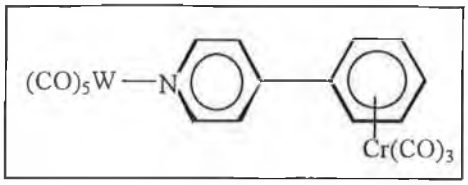

The synthesis and isolation of this compound was difficult and provided very low yields. Consequently only preliminary experiments were conducted.

4.31 NMR Characterisation of [(η^1:η^6-4-phenylpyridine)($W(CO)_5$) ($Cr(CO)_3$)]

A ^1H NMR spectrum was obtained to confirm complexation of both the $W(CO)_5$ and the $Cr(CO)_3$ moieties. Figure 4.17 presents the proton NMR of (η^1-4-phenylpyridine)$W(CO)_5$. The resonance's centred at 8.6ppm are assigned to the protons ortho to the nitrogen on the pyridine ring, those at ~7.6 ppm to the protons meta to the pyridine ring, and those at ~7.2 to the uncomplexed phenyl ring. Figure 4.18 represents the NMR spectrum of the product. The peaks corresponding to the phenyl ring have been shifted upfield to ~ 5.8 - 5.5 ppm. These shifts in resonances are typical of loss of aromaticity upon complexation of an arene ring to a metal tricarbonyl centre.

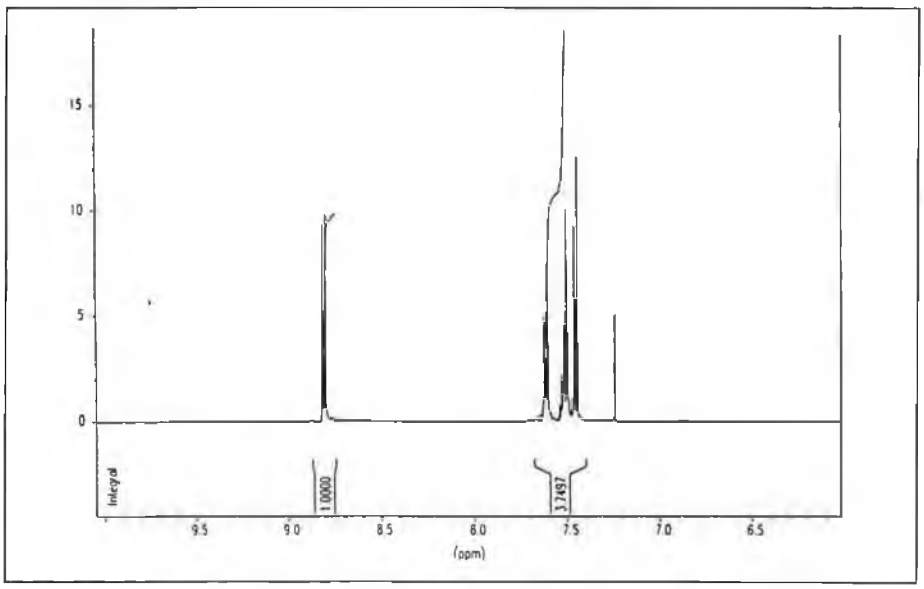

Figure 4.17 $^1H_1$ NMR spectrum of (η^1-4-phenylpyridine)$W(CO)_5$ in $CDCl_3$

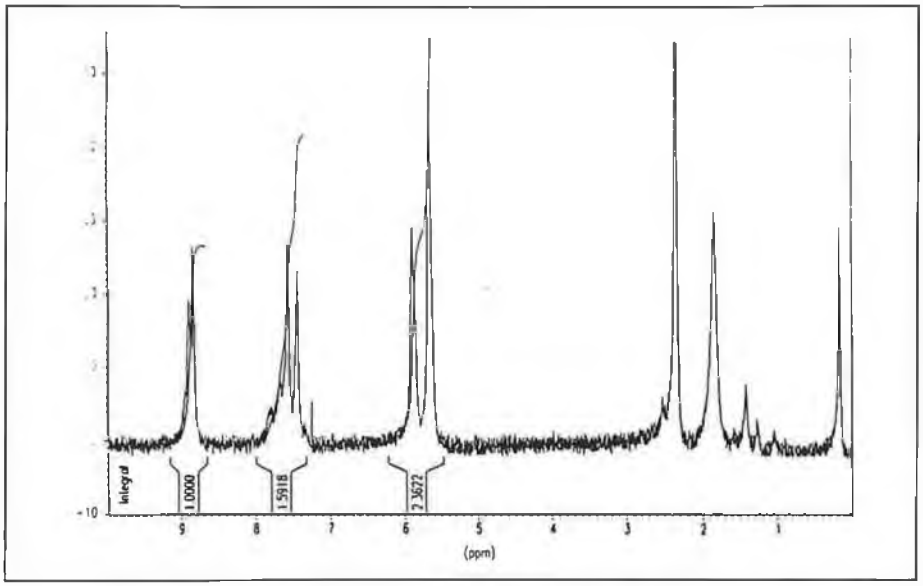

Figure 4.18 ^{1}H NMR spectrum of [(η^1:η^6-4-phenylpyridine)W(CO)$_5$Cr(CO)$_3$] in $CDCl_3$.

4.32 Electronic Absorbance spectrum of [(η^1:η^6-4-phenylpyridine)(W(CO)$_5$) (Cr(CO)$_3$)]

The UV/vis spectra of (η^1-4-phenylpyridine)W(CO)$_5$ and [(η^1:η^6-4-phenylpyridine)(W(CO)$_5$) (Cr(CO)$_3$)] are presented in Figure 4.19. The λ_{max} at ~ 400nm in the pentacarbonyl species is assigned to a LF transition overlapping a W —> (4-phenylpyridine) CT transition.[7] The spectrum of the heterobimetallic complex is significantly different. The λ_{max} is shifted to lower energy and is tentatively assigned to a low energy MLCT band. The Cr(CO)$_3$ would increase the electron withdrawing nature of the arene ring, and so cause a red shift in the W—> (4-phenylpyridine) CT transition.[5] The absorbance at ~320 nm is typical of arene tricarbonyl complexes[6] and can be assigned to a Cr—> metal CT with some Cr —> π^* CO CT.

4.33 UV/vis monitored steady state photolysis of [(η^1:η^6-4-phenylpyridine) ($W(CO)_5$) ($Cr(CO)_3$)]

The sample was prepared in acetonitrile solution because of low solubility in nonpolar solvents. It was outgassed by purging with argon for 20 minutes prior to photolysis. The spectroscopic changes following photolysis at $\lambda > 400$ nm are presented in Figure 4.20. Depletion of the parent bands was accompanied by an increase in absorption at ~ 390 nm and > 580 nm The isosbestic points at 400 nm and 580 nm suggest a reaction uncomplicated by side or subsequent reactions. The band at 390 nm coincides with the λ_{max} of the pentacarbonyl; (η^1-4-phenylpyridine) $W(CO)_5$. The increase in absorption at $\lambda > 580$ nm can tentatively be assigned to the solvated $Cr(CO)_3$ fragment. Prolonged photolysis resulted in the depletion of the pentacarbonyl absorbance at 390 nm.

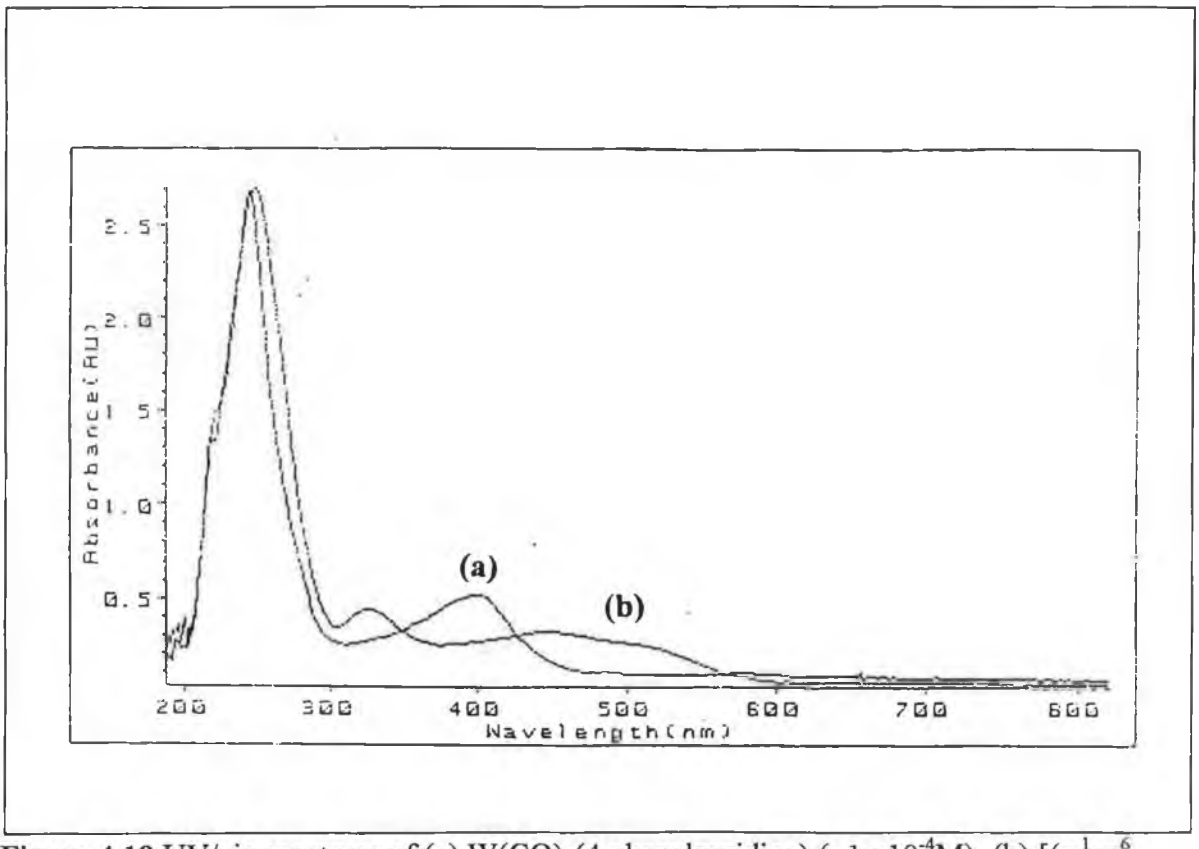

Figure 4.19 UV/vis spectrum of (a) $W(CO)_5$(4,phenylpyridine) (~1 x10^{-4}M), (b) [(η^1:η^6-4-phenylpyridine)($W(CO)_5$) ($Cr(CO)_3$)] in acetonitrile.

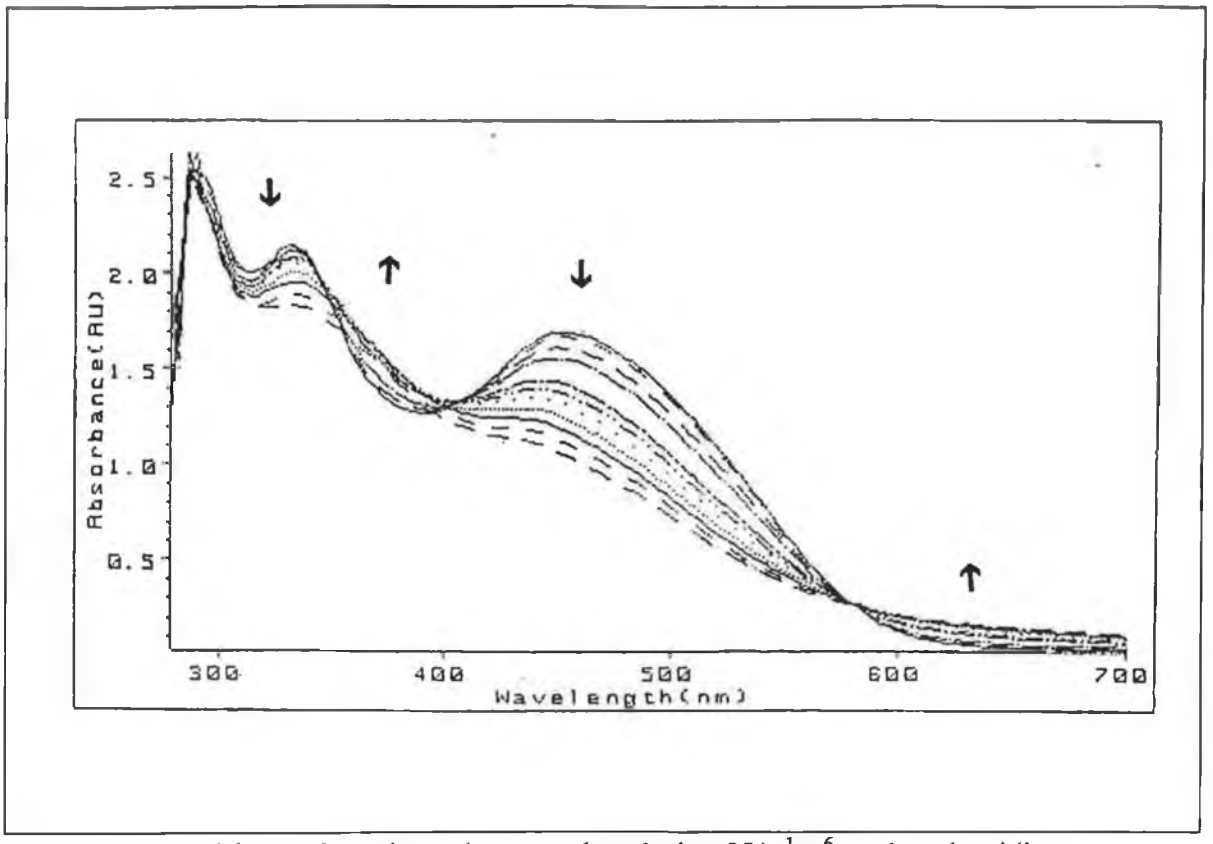

Figure 4.20 UV/vis monitored steady state photolysis of [(η^1:η^6-4-phenylpyridine ($W(CO)_5$) ($Cr(CO)_3$)] in acetonitrile.

4.4 Conclusion

The dominant photoprocess in the *cis* complex is isomerisation to the *trans* complex. This is confirmed by the ^{1}H NMR experiments. Further photoreactions of the *trans* bimetallic species could not be determined by from the NMR monitored photolysis due to the insolubility of the product complex. The isomerisation possibly arises from an IL excited state. Isomerisation at such low energy is unusual as the IL ($\pi \rightarrow \pi^*$) transition of the free ligand lies in the UV region of the spectrum. Complexation of the $Cr(CO)_3$ moieties results in a low energy MLCT transition. This low energy transition ultimately has the same effect as the IL transition; i.e. population of the ligand π^* orbital. This would explain the low energy isomerisation observed. Figure 4.21 portrays the energy difference in occupying the π^* orbital of the ligand for the free ligand and the complex.

A secondary less efficient process appears to be the formation of the mononuclear species; (η^6-*cis*-1,2-diphenylethene) $Cr(CO)_3$. The less efficient arene-loss observed at low energy irradiation can tentatively be assigned to a LF transition lying close in energy to the MLCT transition. While the MLCT transition is efficiently populated the LF transition is less efficiently populated. The laser experiments showed CO-loss to be another photoprocess, so it would appear that upon irradiation at $\lambda = 355$ nm a higher energy LF transition is populated which results in labilisation of the metal-CO bond..

It was more difficult to elucidate the photochemistry of the *trans* species because of its insolubility in alkane solvents. Upon irradiation of the complex at $\lambda > 400$ nm under an atmosphere of argon scission of both Cr-arene bonds was observed. Both the laser flash photolysis and the IR monitored photolysis provide evidence for CO-loss resulting upon higher energy irradiation. The nature of the changes in the IR bands and the transients observed imply that CO-loss occurs from one $Cr(CO)_3$ moiety. The wavelength dependence of the photochemistry can again be rationalised in terms of two LF transitions, the low energy transition resulting in arene-loss, the higher energy transition resulting in CO-loss. A proposed reaction mechanism for the photochemistry of [(η^6-*trans*-1,2-diphenylethene)($Cr(CO)_3)_2$] is presented in Reaction 4.5.

Preliminary studies were only carried out on the photochemistry of [(η^1:η^6-4-phenylpyridine)($W(CO)_5$) ($Cr(CO)_3$)]. Steady state photolysis implied that dissociation of the $Cr(CO)_3$ bond preceded breaking of the $W(CO)_5$-pyridine bond upon low energy photolysis.

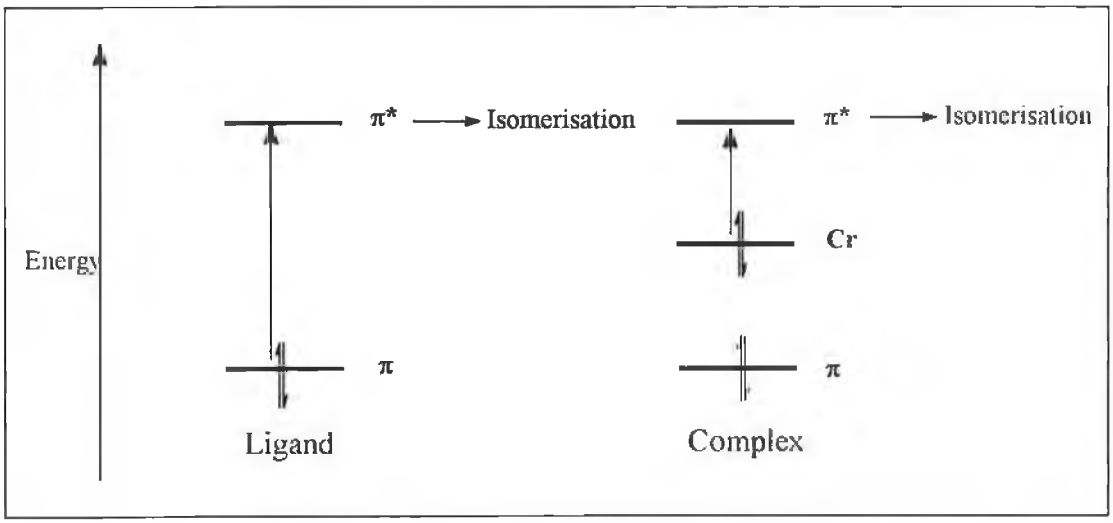

Figure 4.21 The proposed difference in energy for population of the π* orbital in *cis*-1,2-diphenylethene and [(η_6-*cis*-1,2-diphenylethene)($Cr(CO)_3)_2$].

Reaction 4.4

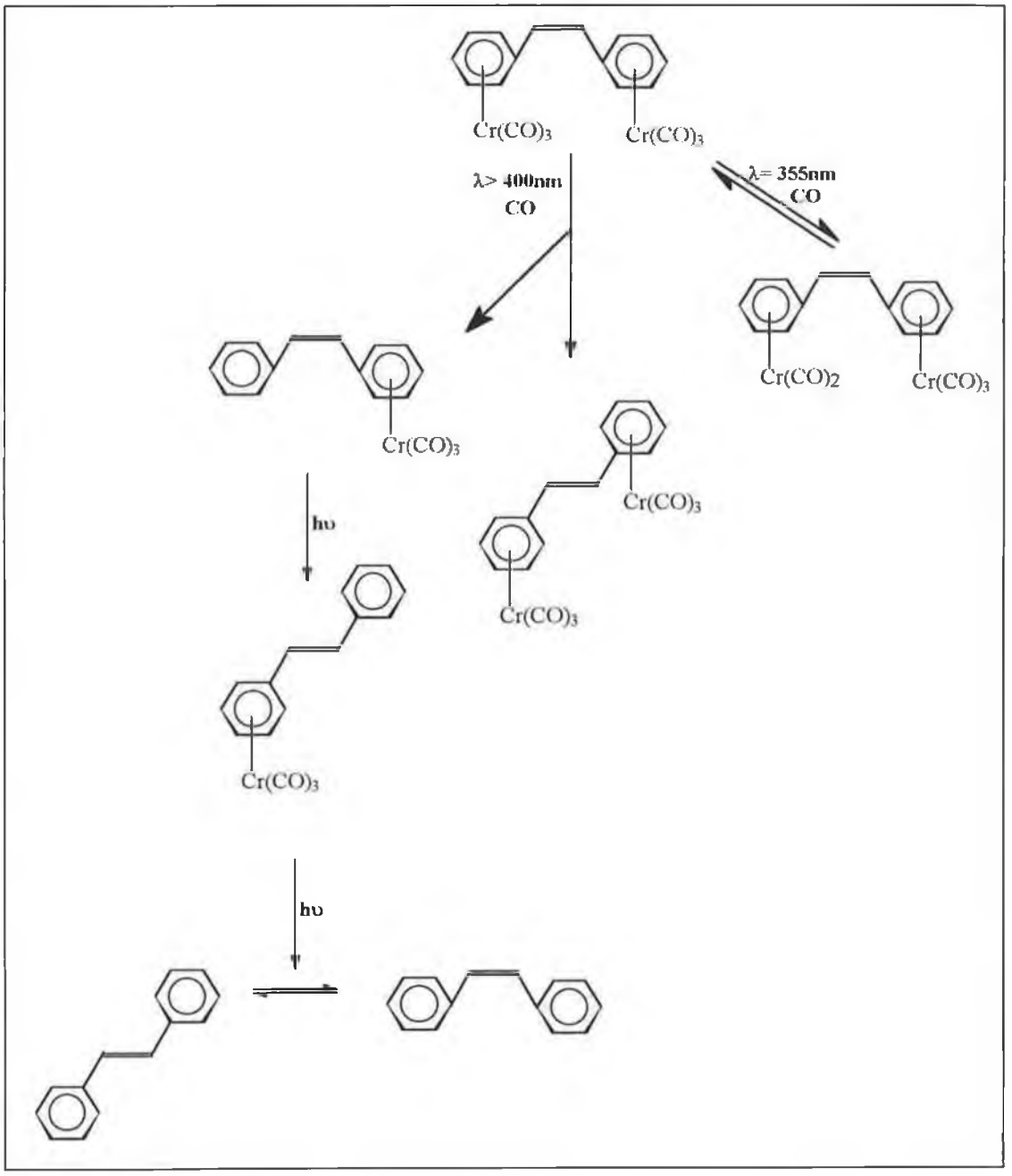
Cr(CO)3
Cr(CO)3
λ> 400nm
CO
λ= 355nm
CO
Cr(CO)2
Cr(CO)3
Cr(CO)3
Cr(CO)3
Cr(CO)3
hυ
hυ

Reaction 4.5

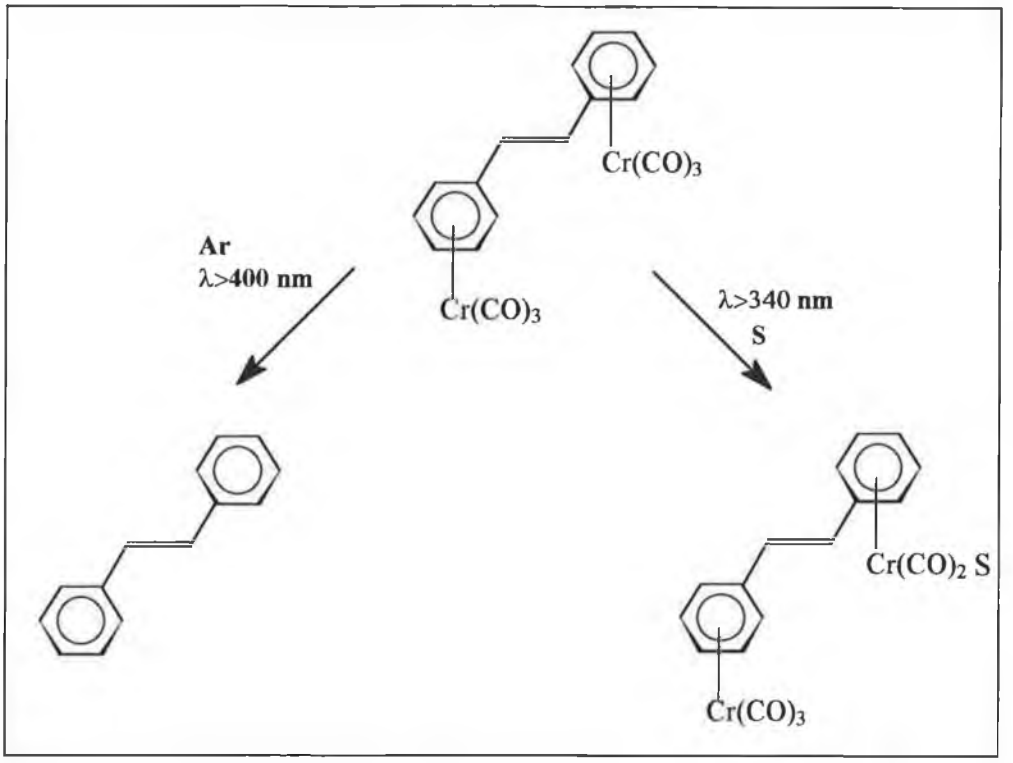

4.5 Crystal and Molecular structure of [(η^6-*trans*-1,2-diphenylethene) ($Cr(CO)_3)_2$]

The crystal and molecular structure of [(η^6-*trans*-1,2-diphenylethene) ($Cr(CO)_3)_2$] was determined. Collection of the crystallographic data was carried out at Trinity College Dublin. The complex contains one molecule per asymmetric unit as presented in Figure 4.22. The twelve carbon atoms of the complexed rings are coplanar, with a plane that is essentially parallel to that of the six oxygen atoms. The C-C distance has an average of 1.4113 Å. This is similar to the C-C bond lengths determined for (η^6-benzene)$Cr(CO)_3$, where the bond distances varied from 1.370 to 1.421 Å.[8] The perpendicular distance from the Cr atom to the plane of the arene-ring is 2.214 Å, which is slightly greater than that of its benzene analogue(1.724 Å). The Crystallographic data is presented in Tables 4.1 to 4.3.

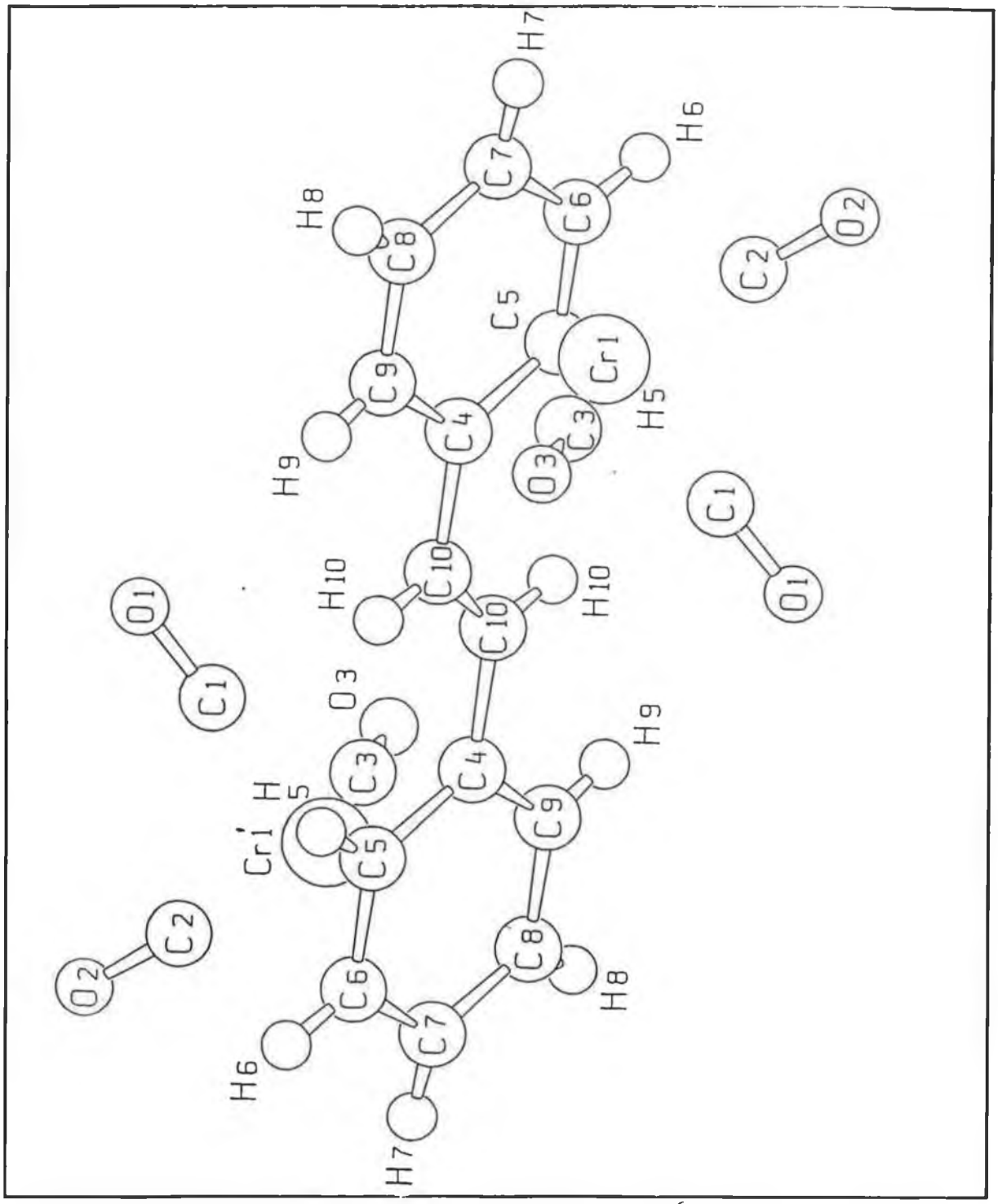

Figure 4.22 SCHAKAL drawing of the crystal structure of [(η^6-*trans*-1,2-diphenylethene)($Cr(CO)_3)_2$].

Table 4.1 Atomic co-ordinates (x 10^4) for non hydrogen atoms with esds's in parentheses for [(η^6-*trans*-1,2-diphenylethene)($Cr(CO)_3)_2$]. U_{eq} x 10^3 {$U_{eq} = (1/3)\Sigma_i\Sigma_j U_{ij} a_i^* a_j^* a_i . a_j$.}

	x	y	z
Cr(1)	1823(1)	3324(1)	7378(1)
C(1)	3238(5)	4557(4)	8003(3)
O(1)	4117(4)	5322(4)	8420(2)
C(2)	42(6)	5871(6)	6773(3)
O(2)	-1031(5)	7495(4)	6405(3)
C(3)	3683(6)	3174(5)	5791(3)
O(3)	4881(6)	3018(5)	4807(3)
C(4)	2960(5)	596(4)	8828(3)
C(5)	950(5)	2029(5)	9405(3)
C(6)	-862(6)	2743(6)	8796(3)
C(7)	-706(6)	2063(6)	7573(4)
C(8)	1233(6)	687(5)	6998(4)
C(9)	3060(6)	-36(5)	7618(3)
C(10)	4931(6)	-161(5)	9417(3)

Table 4.2 Atomic co-ordinates (x 10^4) for the hydrogen atoms in [(η^6-*trans*-1,2-diphenylethene)($Cr(CO)_3)_2$].

	x	y	z	U(eq)
H(5)	837(50)	2507(47)	10128(35)	42(9)
H(6)	-2147(65)	3723(57)	9161(37)	61(11)
H(7)	-1869(61)	2656(53)	7126(35)	52(10)
H(8)	1406(50)	312(47)	6280(34)	37(9)
H(9)	4251(55)	-858(48)	7276(31)	37(9)
H(10)	6138(62)	-960(56)	8898(36)	59(10)

Table 4.3 A complete list of bond lengths angles (°) for [(η^6-*trans*-1,2-diphenylethene)($Cr(CO)_3)_2$].

C(1)-Cr(1)-C(3)	89.66(14)
C(1)-Cr(1)-C(2)	88.24(14)
C(3)-Cr(1)-C(2)	89.5(2)
C(1)-Cr(1)-C(5)	89.96(13)
C(3)-Cr(1)-C(5)	151.0(2)
C(2)-Cr(1)-C(5)	119.49(14)
C(1)-Cr(1)-C(9)	117.59(12)
C(3)-Cr(1)-C(9)	88.38(14)
C(2)-Cr(1)-C(9)	154.06(14)
C(5)-Cr(1)-C(9)	66.29(13)
C(1)-Cr(1)-C(8)	154.79(14)
C(3)-Cr(1)-C(8)	90.01(14)
C(2)-Cr(1)-C(8)	116.96(14)
C(5)-Cr(1)-C(8)	78.37(13)
C(9)-Cr(1)-C(8)	37.21(13)
C(1)-Cr(1)-C(6)	116.00(13)
C(3)-Cr(1)-C(6)	154.3(2)
C(2)-Cr(1)-C(6)	93.1(2)
C(5)-Cr(1)-C(6)	36.80(13)
C(9)-Cr(1)-C(6)	78.26(14)
C(8)-Cr(1)-C(6)	66.06(14)
C(1)-Cr(1)-C(7)	153.19(14)
C(3)-Cr(1)-C(7)	117.14(14)
C(2)-Cr(1)-C(7)	92.0(2)
C(5)-Cr(1)-C(7)	66.68(13)
C(9)-Cr(1)-C(7)	66.23(14)
C(8)-Cr(1)-C(7)	36.19(14)
C(6)-Cr(1)-C(7)	37.20(13)
C(1)-Cr(1)-C(4)	90.34(12)
C(3)-Cr(1)-C(4)	113.61(14)
C(2)-Cr(1)-C(4)	156.85(14)
C(5)-Cr(1)-C(4)	37.38(12)
C(9)-Cr(1)-C(4)	36.69(12)
C(8)-Cr(1)-C(4)	66.82(13)
C(6)-Cr(1)-C(4)	66.93(12)
C(7)-Cr(1)-C(4)	79.05(13)
O(1)-C(1)-Cr(1)	178.8(3)
O(2)-C(2)-Cr(1)	177.7(3)

Table 4.3(continued) A complete list of bond angles (°) for [(η^6-*trans*-1,2-diphenylethene) ($Cr(CO)_3)_2$].

O(3)-C(3)-Cr(1)	177.9(3)
C(9)-C(4)-C(5)	117.5(3)
C(9)-C(4)-C(10)	119.4(3)
C(5)-C(4)-C(10)	123.0(3)
C(9)-C(4)-Cr(1)	70.5(2)
C(5)-C(4)-Cr(1)	70.2(2)
C(10)-C(4)-Cr(1)	128.0(2)
C(6)-C(5)-C(4)	121.1(3)
C(6)-C(5)-Cr(1)	72.0(2)
C(4)-C(5)-Cr(1)	72.4(2)
C(5)-C(6)-C(7)	119.9(3)
C(5)-C(6)-Cr(1)	71.2(2)
C(7)-C(6)-Cr(1)	71.6(2)
C(8)-C(7)-C(6)	119.7(4)
C(8)-C(7)-Cr(1)	71.7(2)
C(6)-C(7)-Cr(1)	71.2(2)
C(7)-C(8)-C(9)	120.3(4)
C(7)-C(8)-Cr(1)	72.2(2)
C(9)-C(8)-Cr(1)	71.0(2)
C(4)-C(9)-C(8)	121.5(3)
C(4)-C(9)-Cr(1)	72.8(2)
C(8)-C(9)-Cr(1)	71.7(2)
C(10)#1-C(10)-C(4)	126.8(4)

Table 4.4 Selected bond lengths (Å) for [(η^6-*trans*-1,2-diphenylethene)($Cr(CO)_3)_2$].

Cr(1)-C(1)	1.830(3)
Cr(1)-C(3)	1.832(4)
Cr(1)-C(2)	1.837(4)
Cr(1)-C(5)	2.201(3)
Cr(1)-C(9)	2.201(3)
Cr(1)-C(8)	2.210(3)
Cr(1)-C(6)	2.212(3)
Cr(1)-C(7)	2.217(3)
Cr(1)-C(4)	2.230(3)
C(1)-O(1)	1.154(4)
C(2)-O(2)	1.151(4)
C(3)-O(3)	1.148(4)
C(4)-C(9)	1.395(5)
C(4)-C(5)	1.420(5)
C(4)-C(10)	1.472(5)
C(5)-C(6)	1.393(5)
C(6)-C(7)	1.413(5)
C(7)-C(8)	1.375(5)
C(8)-C(9)	1.408(5)
C(10)-C(10)#1	1.308(7)

References

[1] Ford, P.; Rudd, De F. P.; Gaunder, R.; Taube, H.; *J. Amer.Chem. Soc.* **90,** 1968.

[2] (a) Wrighton, M.; Hammond, G. S.; Gray, H. B.; *J. Amer. Chem. Soc.* **90,** 1187, 1968.
(b) Wrighton, M.; Hammond, G. S.; Gray, H. B.; *J. Amer. Chem. Soc.* **93,** 4336, 1971.
(c) Wrighton, M.; Abrahamson, H. B.; Morse, D. L.; *J. Amer. Chem. Soc.* **98**, 4105, 1976.

[3] Wrighton, M.; Hammond, G. S.; Gray, H. B.; *Mol. Photochem.* **5,** 179, 1973.

[4] Rest, A. J.; Sordeau, J. R.; J. Chem. Soc. Chem. Comm. 696, 1975.

[5] Pryce, M. T.; *Ph.D. Thesis*, Dublin City University 1994.

[6] Carroll, D. G.; McGlynn, S. P.; *Inorg. Chem.* 7, 1285, 1968.

[7] Geoffroy, G. L.; Wrighton, M. S.; *Organometallic Photochemistry,* Academic Press, New York, 1979.

[8] Bailey, M. F.; Dahl, L. F.; *Inorg. Chem.* **4**, 1314, 1965.

CHAPTER 5
Experimental Section

5.1 Materials

The following solvents were of spectroscopic grade and used without further purification; cyclohexane, toluene, acetonitrile, pyridine, methylcyclohexane, ethanol, methanol. Argon and carbon monoxide were supplied by Air Products and IIG. (η^6-mesitylene)$W(CO)_3$(Strem chemicals), *trans*-1,1-diphenylethene, *cis*- 1,1-diphenylethene, mesitylene, allylbenzene, 1,10 phenanthroline, potassium hydrogen phthalate, naphthalene, 4-phenylpyridine, boron triflouride etherate, (Aldrich chemical Co.), were used without further purification. Chromium hexacarbonyl, tungsten hexacarbonyl, molybdenum hexacarbonyl (Aldrich chemical Co.) were sublimed where necessary. Tetrahydrofuran (THF) diethyl ether and 1,4-dioxan, were dried over sodium and benzophenone and stored with sodium under argon the dioxan was filtered through activated alumina prior to use. Dibenzene chromium iodide was synthesised by Dr. Charles Gordon, dibenzene chromium chloride was prepared by passing an aqueous solution of the iodide salt through an amberlite column which was washed with hydrogen chloride.

5.2 Equipment

Infrared spectra were recorded on a Perkin Elmer 2000 FTIR spectrometer, or a Perkin Elmer 1600 FTIR spectrometer using a sodium chloride solution cell d = 0.1 mm. UV/vis spectra were recorded on a Hewlett Packard 8453A photodiode array spectrometer using a quartz cell of 1cm pathlength. NMR measurements were carried out on a Brüker model AC 400 MHz spectrometer.

5.3 Synthesis of [(η^6-*cis* and *trans*-1,2-Diphenylethene)$(Cr(CO)_3)_2$

Both the *cis* and *trans* complexes were synthesised by heating to reflux temperature; $Cr(CO)_6$ (2.2g, 10 mmol) and *cis* or *trans* 1,2-diphenylethene (0.9g, 5mmol) in an argon purged mixture of 50 cm^3 dibutyl ether with 5 cm^3 THF for 4 days under argon. A crude product precipitated overnight at -20°C. Vacuum filtration yielded a red product in the case of the *trans* complex and a yellow/orange product in the case of

the *cis* complex. The *trans* complex was purified by washing with dichloromethane, to yield dark red crystals. The *cis* complex was purified by recrystallisation from THF/pentane solution.

5.4 Synthesis of (η^6-arene)$Cr(CO)_3$ complexes

(η^6-Mesitylene)$Cr(CO)_3$ was synthesised as described by Mahaffy *et al*[1]. $Cr(CO)_6$ (1g, 4.5mmol) and mesitylene (~40cm^3) were brought to reflux temperature for 4 hours under an atmosphere of argon. The resultant yellow solution was filtered through silica using a glass centred crucible and the solvent removed under reduced pressure. The complex was recrystallised from diethyl ether.(η^6-naphthalene)$Cr(CO)_3$ was synthesised using the method of Hudecek *et al.* [2]; $Cr(CO)_6$ (1.1g, 5mmol), naphthalene (1.28g, 10mmol) was brought to reflux temperature in decalin for three hours. A red product precipitated at -20°C overnight. The product was recrystallised from toluene/pet ether to yield a red crystalline solid.(η^6-allylbenzene)$Cr(CO)_3$ was synthesised by refluxing $Cr(CO)_6$ (4g, 18mmol), and allylbenzene (10cm^3, 75mmol) in 125ml of butyl ether with 10cm3 THF for 72 hours. The solvent was removed under reduced pressure to yield a yellow/brown oil. This was taken up into hexane and upon removing the hexane a yellow oil remained. For each of these methods the solutions were purged for ~20 minutes prior to reflux and each was carried out under an atmosphere of argon.

5.5 Synthesis of (η^6-arene)$Mo(CO)_3$ complexes

(η^6-Mesitylene)$Mo(CO)_3$ was synthesised by bringing to reflux temperature an argon purged solution of $Mo(CO)_6$ (1g, 3.7mmol) and mesitylene (~ 40 cm^3) for three hours. Upon cooling to room temperature a yellow solid crystallised, addition of hexane aided further precipitation. The complex was recrystallised from chloroform/hexane solution. (η^6-allylbenzene)$Mo(CO)_3$ was synthesised using the method described by Nesmeyanov *et al.*[3]; boron triflouride etherate (0.64g, 4.5mmol) was added dropwise with stirring to finely dispersed [$Mo(CO)_3$(pyridine)$_3$][4] (0.63g, 1.5mmol) and allylbenzene

(0.177g,1.5mmol) in 50ml of dry argon purged diethyl ether. After 2 hours stirring at room temperature the mixture was diluted with 100cm^3 of hexane, and this was washed with 3 x 100cm^3 of cold (milli Q) water. The hexane layer was then dried over magnesium sulphate and the hexane removed under reduced pressure until a solid yellow product began to crystallise. Further crystallisation occurred on allowing the solution to stand in dry ice for several hours. The yellow powder solid was washed with cold pentane and dried under vacuum. Again all reactions were carried out under argon.

5.6 Synthesis of [(η^1:η^6-4-phenylpyridine)W(CO)$_5$Cr(CO)$_3$]

5.61 Photolysis Apparatus

Preparative photolysis work was carried out using an Applied Photophysics 400 watt medium pressure mercury vapour lamp; a double walled quartz glass vessel houses the lamp which is water cooled, while an external vessel holds the sample solution to be irradiated. Argon is continuously bubbled through the solution during the irradiation to expel the carbon monoxide liberated during the photolysis.

5.62 Synthesis of (η^1-4-phenylpyridine)W(CO)$_5$

W(CO)$_6$ (1g, 2.8mmol) and dry THF (~200cm^3) was purged with argon and the photolysed in the apparatus described in Section 5.61. After 2 hours the resultant yellow solution of the W(CO)$_5$THF adduct was transferred in the dark to a round bottom flask containing 4-phenylpyridine (0.44g, 2.8mmol) and THF (100cm^3). The mixture was stirred in the dark at room temperature overnight. The THF was removed by rotary evaporation to yield an orange solid. The product was purified by recrystallisation from dichloromethane/hexane.

5.63 Synthesis of [(η^1:η^6-4-phenylpyridine)W(CO)$_5$Cr(CO)$_3$]

Numerous attempts were made to synthesise the bimetallic complex. The reaction of the pentacarbonyl species with [Cr(CO)$_3$(MeCN)$_3$] showed no evidence for complexation of the phenyl ring. Upon refluxing Cr(CO)$_6$ (0.46g, 2.1mmol) and (η^1-4-phenylpyridine)W(CO)$_3$ for several hours a deep red colour resulted. The dioxan was removed under reduced pressure to yield a red crude product. The starting materials

were separated from the product by flash chromatography under a positive pressure of argon and eluting with 40:60 dichloromethane: hexane. The solvent mixture was removed under reduced pressure.

5.7 Laser Flash Photolysis

5.71 Sample preparation for flash photolysis experiments

Samples for flash photolysis experiments were prepared in a degassing bulb attached to a flourescence cell. All samples were adjusted such that the absorbance at the λ_{exc} (266 or 355 nm) was between 0.8 and 1.5. All absorbance readings were recorded on a Hewlett-Packard 8452a UV/vis spectrometer and any changes that occurred in the UV/vis spectrum during the experiment were also recorded. The samples were degassed by three cycles of a freeze-pump-thaw procedure to ~10^{-3} Torr and finally liquid-pumping to remove any impurities such as water. Argon or carbon monoxide was then placed over the sample depending on the experiment. The samples were protected from light during the preparation process.

5.72 Laser Flash Photolysis with UV/vis detection

A schematic diagram of the flash photolysis apparatus is presented in figure 5.2. The excitation source is a neodynium yttrium aluminium garnet (Nd-YAG) laser which operates at 1064 nm, however the frequency can be doubled, tripled, or quadrupled to generate a second, third or fourth harmonic frequency at 532, 355, or 266 nm respectively. The power of the laser can be amplified by applying different voltages across the amplifier flash tube. The pulse time is approximately 10 ns. In this study both the 266 nm and the 355 nm frequencies were employed, the energy typically is 40 mJ per pulse and 55 mJ per pulse respectively. The circular laser pulse is directed *via* two Pellin-Broca prisms onto the sample cuvette. A power meter is situated after the first prism but before the sample cuvette. When the pulse passes through the power meter the oscilloscope is triggered. The monitoring light source is an air cooled 275 watt Xenon

arc lamp arranged at right angles to the laser beam. The monitoring beam passes through the sample and is directed to the entrance slit of an Applied Photophysics f/3 monochromator *via* a circular lens. UV/vis filters were employed ($\lambda > 400$ nm or $\lambda > 340$ nm) between the monitoring source and the sample to prevent excessive photolysis/ photodegradation of the sample. At the exit stage of the monochromator a Hamadsu five stage photomultiplier operating at 850 V detects absorbance changes and relays them to the oscilloscope *via* a variable load resistor. The oscilloscope (Hewlett-Packard 5410A) is interfaced with an Olivetti PCS286 microcomputer *via* an IEEE bus.

The transient signals were recorded in the following manner. An I_o was recorded which corresponds to the absorbance of the sample prior to the laser flash. This was measured by obtaining the difference in mV of the light transmitted by the sample when the shutter on the monitoring source was closed and open. A typical trace shows the change of voltage with time which corresponds to the change in absorbance. The resultant transients were analysed employing either first or second order kinetics depending on the sample in question. When all the data is obtained with the same time bases and voltages settings, a two dimensional spectrum can be obtained in a point by point manner, so that a series of transients are accumulated at fixed intervals after the flash.

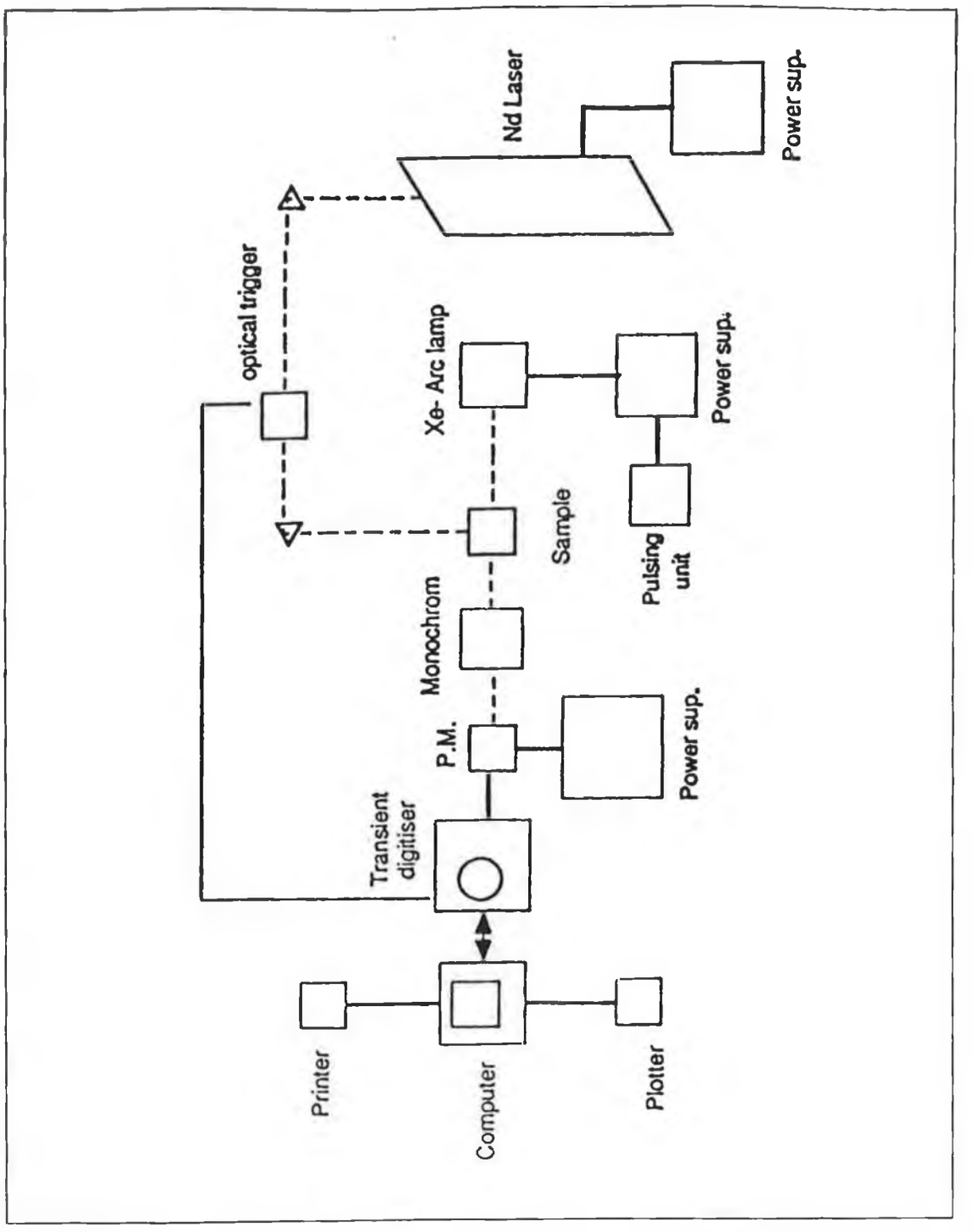

Figure 5.1 Schematic diagram of the instrumentation used in the laser flash photolysis experiments.

5.8 NMR monitored photolysis

The samples were prepared in a degassable quartz NMR tube in the deuterated solvent of choice. The samples were degassed by three cycles of freeze-pump-thaw procedure to ~10^{-3} Torr. The NMR tube was thawed slowly during each cycle as the tube was very delicate. The sample was then liquid pumped and placed under 1 atm of carbon monoxide. The sample was protected from light as much as possible, to prevent premature photoreactions. The changes in the sample were then monitored upon photolysis at various time intervals.

5.9 Determination of extinction coefficients

Extinction coefficients were determined for compounds at the wavelength of excitation in the relevant solvents. The Beer-Lambert law then allows calculation of the concentration of a sample when the absorbance is known. The Beer-Lambert law is given by :

$$\boxed{A = \varepsilon c l}$$

where;

A = absorbance at the excitation wavelength (A.U.)

ε = molar extinction coefficient (L mol^{-1} cm^{-1})

c = concentration (mol L^{-1})

l = pathlength (1cm)

5.10 Determination of quantum yields for the photosubstitution of CO in (η^6-mesitylene)$Mo(CO)_3$.

The Quantum yield for a photochemical reaction is given by;

$$\Phi = \frac{\text{no. of moles of product formed}}{\text{no. of quanta absorbed}}$$

The number of quanta absorbed was determined using the potassium ferrioxalate actinometer. When a solution of $K_2(FeC_2O_4)_3$ in aqueous sulphuric acid is irradiated with in the range 253 to 577 nm the Fe^{3+} ions are reduced to Fe^{2+}. The yield of Fe^{2+} ions can then be determined experimentally; a red coloured complex is formed with 1,10 phenanthroline which can be monitored at 510 nm.

5.101 Preparation of the potassium ferrioxalate actinometer

The actinometer was prepared as described by Rabek[5]; $FeCl_3$ (1.5 M) and $K_2C_2O_4$ (1.5 M) were mixed 1:3 by agitation. The bright green precipitate of $K_3Fe(C_2O_4)_3 .3H_2O$ was recrystallised from water and dried under vacuum in a stream of warm air. The salt was stored in the dark. For actinometric measurements $K_3Fe(C_2O_4)_3$ (2.947g) was dissolved in 800cm^3 of milli-Q water, 100cm^3 of 1M H_2SO_4 was added and the solution made up to 1000 cm^3. All preparation and measurements were carried out in the darkroom using a red photographic light. All solutions were degassed prior to measurements.

5.102 Preparation of solution Filters

The filters were prepared as described by Murov[6];

λ_{exc} = **334nm**

$NiSO_4.6H_2O$ (0.38M soln.)/ K_2CrO_4 (5×10^{-4}M soln.)/ K biphthalate (0.025M soln.)/ Corning 7-54 filter.

λ_{exc} = **313nm**

$NiSO_4$ (0.178M soln.)/ Naphthalene in isootane (0.11M)/ Corning 7-51 filter.

λ_{exc} = **266 nm**

The 266 nm laser frequency was employed.

5.103 Determination of Light intensity of source

A $4cm^3$ solution of the actinometer was irradiated at the desired wavelength, this was then transferred to a $10cm^3$ volumetric flask along with of buffer solution (1 N CH_3COONa ($600cm^3$) and 1 N H_2SO_4 ($360cm^3$) to 1L) and $0.8cm^3$ phenthroline, and made up to volume. The mixture was shaken well and allowed to develop for 1 hour. The absorbance at 510 nm was then recorded. The number of moles of Fe^{2+} could then be determined from;

$$n_{Fe^{2+}} = \frac{6.023 \times 10^{20} \times V_1 \times V_3 \times A}{V_2 \times l \times \varepsilon}$$

where

V_1 = Volume of actinometer irradiated (cm^3).

V_2 = Volume of actinometer transferred into volumetric flask.

V_3 = Final volume

A = Absorbance at 510 nm

l = Cell path length (1 cm)

ε = extinction coefficient of Fe^{2+}/ phenanthroline complex at 510 nm (L mol^{-1} cm^{-1})

The number of quanta absorbed per second can then be determined from;

$$n_a = \frac{n_{Fe^{2+}}}{\Phi \times t}$$

where

n_a = The number of quanta absorbed per second.

Φ = The quantum yield of Fe^{2+} at λ_{exc}.[5]

t = Irradiation time in seconds.

5.104 Determination of the number of moles of (η^6-mesitylene)$Mo(CO)_2$(pyr) formed.

Solutions of (η^6-mesitylene)$Mo(CO)_3$ in cyclohexane with excess pyridine were degassed for 20 minutes and irradiated in the same manner as the actinometer for set intervals of time. The photoreaction was allowed precede to ~20% completion to avoid absorbance of the photoproduct. The depletion of the parent was monitored at 324 nm and using the Beer-Lambert law as previously described (Section 5.8) the number of moles of depleted complex could be determined. The experiment with λ_{exc} = 266 nm employed Z-cyclooctene as the substitution ligand as pyridine absorbed at this wavelength. Corrections were made for internal filtering of light in all cases.

5.11 Peakfit Analysis of UV/vis Spectra

Although a peak may be just discernible in a UV/vis spectrum it may not produce a local maxima in the data stream. A Jandel Scientific peakfit package was employed to observe low intensity overlapped absorption's. Initially a smoothing algorithm is applied to the spectrum; the Savitzky-Golay procedure was employed in this study. The algorithm is based on least squares quatic polynomial fitting across a moving window within the data. The line-shape of the spectra are Voigt in nature; a convolution of Gaussian and Lorentzian line shape. The Lorentzian line shape is the "natural" shape for spectra consisting of energy absorption or emission due to a transition between energy states. The line broadening is attributed to the lifetimes of the energy states and the Heisenberg principle. The Gaussian line broadening originates from instrument optical and electrical effects, and is often referred to as the spread function. The spectral lines are deconvoluted during the peakfitting to yield the Lorentzian and instrument response width. In this study a residual method was employed to elucidate "hidden" peaks in the UV/vis spectra of some compounds. A residual may be defined as the difference in Y-value between a data point and the sum of component peaks evaluated at the data points X-value. The peaks are then arranged in such a way that their total area equals the area of the data, and so "hidden" peaks are revealed by residuals.

References

[1] Mahaffy, C. A. L.; Pauson, P.L.; *Inorg. Synth.* **19,** 154, 1979.

[2] Hrnciar, P.; Hudecek, M.; Magamedov, G. K. I.; Toma, S.; *Collect. Czech. Comm* **56**, 1477, 1991.

[3] Nesmeyanov, A. N.; Krivykh, V. V.; Kaganovich, V. S.; Rubinskaya, M. I.; *J. Organomet. Chem.* **102,** 185, 1975.

[4] Hieber, W.; Muhlbauer, F.; *Z. Anorg. Allg. Chem.* **221,** 337, 1935.

[5] Rabek, J. F.; *Experimental Methods in Photochemistry and Photophysics*, Wiley, NewYork, 1982.

[6] Murov, R; *Hand Book of Photochemistry*, New York, 1973.

Appendix

Extinction Coefficients

$[(\eta^6\text{-benzene})_2Cr]^+I^-$ in water at 266 nm

Conc. ($x10^{-4}M$)	Absorbance (A.U.)
0.0	0.0
1.0	0.42722
2.0	0.84175
3.0	1.22952
4.0	1.66333

Beer-Lambert law Fit

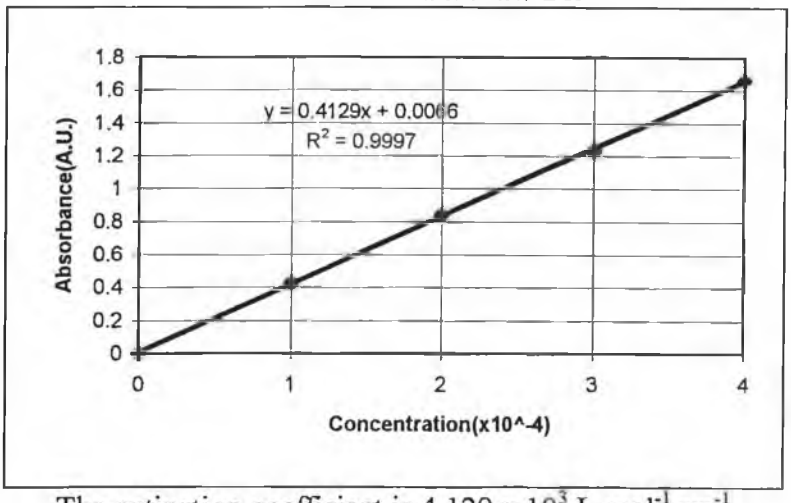

The extinction coefficient is 4.129×10^3 L mol^{-1} cm^{-1}

$[(\eta^6\text{-benzene})_2Cr]^+I^-$ in acetonitrile at 266 nm

Conc. ($x10^{-4}M$)	Absorbance (A.U.)
0.0	0.0
1.0	0.52899
2.0	0.98415
3.0	1.5473
4.0	1.91963

Beer-Lambert Law Fit

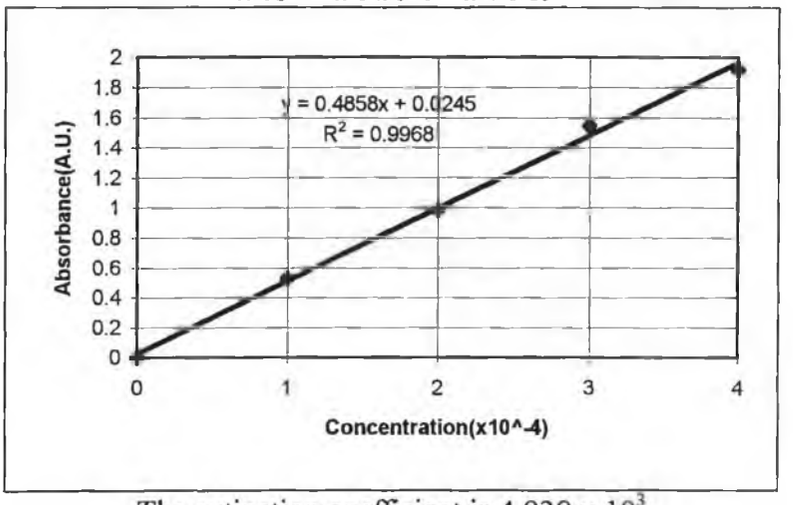

The extinction coefficient is 4.939×10^3

$[(\eta^6\text{-benzene})_2Cr]^+I^-$ in water at 354nm

Conc. ($x10^{-4}M$)	Absorbance (A.U.)
0.0	0.0
1.0	0.29979
2.0	0.58481
3.0	0.85849
4.0	1.1683

Beer-Lambert Law Fit

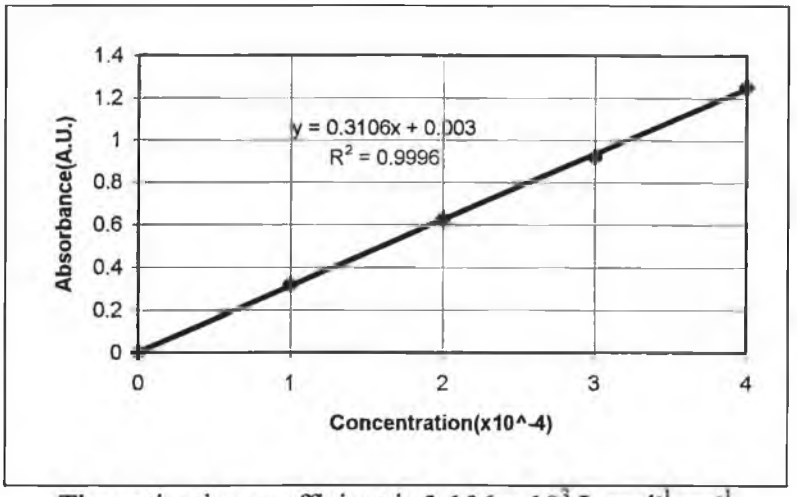

The extinction coefficient is 3.106×10^3 L mol^{-1} cm^{-1}

$[(\eta^6\text{-benzene})_2Cr]^+I^-$ in Acetonitrile at 354nm

Conc. ($x10^{-4}M$)	Absorbance (A.U.)
0.0	0.0
1.0	0.35918
2.0	0.66522
3.0	1.003624
4.0	1.32379

Beer-Lambert Law Fit

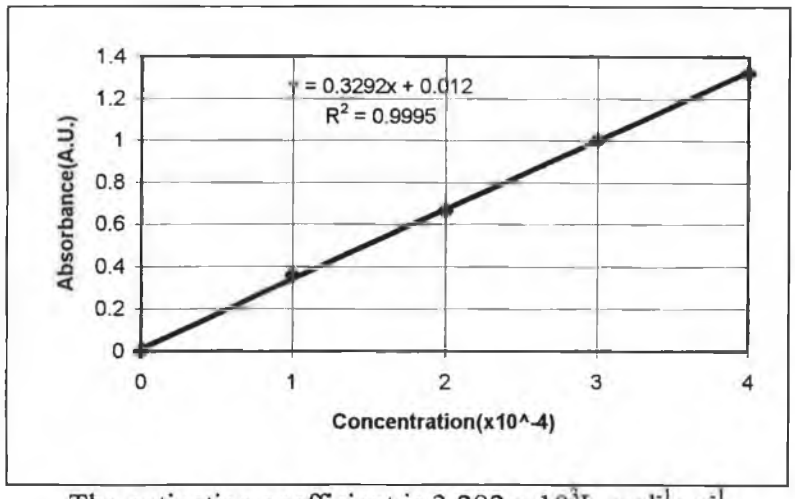

The extinction coefficient is $3.292 \times 10^3 L\ mol^{-1}cm^{-1}$

$[(\eta^6\text{-benzene})_2Cr]^+Cl^-$ in water at 266nm

Conc. ($x10^{-4}M$)	Absorbance (A.U.)
0.0	0.0
1.0	0.41839
2.0	0.83472
3.0	1.1994
4.0	1.59325

Beer-Lambert Law Fit

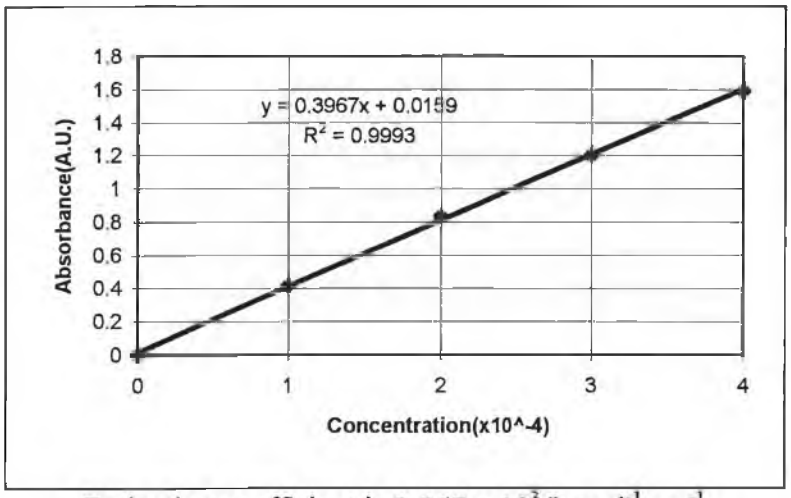

Extinction coefficient is 3.967×10^3 L mol^{-1} cm^{-1}

$[(\eta^6\text{-benzene})_2Cr]^+Cl^-$ in Acetonitrile at 266nm

Conc. ($x10^{-4}M$)	Absorbance (A.U.)
0.0	0.0
1.0	0.45004
2.0	0.87583
3.0	1.24051
4.0	1.63446

Beer -Lambert Law Fit

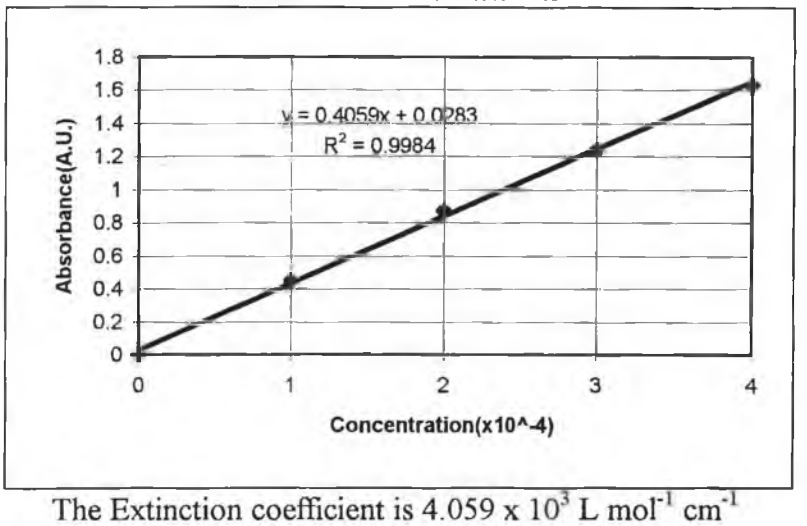

The Extinction coefficient is 4.059×10^3 L mol^{-1} cm^{-1}

$[(\eta^6\text{-benzene})_2Cr]^+Cl^-$ in Water at 354 nm

Conc. ($x10^{-4}M$)	Absorbance (A.U.)
0.0	0.0
1.0	0.28995
2.0	0.57596
3.0	0.95609
4.0	1.2304

Beer -Lambert Law Fit

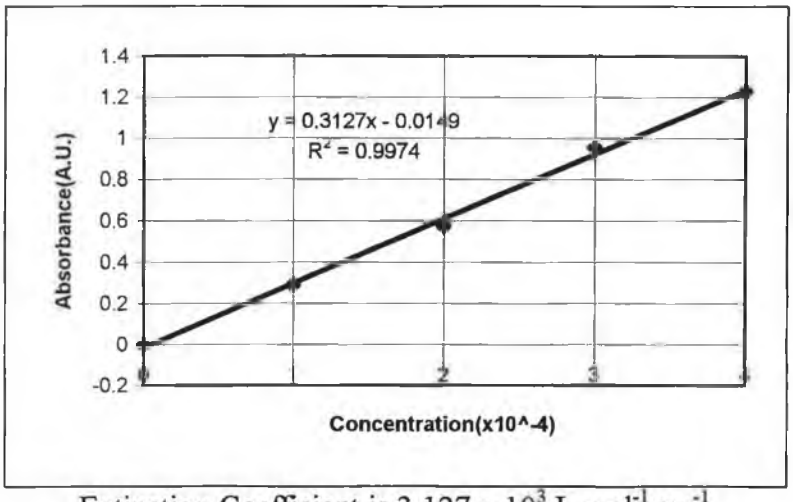

Extinction Coefficient is 3.127×10^3 L mol^{-1} cm^{-1}

$[(\eta^6\text{-benzene})_2Cr]^+Cl^-$ in Acetonitrile at 354 nm

Conc. ($x10^{-4}M$)	Absorbance (A.U.)
0.0	0.0
1.0	0.34117
2.0	0.65637
3.0	1.02122
4.0	1.28853

Beer -Lambert Law Fit

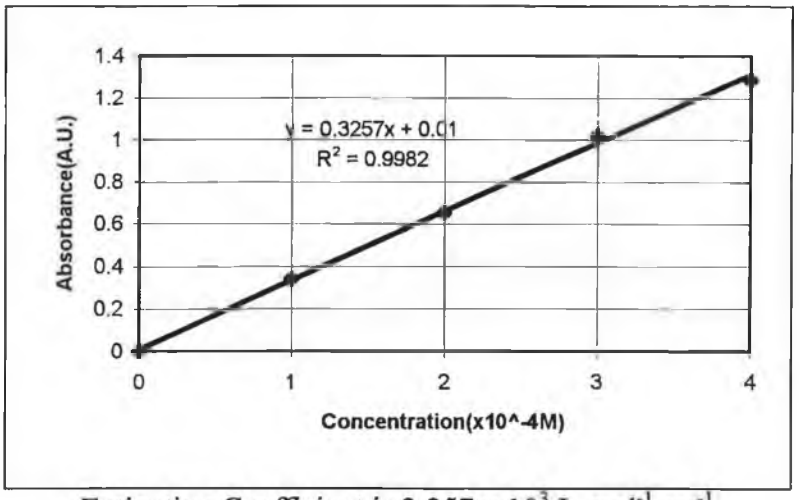

Extinction Coefficient is 3.257×10^3 L mol^{-1} cm^{-1}

[(η^6-*cis*-1,2-diphenylethene)($Cr(CO)_3)_2$] in cyclohexane at 354 nm

Conc. ($x10^{-5}$M)	Absorbance (A.U.)
0.0	0.0
1.0	0.34117
2.0	0.65637
3.0	1.02122
4.0	1.28853

Beer -Lambert Law Fit

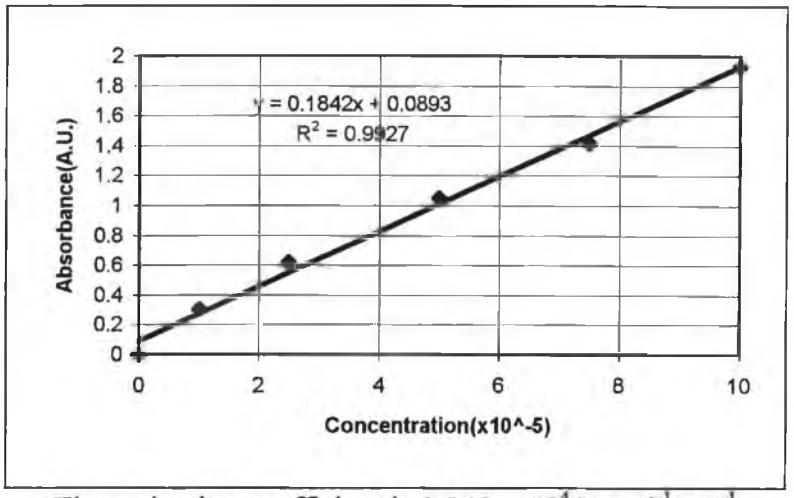

The extinction coefficient is 1.842 x 10^4 L mol^{-1} cm^{-1}

(η^6-mesitylene)$Cr(CO)_3$ in cyclohexane with excess pyridine at 324 nm

Conc. ($x10^{-5}M$)	Absorbance (A.U.)
0.0	0.0
1.0	0.34117
2.0	0.65637
3.0	1.02122
4.0	1.28853

Beer -Lambert Law Fit

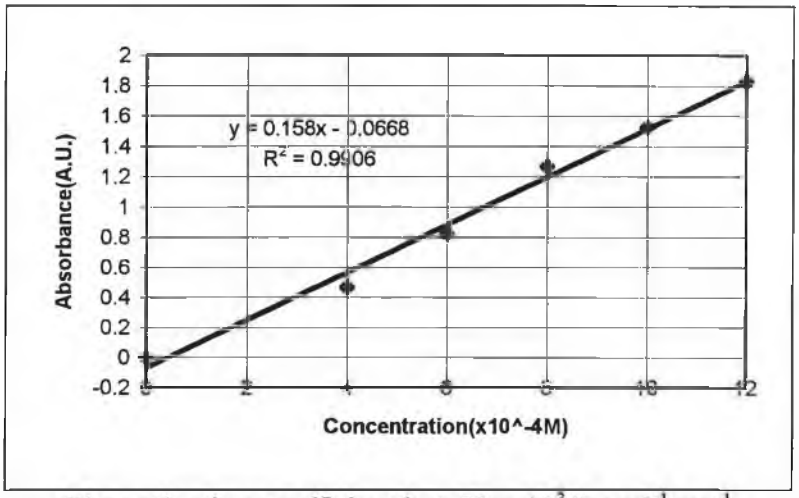

The extinction coefficient is 1.58 x 10^3 L mol^{-1} cm^{-1}

(η^6-mesitylene)$Cr(CO)_3$ in cyclohexane with excess Z-cyclooctene at 324 nm

Conc. ($x10^{-5}M$)	Absorbance (A.U.)
0.0	0.0
1.0	0.34117
2.0	0.65637
3.0	1.02122
4.0	1.28853

Beer -Lambert Law Fit

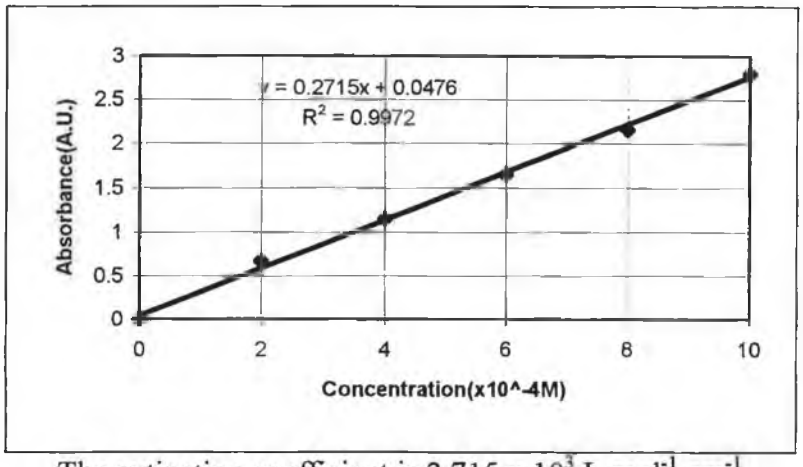

The extinction coefficient is 2.715 x 10^3 L mol^{-1} cm^{-1}